NAG 3-1

NAG 3-382

Drexel University

College of Engineering
Department of
Mechanical Engineering
and Mechanics
Philadelphia, PA 19104

(215) 895-2352-53

(NASA-CR-176373) OXIDES OF NITROGEN EMISSIONS FROM THE COMBUSTION OF MONODISPERSE LIQUID FUEL SPRAYS Ph.D. Thesis (Drexel Univ.) 173 p HC A08/MF A01 CSCL 13B

N86-14770

Unclas
G3/45 04930

OXIDES OF NITROGEN EMISSIONS FROM THE COMBUSTION OF

MONODISPERSE LIQUID FUEL SPRAYS

by

Hamid Sarv

Submitted in partial fulfillment of the requirements for the degree of

Doctor of Philosophy

Approved by Nicholas P. Cernansky

Dr. Nicholas P. Cernansky
Principal Investigator

Research Sponsored by the NASA Lewis Research Center through research grant NAG 3-1

Department of Mechanical Engineering and Mechanics
Drexel University, Philadelphia, PA 19104

June 1985

ABSTRACT

A study of NO_x formation in a one dimensional monodisperse spray combustion system, which allowed independent droplet size variation, was conducted. Temperature, NO and NO_x concentrations were measured in the transition region, encompassing a 26-74 micron droplet size range. Emission measurements of hydrocarbons, carbon monoxide, carbon dioxide and oxygen were also made. The equivalence ratio was varied between 0.8 and 1.2 for the fuels used in this study, including methanol, isopropanaol, n-heptane and n-octane. Pyridine and pyrrole were added to n-heptane as nitrogen-containing additives in order to simulate synthetic fuels.

Results obtained from the postflame regions using the pure fuels indicate an optimum droplet size in the range of 43-58 microns for minimizing NO_x production. For the fuels examined, the maximum NO_x reductions relative to the small droplet size limit were about 10-20% for lean and 20-30% for stoichiometric and rich mixtures. This behavior is attributed to droplet interactions and the transition from diffusive to premixed type of burning. Preflame vaporization controls the gas phase stoichiometry which has a significant effect on the volume of the hot gases surrounding a fuel droplet, where NO_x is formed. On the other hand, the release of fuel vapor from the droplet to the reaction zone is influenced by droplet interactions which reduce the volume of the hot gases and NO_x production by bringing the flame closer to the droplet surface.

For small droplets, gas phase combustion and droplet ignition are intensified by the high preflame extent of vaporization. Much of the NO_x is formed in the hot gases surrounding the burning fuel droplets, where premixed type of burning appears to dominate. Large droplets burn in a diffusive fashion, due to lower droplet vaporization before the flame front and the slow propagation of the fuel vapor emerging from the surface of the burning droplets. However, NO_x production for large droplets increases as they achieve elevated flame temperatures due to their higher Damkohler number. At some intermediate size, where minimum NO_x is predicted, the flame temperature

and the fuel vapor concentration in the gas phase fall in between the values observed for the small and large droplets. Under this situation, droplet interactions reduct the burning rate and lower NO_x formation by confining its production to a thin reaction zone. These interaction effects are also believed to be responsible for higher CO and O_2, and lower CO_2 emissions.

The occurrence of the minimum NO_x point at different droplet diameters for the various fuels appears to be governed by the fuel vaporization characteristics. This point was verified by air preheating and synthetic oxidizer experiments.

Experiments with nitrogen-bearing additives revealed that under stoichiometric and rich conditions, reducing the droplet size increases the efficiency of fuel-N conversion to NO_x. This observation is associated with improved oxidation of the pyrolysis fragments of the additive by better oxygen penetration through the droplet flame zone.

Preflame spray vaporization and NO_x formation from spray combustion are also studied analytically. Temperature and fuel, oxidizer and NO mass fractions around the burning droplets were determined from the numerical solution of the governing energy and species equations. A qualitative agreement between the predicted and experimental results was found.

OXIDES OF NITROGEN EMISSIONS FROM THE COMBUSTION OF MONODISPERSE LIQUID FUEL SPRAYS

A Thesis

Submitted to the Faculty

of

Drexel University

by

Hamid Sarv

in partial fulfillment of the

requirements for the degree

of

Doctor of Philosophy

June 1985

ACKNOWLEDGEMENTS

It is with deep appreciation that I express gratitude to my thesis advisor, Professor Nicholas P. Cernansky for his guidance and continuous interest throughout this effort. His patient supervision and enthusiasm have been necessary in making this work possible.

I am also greatful to my thesis committee members, Professors Bakhtier Farouk, Chung W. Lau, Arthur M. Mellor, Izak Namer and Charles B. Weinberger, for their suggestions and recommendations that were essential to the improvement of this research. Many thanks are due to Professors Richard S. Cohen and Ahtisham A. Nizami and Dr. Surendra Singh for their thoughtful comments and valuable conversations. Thanks are also given to many of my fellow graduate students and collegues, in particular, to Richard D. Wilk, for numerous informative and helpful discussions. The assistance of the staff of the Mechanical Engineering Labs, Altimus Seneca, Jake Stineman, Henry Mocarsky and Louis Haas, in the design, fabrication and trouble shooting of the experimental setup is greatly appreciated.

This work was sponsored by the NASA Lewis Research Center through research grant NAG 3-1 to the Mechanical Engineering and Mechanics Department, Drexel University.

Finally, I would like to thank my parents for their support, encouragement and personal sacrifice, to whom I will always remain indebted.

TABLE OF CONTENTS

LIST OF FIGURES

Page

Page

LIST OF TABLES

NOMENCLATURE

A = pre-exponential collision frequency factor

B = mass transfer number

C_1 = defined by equation (5-15)

C_2 = defined by equation (5-16)

C_D = drag coefficient

C_p = Specific heat at constant pressure

d = burner diameter in terms of droplet radius

D = droplet diameter

$\mathcal{D}$ = mass diffusivity

ΔH = heat of reaction

E = activation energy

f = disturbance frequency

h = burner height in terms of droplet radius

i = radial index

j = species index

k = droplet index

K = thermal conductivity

ℓ = droplet index

L = latent heat of vaporization

$\mathcal{L}$ = center-to-center droplet spacing in terms of droplet radius

m = mass

$\dot{m}$ = vaporization/burning rate of fuel spray

$\dot{M}$ = burning rate of a single fuel droplet

N = number of droplets

N_r = number of radial meshes

N' = number of species

P = pressure

Q = fuel flow rate

r = radial coordinate

r_s = droplet radius

$\tilde{r}$ = normalized radial coordinate (r/r_s)

Re_D = Reynolds number $(\rho U' D/\mu)$

$\mathring{R}$ = Universal gas constant

S = surface area of droplet

t = time

T = temperature

U = droplet velocity

U' = relative velocity between a droplet and gas phase

v = radial velocity

w = source term

W = molecular weight

X = mole fraction

Y = mass fraction

<u>Subscripts</u>

b = boiling point

f = liquid

F = fuel vapor

g = gas phase

O = oxidizer

o = initial

s = surface

∞ = ambient

Greek Symbols

α = thermal diffusivity

α' = droplet interaction matrix

β = defined by equation (5-29)

γ = defined by equation (5-30)

ϵ = fraction of fuel droplet vaporized

η = burning rate correction factor

μ = absolute viscosity

ν = stoichiometric molar coefficient

ρ = density

ϕ = equivalence ratio, $(\text{Fuel/Ox})_{\text{actual}}/(\text{Fuel/Ox})_{\text{stoichiometric}}$

ψ = velocity potential defined by equation (5-51)

ABSTRACT

OXIDES OF NITROGEN EMISSIONS FROM THE COMBUSTION OF MONODISPERSE LIQUID FUEL SPRAYS

Hamid Sarv

and

Nicholas P. Cernansky

A study of NO_x formation in a one dimensional monodisperse spray combustion system, which allowed independent droplet size variation, was conducted. Temperature, NO and NO_x concentrations were measured in the transition region, encompassing a 26-74 micron droplet size range. Emission measurements of hydrocarbons, carbon monoxide, carbon dioxide and oxygen were also made. The equivalence ratio was varied between 0.8 and 1.2 for the fuels used in this study, including methanol, isopropanol, n-heptane and n-octane. Pyridine and pyrrole were added to n-heptane as nitrogen-containing additives in order to simulate synthetic fuels.

Results obtained from the postflame regions using the pure fuels indicate an optimum droplet size in the range of 43-58 microns for minimizing NO_x production. For the fuels examined, the maximum NO_x reductions relative to the small droplet size

limit were about 10-20% for lean and 20-30% for stoichiometric and rich mixtures. This behavior is attributed to droplet interactions and the transition from diffusive to premixed type of burning. Preflame vaporization controls the gas phase stoichiometry which has a significant effect on the volume of the hot gases surrounding a fuel droplet, where NO_x is formed. On the other hand, the release of fuel vapor from the droplet to the reaction zone is influenced by droplet interactions which reduce the volume of the hot gases and NO_x production by bringing the flame closer to the droplet surface.

For small droplets, gas phase combustion and droplet ignition are intensified by the high preflame extent of vaporization. Much of the NO_x is formed in the hot gases surrounding the burning fuel droplets, where premixed type of burning appears to dominate. Large droplets burn in a diffusive fashion, due to lower droplet vaporization before the flame front and the slow propagation of the fuel vapor emerging from the surface of the burning droplets. However, NO_x production for large droplets increases as they achieve elevated flame temperatures due to their higher Damkohler number. At some intermediate size, where minimum NO_x is predicted, the flame temperature and the fuel vapor concentration in the gas phase fall in between the values observed for the small and large droplets. Under this situation, droplet interactions reduce the burning rate and lower NO_x formation by confining its production to a thin reaction zone. These interaction effects are also believed to be responsible for higher CO and O_2, and lower CO_2 emissions.

The occurrence of the minimum NO_x point at different droplet diameters for the various fuels appears to be governed by the fuel vaporization characteristics. This point was verified by air preheating and synthetic oxidizer experiments.

Experiments with nitrogen-bearing additives revealed that under stoichiometric and rich conditions, reducing the droplet size increases the efficiency of fuel-N conversion to NO_x. This observation is associated with improved oxidation of the pyrolysis fragments of the additive by better oxygen penetration through the droplet flame zone.

Preflame spray vaporization and NO_x formation from spray combustion were also studied analytically. Temperature and fuel, oxidizer and NO mass fractions around the burning droplets were determined from the numerical solution of the governing energy and species equations. A qualitative agreement between the predicted and experimental results was found.

CHAPTER 1

Introduction

Based on energy consumption figures published in 1982 (Gustaferro, 1982), combustion of liquid hydrocarbon fuels constitutes 47% of the total energy usage in the United States. Despite the increasing contributions of other forms of energy such as nuclear, solar, and geothermal, our energy systems rely heavily upon the supply of fossil fuels. The forecast predicts that the combustion of liquid fuels will remain as the dominant source of power generation for years to come. Another intriguing fact is that about 42 percent of the liquid fuel is consumed in sprays. The ease in storage, handling, and atomization of liquid fuel has made spray combustion the driving force in large scale stationary gas turbines and boilers, as well as in air and some ground transportation vehicles.

Because of the wide use of fuel spray combustion, the efficiency and pollutant formation from such applications have become of major concern to both government and private industry. Although there have been many analytical studies to characterize the combustion of fuel sprays, in most cases our knowledge is based on empirical relationships (obtained from experimental results), which are often scale dependent. As a consequence, there is still a lack of understanding of the most fundamental processes that occur during the combustion of fuel sprays. Most of the difficulty is associated with simultaneous occurrence of complex physical and chemical processes which make the formulation of a descriptive model of spray burning a strenuous task. Recently, a number of extensive reviews (Williams, 1973; Faeth, 1979; Chigier, 1983; Sirignano, 1983) have discussed the state of the art in the area of liquid fuel spray combustion and have also suggested future directions for experimental and analytical developments.

Oxides of nitrogen are among the major pollutants emitted from combustion sources. In spray combustion, NO_x ($NO+NO_2$) emission levels have been found to be influenced by the fuel spray characteristics. While some researchers believe in a droplet size effect, others have attributed their observations to aerodynamic and mixing effects. Unfortunately, due to the operational inflexibilities in their experimental systems, the importance of the individual factors could not be distinguished. For instance, change of droplet size often required substantial variations in fuel and air flow rates which may have influenced the combustion processes. Also, the related analytical studies have deviated from modeling the physical system by limiting their attention to the combustion of single droplets. This study was undertaken to resolve some of the contradictions by isolating the important parameters that could lead to lower NO_x formation.

A well-characterized spray combustion facility was used to simulate some of the basic processes that occur in practical combustors such as diesel engines or gas turbines. The experimental variables include droplet size, stoichiometry, fuel type, oxidizer composition, etc. Oxides of nitrogen and temperature constitute the major portion of the experimental measurements made in this study.

Experimental results that are presented for a range of operating conditions indicate an optimum droplet size for minimizing NO_x production. Droplet interactions and transition from diffusive to premixed type of burning are considered to be responsible for the observed behavior. This point has also been examined through additional measurements and analytical calculations. Numerical predictions are compared with the experimental results and possible refinements to the model are discussed.

Chapter 2 includes a review of some of the previous work in the area of spray combustion and pollutant formation. The experimental facility and measurements are reported in Chapters 3 and 4, respectively. The analytical calculations and predictions are presented in Chapter 5. Finally, the conclusions of the study and recommendation for future work are given in Chapter 6.

CHAPTER 2

Background and Literature Review

As noted, a number of extensive reviews dealing with fuel spray combustion have appeared in the literature (Williams, 1973; Faeth, 1979; Chigier, 1983; Sirignano, 1983). No attempt is made to duplicate or summarize these landmark efforts here. Instead, only the previous work particularly germane to the present study is reviewed in this chapter. The three major areas covered are liquid fuel spray combustion, transition region phenomena and NO_x formation. Some of the specific topics such as droplet interactions and NO_x formation mechanisms for fuels with chemically bound nitrogen are examined more closely along with the relevant findings of this study, in later chapters.

2.1 Liquid Fuel Spray Combustion

The most fundamental aspect of spray combustion involves the burning of single fuel droplets. Experiments with droplets suspended from filaments (Godsave, 1953), porous spheres fed by liquid fuel (Spalding, 1953), freely falling droplets (Kumagai and Isoda, 1956), and dilute sprays (Bolt and Boyle, 1956) have shown that the surface regression rate of a fuel droplet during evaporation or combustion varies linearly with time and is governed by the "D^2 law". For isolated droplets, theoretical calculations relate this rate to the droplet size, fuel/ambient gas composition, local temperature, pressure, and the relative velocity between the fuel droplet and the gas phase. Excellent agreement has been found between the physical model and the experimental results.

Development of a chemical model for predicting the concentration of the combustion products requires consideration of heat, mass, and momentum transfer in addition to a knowledge of the major chemical reactions. Certain assumptions, including single fuel droplet, spherical symmetry, equal thermal and molecular diffusivities, and a one step fuel oxidation reaction, are commonly made to simplify the analysis. In spite of the simplifications, the problem remains complex and numerical treatment becomes necessary. One of the first analyses of this type was done by Lorell et al. (1956) who determined the flame structure around a single ethanol droplet under steady state conditions. In their analysis, the flame temperature and its thickness were found to be sensitive to the chemical reaction rates. When the reactions become infinitely fast, the reaction zone reduces to a flame shell of infinitesimal thickness. In this situation, temperature and concentration profiles as well as flame location can be determined explicitly (Williams, 1965). Unsteady combustion of a single fuel droplet placed in a hot and reactive environment was numerically investigated by Botros et al. (1980). Their study showed that diffusional or premixed type of burning depends on the fuel concentration in the droplet environment. In contrast with the D^2 law predictions, they demonstrated an unsteady flame front relative to the receding droplet radius.

New complications arise when one attempts to characterize the behavior of fuel sprays. For instance, droplet size distribution and air flow patterns require special considerations due to their effects on spray combustion (Beèr and Chigier, 1983). Spray vaporization results in fuel enrichment and cooling of the gas phase (Law, 1977; Rao and Lefebvre, 1981) which can have significant effects on ignition and burning of the droplets.

An individual droplet in a spray has to compete with its neighbors for the available oxygen. This competition becomes stronger for smaller droplet spacings and leads to an increase in the droplet lifetime compared to that of an isolated droplet with the same diameter.

Kanevsky (1956) showed that for a stationary array of nine droplets, the burning rate for the center droplet reduced when the droplet flame boundaries merged at decreased droplet spacings. Similar results have also been obtained by others (Nuruzzaman et al., 1971; Miyasaka and Law; 1981; Sangiovanni and Labowsky, 1982; Xiong et al., 1985) using linear arrays of monodisperse fuel droplets.

The theoretical work of Labowsky (1976-1980), Umemura et al. (1981a,1981b), and Marberry et al. (1984), assuming a quasi-steady mass flux transport model, show that the evaporation rates of interacting droplets decrease when the droplet spacing is reduced. Their calculations indicate that the spray evaporation rate can be determined by applying a correction factor to the single droplet model which is only dependent on the array geometry.

Chiu *et al.* (1977,1983) have identified four classes of sprays that exhibit external sheath, external group, internal group, and single droplet modes of combustion. These regimes are separated by a group combustion number which is defined as the ratio of the heat transfer in the gas phase to the heat transfer between the gas and the liquid phase. In a recent study, Bellan and Cuffel (1983) presented a spray evaporation model in which the interacting droplets were separated by spheres of influence, and each droplet in the spray evaporated inside a finite surroundings. Their predicted results show that the evaporation of interacting droplets cannot be described by the D^2 law over the entire droplet lifetime.

2.2 Transition Region Effects

Another point of interest in spray combustion is the behavior of spray systems in the "transition region". In this region, which covers a range of 15-80 μm droplet diameter, the local conditions around the droplets are influenced by their size and spacings. For these sprays, the dominance of heterogeneous or homogeneous type of burning depends on the amount of prevaporization before the flame and the strength of droplet interactions in the flame. Such factors have been determined to be responsible for a number of interesting and important observations including increased burning velocities (Polymeropoulos and Das, 1975; Hayashi *et al.*, 1976; Polymeropoulos, 1984), broadened flammability limits (Burgoyne and

Cohen, 1954; Hayashi et al., 1981), lower ignition energies (Chan and Polymeropoulos, 1981), and reduced NO_x emissions (Nizami et al., 1978–82). These findings are of significant value for the design and development of high efficiency and low emission spray combustors.

2.3 NO_x Formation in Spray Combustion Systems

Prediction of NO_x emissions from spray combustion sources by isolating the contributing factors has been the subject of many investigations. Nitric oxide formation in the vicinity of a diffusion flame around a single droplet has been analytically treated by Kesten (1972) and Bracco (1973). The former study dealt with transient NO formation, assuming quasi-steady droplet combustion and an infinitely fast fuel oxidation reaction, while in the latter case, steady state droplet combustion at a finite reaction rate was considered. Both studies showed that the NO production per mass of fuel (Emission Index) increases with increasing droplet diameter. Kesten also demonstrated that under certain constraints (residence time equal to the droplet lifetime and near stoichiometric values), the NO emission index for homogeneous gas phase combustion can be more significant than that from the droplet combustion.

Exit plane measurements from a variety of experimental and practical combustion systems have also indicated the effects of droplet size and spray characteristics on NO_x emissions. Increased NO emissions with increasing Sauter Mean Diameter (SMD) have been measured from a marine gas turbine engine (Opdyke, 1983). Mellor and co-workers (1976, 1980) showed that the NO_x emissions from a gas turbine combustor can be correlated to the characteristic times for droplet evaporation, mixing, and chemical reactions. In a different study using a research gas turbine combustor, Nicolls _et al_. (1980) reported a decrease in the NO_x levels when the droplet size was increased from 10 to 57 microns at a constant residence time.

Murphy and Borman (1979) evaluated the contribution of droplet burning to the total NO_x formed in their laminar mist flame. Their result indicated higher NO_x emissions for larger droplets. With a monodisperse fuel spray burning in an aerodynamically stabilized flame inside a combustion tunnel, Nizami and Cernansky (1978-1982) showed the existence of an optimum droplet diameter (around 50 μm) for minimum NO_x production.

Combustion of fuels which contain chemically bound nitrogen contributes to additional NO_x emissions over what is formed from atmospheric nitrogen. Unfortunately, very little is known about the effect of droplet diameter on fuel-N conversion to NO_x. Perhaps the only qualitative study in this area was done by Appleton and Heywood (1973) who showed a strong influence of the degree of atomization and fuel/air mixing on the conversion efficiency. In a similar study, Foster and Keck (1980) reported significant levels of hydrogen cyanide in fuel-rich turbulent diffusion flames as far as five burner diameters downstream of a fuel atomizer nozzle. Increasing atomization pressure led to intense mixing and resulted in major reductions in HCN and a moderate rise in NO concentrations. Crowhurst and Simmons (1985a) utilized a hollow sintered cylinder burner for a structural examination of methane-acetonitrile-argon diffusion flames burning in a stream of oxygen and argon. They concluded that nitric oxide forms primarily on the oxygen side of the main reaction zone, with some of the NO diffusing back into the pyrolysis region of the flame and reacting with the nitrogenous radicals to form molecular nitrogen.

Most mechanistic studies have concentrated on prevaporized and premixed fuel/air mixtures doped with a nitrogen containing compound. Overall, the NO_x formation reactions from fuel-N involve the oxidation of the pyrolysis fragments of the nitrogen additive. Such mechanisms are affected by the flame stoichiometry and have been discussed by Fenimore (1976a, 1976b), Haynes (1977a), Crowhurst and Simmons (1983, 1985a, 1985b), Dasch and Blint (1984), and others. Previous work of Fenimore (1976a), Foster and Keck (1980), Sapre and Quader (1983) and Chen and Malte (1984), have shown little or no effect of the type of doping compound on NO_x yield.

CHAPTER 3

Experimental Set-Up and Procedures

3.1 Introduction

In this chapter the basic combustion facility and the NO_x and temperature measurement systems are described. The operating conditions and the actual measurements are discussed in Chapter 4. Other instrumentation including the exhaust analyzers and the fuel vaporizing system are specified in Appendix A.

3.2 Spray Combustion Facility

3.2.1 Monodisperse Spray Generation System

A Berglund-Liu Vibrating Orifice Monodisperse Aerosol Generator, Model 3050 (Berglund and Liu, 1973), is used to supply a monosized spray of droplets to the combustion facility. This generator has been employed successfully in other monodisperse spray combustion studies (Nizami *et al.*, 1978-1982; Koshland and Bowman, 1983, 1985).

Monodisperse droplet generation is achieved by applying periodic disturbances to a piezoelectric ceramic which exerts mechanical vibrations to a liquid jet emerging from an orifice plate. The oscillation frequency is applied from a function generator (Hewlett Packard Model 3310A). The perturbed jet then breaks up into discrete droplets with a standard deviation of approximately 1% of the mean diameter. Since one droplet is generated per cycle of disturbance, the droplet diameter can be calculated from the liquid feed rate (Q) and the frequency of disturbance (f) and is given by : $D=(6Q/\pi f)^{1/3}$. Thus, droplet size can be varied by changing the frequency or the fuel flow rate.

Although the actual orifice size is not used in the calculation of droplet diameter, an orifice plate is only capable of providing monosized droplets within a relatively narrow range. However, the monodispersion range can be extended easily by using a set of orifice plates with various orifice diameters.

3.2.2 Fuel and Air Flow Systems

A schematic of the experimental facility is shown in Figure 3.1. A high infusion syringe pump (Harvard Apparatus Model 901) supplies liquid fuel to the aerosol generator. Air is supplied at a regulated pressure of 35 psig from the house air compressor.

The stream of uniform droplets emerging from the orifice plate is subjected to a turbulent jet of dispersion air to prevent coagulation. A secondary flow of dilution air is also added to achieve the desired stoichiometry. For minimum fluctuations in the flow rates, the air flows are adjusted by electronic flow controllers (Tylan Model FC-260), and monitored by Mass Flow meters (Hastings Model ALL-5K).

A tapered baffle plate with 3 cm I.D. is positioned at 2 cm above the droplet generator to improve the mixing of the dilution air with the dispersed aerosol. The air/fuel aerosol then passes

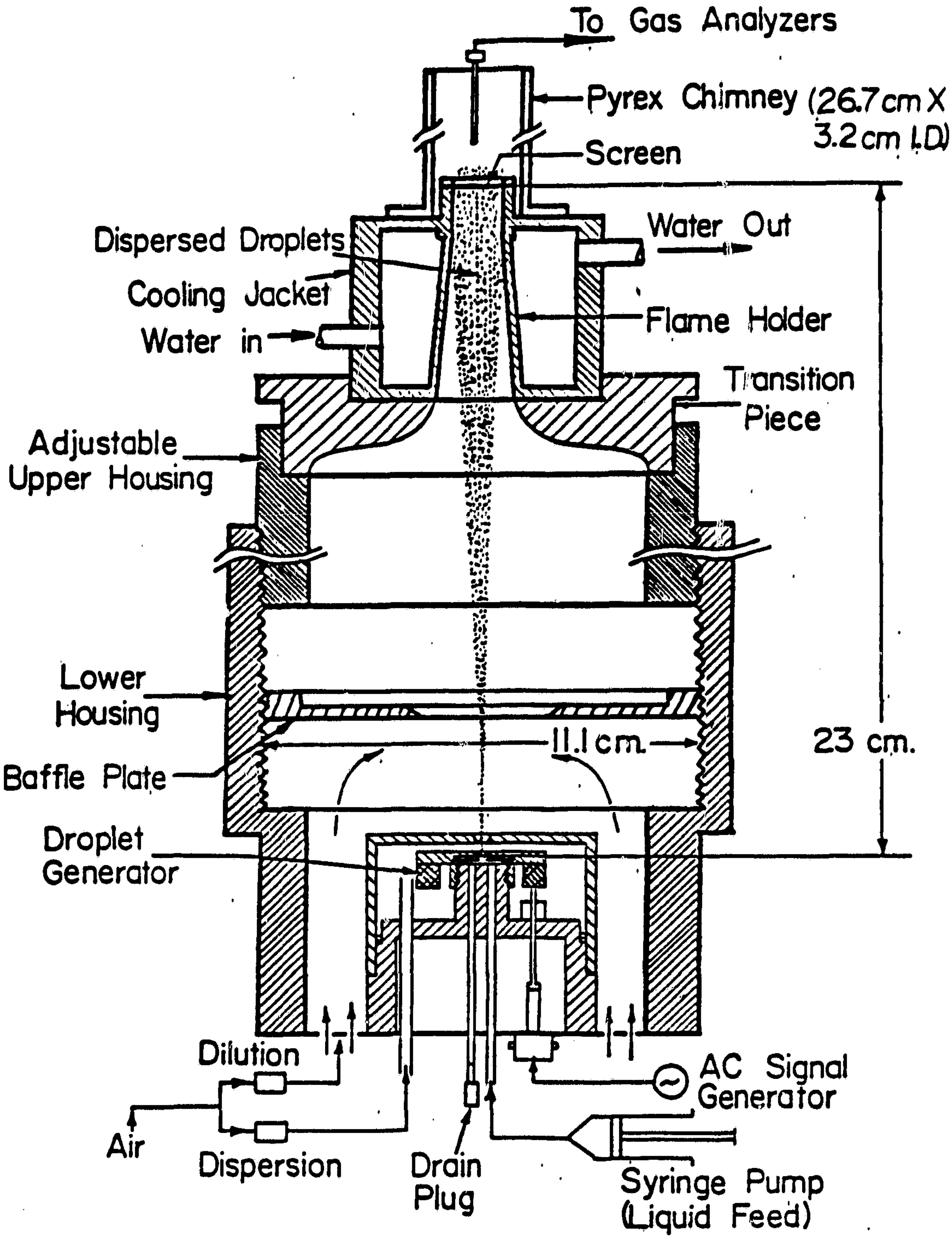

Figure 3.1. One-Dimensional spray combustion facility.

through a transition piece with smooth curvatures designed to minimize any recirculation. Above the transition piece are flow reducing sections which direct the laminarized aerosol to a flame holder where the monodisperse fuel spray is burned inside a screen stabilized one dimensional flame. The flame is surrounded by a long Pyrex tube to avoid outside air entrainment.

3.2.3 Flame Holders

In order to maintain one dimensional and stable flames for all equivalence ratios, a series of 40x40 mesh stainless steel screen flame holders (0.25 mm wire diameter) with matching flow reducing sections were designed and fabricated. The wire meshes block 50% of the area. In the absence of a flame, the fraction of droplets that survive the screen flame holder was determined using a dual beam He-Ne laser operated in the back scatter mode. By traversing the focal volume across the burner, a count rate of the droplets was determined both with and without the screen in place. The measurements indicate that the percentage of droplets which survive impaction on the screen are 37 and 24% for the 37 and 70 μm droplets, respectively. In the presence of a flame, those droplets which do not make it through the screen and agglomerate on the screen wires will flash evaporate and add to the vapor phase in the fuel aerosol entering the flame. The flame holders have exit diameters of 9.5, 12.7, 14.3, and 17 mm and are used for equivalence ratios between 0.8 and 1.2. Both the flame holder and the flow reducing section are water cooled to prevent uncontrolled droplet vaporization.

3.2.4 Other Design Considerations

The design of the spray burner facility allows for adjustment in the burner height from 16–23 cm above the orifice plate. A burner height of 17.8 cm was selected experimentally based on the aerodynamics of the dispersed aerosol. Below this optimum burner height, the fuel spray jet is not completely spread and diffused, resulting in a nonuniform velocity and fuel/air concentration at the screen, as indicated by the shape and luminosity of the flame. Above this optimum height, a significant number of droplets begin to settle out and accumulate on the droplet generator, leaving them unburnt. Thus, the burner height is fixed by these practical considerations.

3.3 Sampling and Analytical Instrumentation

3.3.1 NO_x Measurement System

Nitric oxide and total NO_x are collected using an uncooled aerodynamic stainless steel sampling probe with an orifice diameter of 0.3 mm as shown in Figure 3.2. For comparative studies of the effect of sampling probes on NO_x measurements, a water cooled probe having an orifice size of 0.25 mm (Figure 3.3) is used. The probe is cooled to 50°C during all measurements. The gases are sampled at a line pressure of 80 torr to prevent water condensation in the sampling line. Initially, the probes were designed to achieve aerodynamic quenching. However, Colket et al. (1982) have argued that a single probe may not be capable of aerodynamic quenching for all ambient conditions. But, as

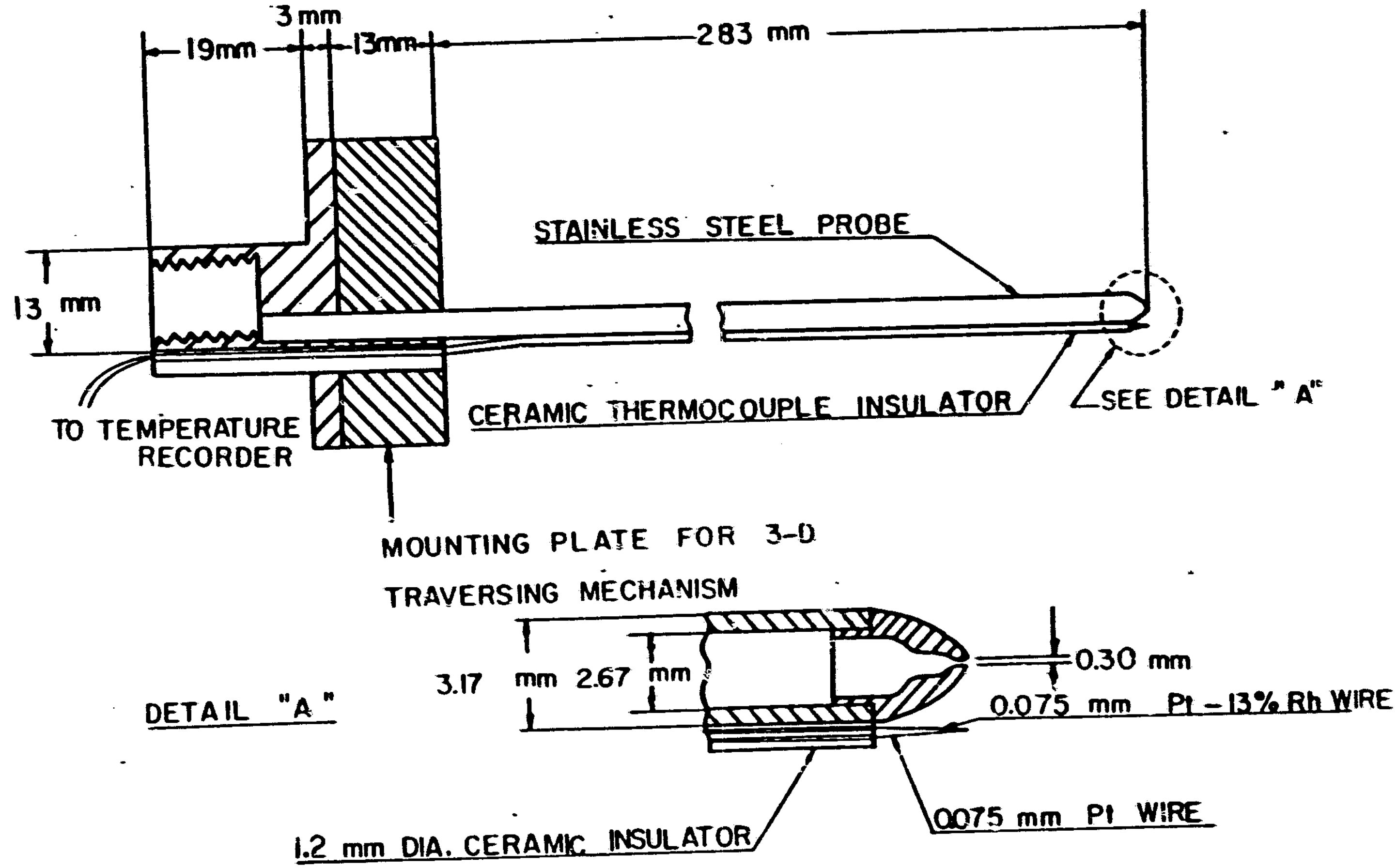

Figure 3.2. Temperature and gas sampling combination probes.

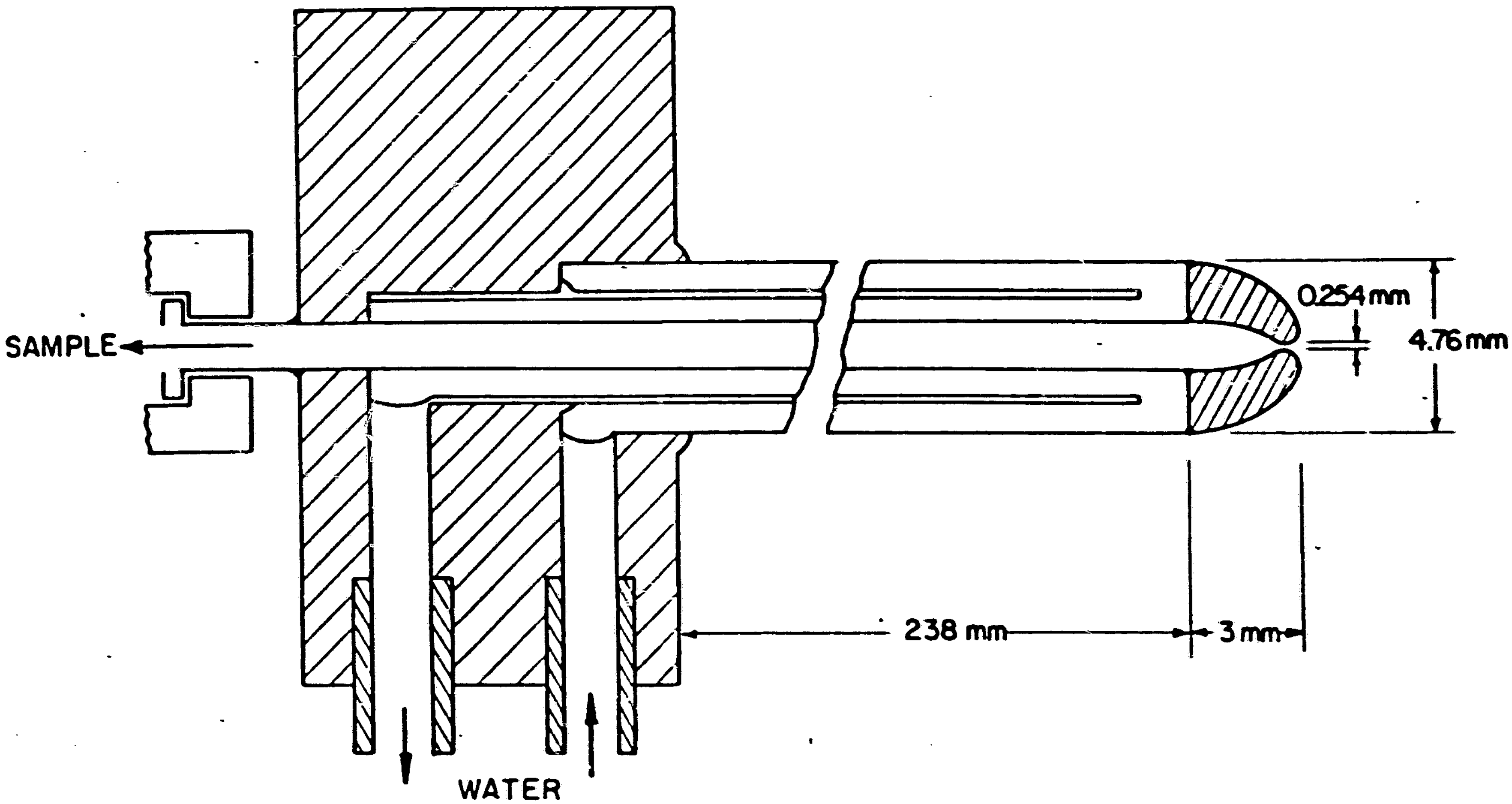

Figure 3.3. Water cooled gas sampling probe.

pointed out in section 4.7.1, the use of cooled or uncooled sampling probes did not have a noticeable effect on the measured NO_x values and only resulted in differences between the NO_2 levels.

The concentrations of NO and NO_x are measured by a chemiluminescent NO analyzer (TECO Model 12A), equipped with a Molybdenum NO_2 to NO converter. This system had been modified for low pressure sampling (Nizami, 1978). A high vacuum sampling pump and a variable sample capillary are used to maintain the analyzer reaction chamber pressure at 8 torr. For each steady state burner operating condition, continuous NO_x sampling and measurements are carried out for a period of two minutes and the measurements are plotted by a strip chart recorder for accurate NO_x concentration readings. Using this method, all NO_x readings were accurate to within 1 ppm, with a day to day reproducibility of 5 percent.

3.3.2 Temperature Measurement System

Temperature measurements are made with a Pt/Pt-13% Rh fine wire thermocouple (0.075 mm diameter) with a bead diameter of approximately 0.11 mm. The wires are inserted into a two-hole ceramic support which is attached to the side of the uncooled sampling probe (see Figure 3.2). This arrangement allows simultaneous NO_x and temperature measurements. The thermocouple is connected to a digital display Trendicator (Doric Type 400 A) as well as to a strip chart recorder for accurate measurements of the mean temperature at a particular location in the burner system. Positioning of the combination gas sampling/thermocouple probe is achieved by a 3-D traversing mechanism.

In order to determine the actual temperature at a sampling position, the measured value must be corrected for conduction and radiation losses. Such corrections are laborious and contain some level of uncertainty as discussed in Appendix D. For this reason, no corrections were applied and the temperature results reported in Chapter 4 represent the raw measurements only. Uncorrected temperature readings are accurate to within 20°C, with a day to day reproducibility of 5 percent.

CHAPTER 4

Experimental Results and Discussion

4.1 Introduction

Selected results on the effects of fuel type, stoichiometry, air preheating, oxidizer composition and fuel nitrogen additives on temperature and NO_x formation are presented and discussed in this chapter. Additional experimental results are given in Appendix B.

In some cases, slight modifications to the experimental facility were necessary to attain the desired operating conditions. Those changes are described appropriately.

The burner was operated under atmospheric pressure and in the monodisperse droplet size range at a constant fuel feed rate of 0.382 cc/min. To achieve the desired stoichiometry, the dilution air flow rate was varied, keeping the dispersion air flow rate at 1300 cc/min.

4.2 System Verification

4.2.1 Monodispersion Range

Since a single orifice plate can only operate in a narrow monodisperse range of droplets, a set of 20, 25, and 35 µm orifice plates were selected to cover a combined range of 36 to 74 µm droplet diameter. Figure 4.1 shows the monodisperse operating range of the aerosol generator determined by the manufacturer's suggested "jet deflection" method (Thermo System Inc., 1977) and further confirmed by a slide impaction technique recommended by Berglund and Liu (1973). All droplets in a collected sample must have the same size in order to be considered monodisperse. Typical slide impaction results of monodisperse droplets are shown in Figure 4.2.

4.2.2 Radial Temperature and NO_x Mapping

One dimensionality and radial symmetry of the flame for three different droplet sizes were examined by temperature and NO_x traverses at a height of 4 mm across the 17 mm flame holder.

In general, the flames appeared as pale blue and, for small droplets, it looked as if tiny streaks were burning in a 1 mm thick envelope flame with a luminous region extented to about 3 mm. Large droplets seemed to have occasional merging individual flamelets and were luminous up to 6 mm above the flame holder. The luminous region was relatively longer for lower volatility fuels.

The radial temperature and NO_x profiles shown in Figures 4.3 and 4.4* indicate some asymmetry for the 69.1 µm droplets, but for most part they are flat, thus confirming the one dimensionality of the burner system.

---

* A 15 µm orifice plate was used to produce the 26.7 µm droplets.

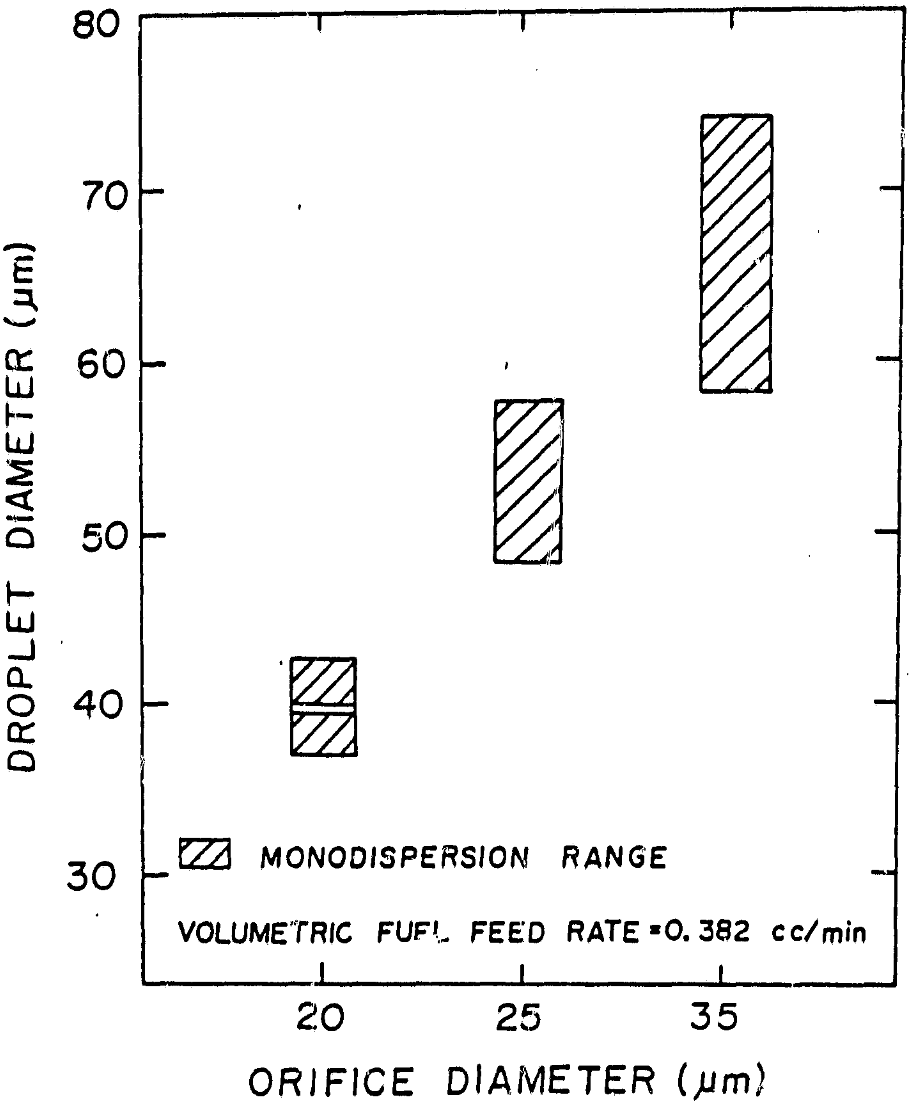

Figure 4.1. Monodispersion ranges of single orifice aerosol generation system.

37.5 micron droplets   70.0 micron droplets

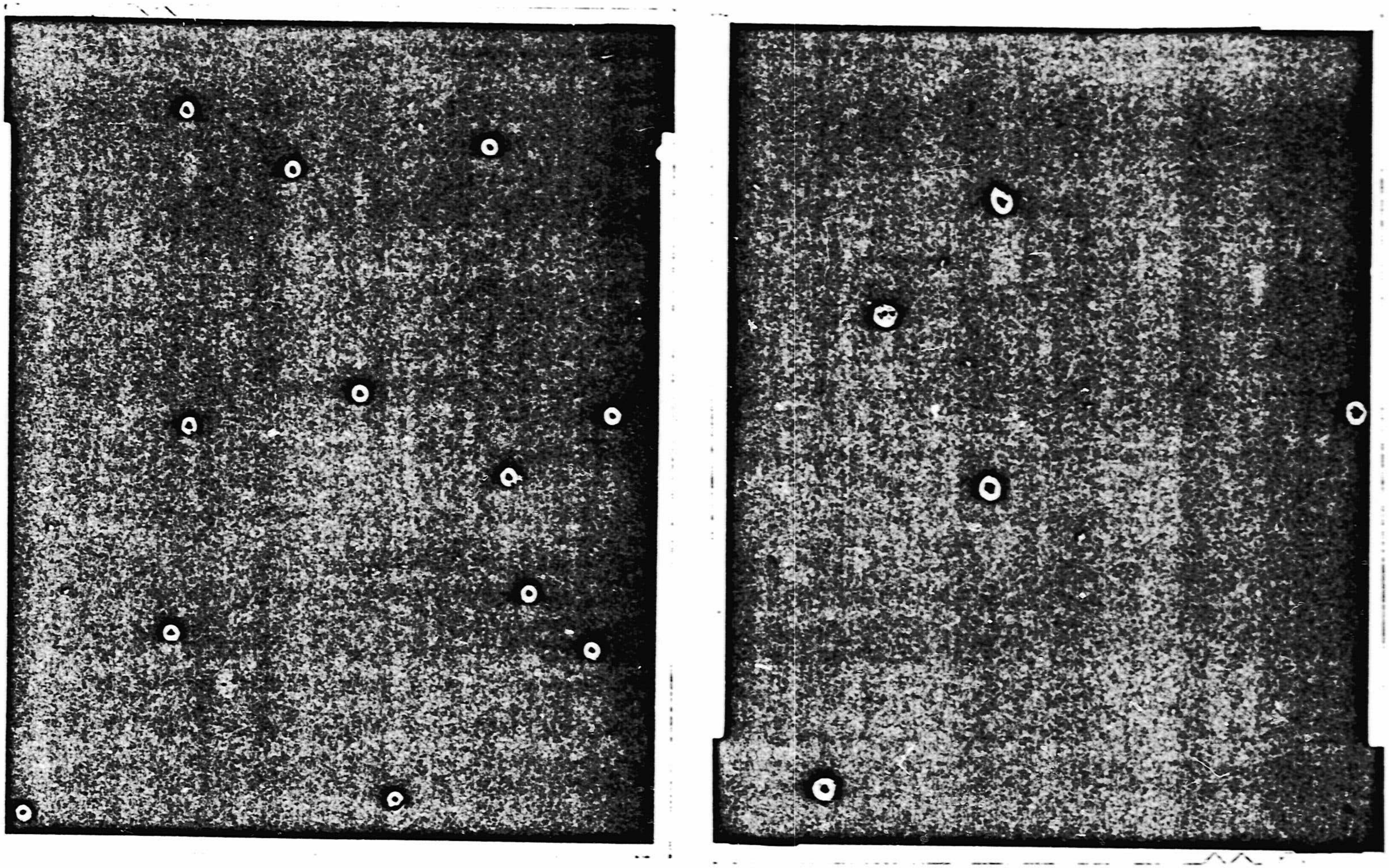

Figure 4.2. Microscopic photographs of droplet impactions on glass slides.

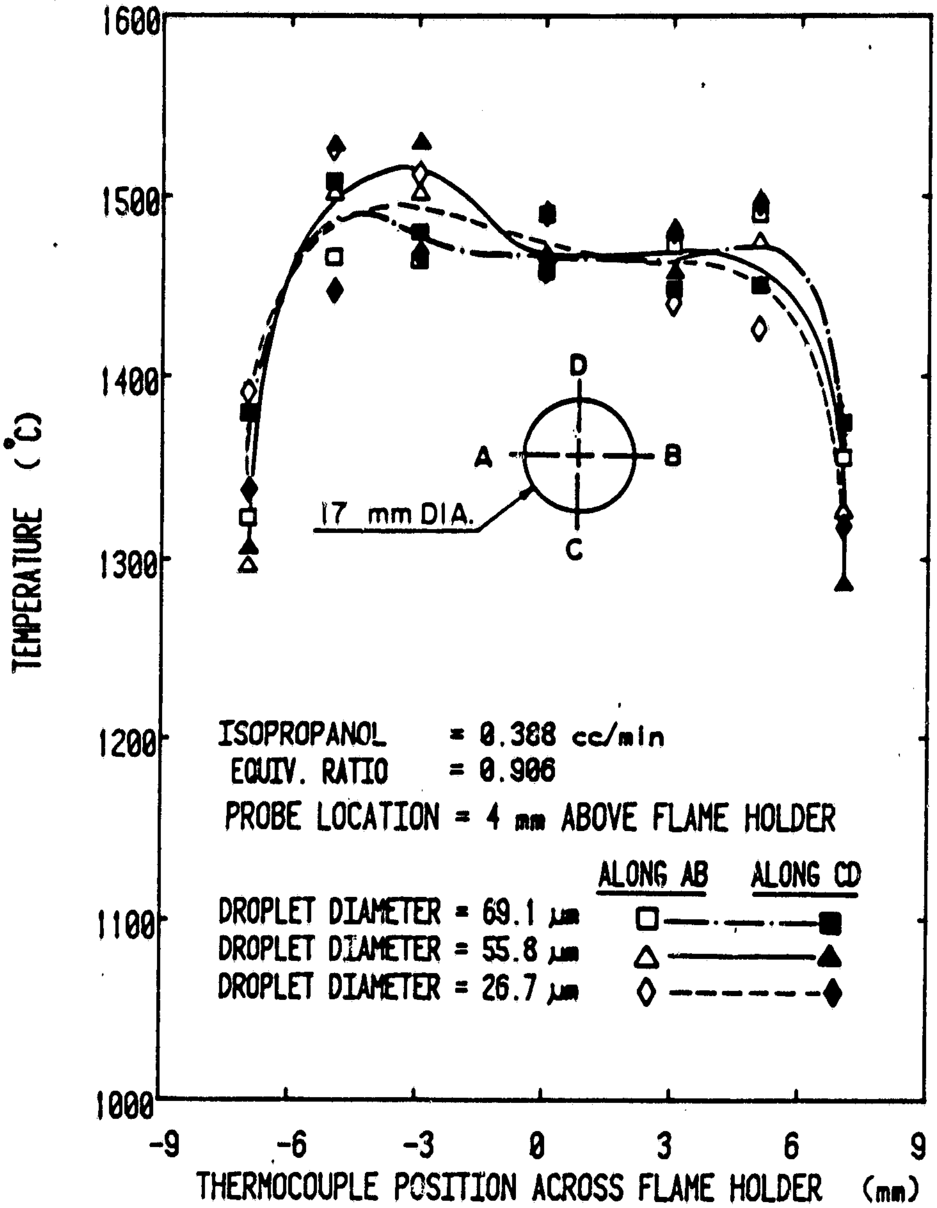

Figure 4.3. Temperature traverses across the burner.

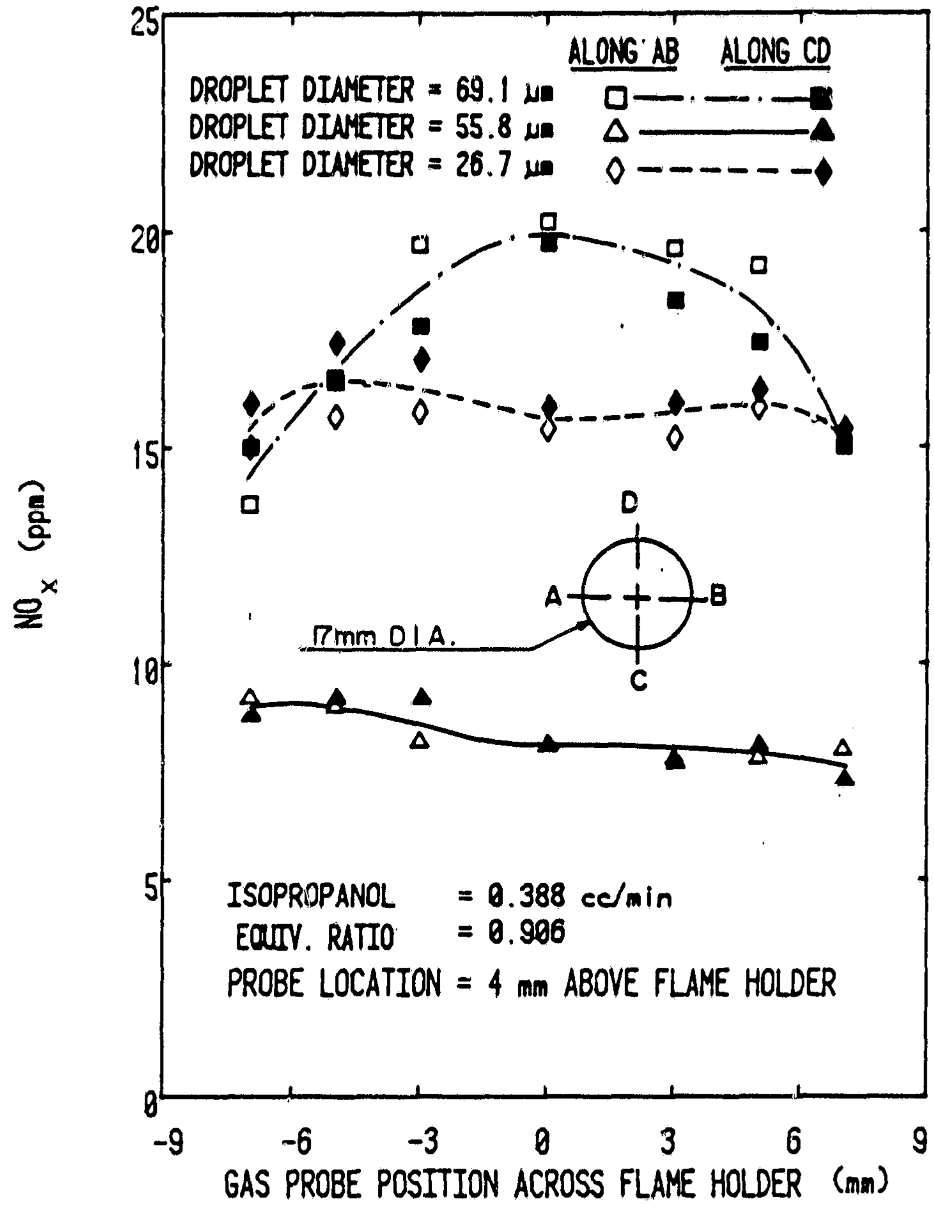

Figure 4.4. NO_X traverses across the burner.

4.3 Fuel Type and Stoichiometry

Post flame temperature, NO, and NO_x were measured in the 36 to 70 μm droplet size range. Several hydrocarbon fuels were used including isopropanol, methanol, n-heptane, and n-octane. All fuels, except for n-octane were HPLC grade and had a purity of greater than 99 percent (n-octane had a purity of 95%). A fixed sampling location on the burner centerline at 5 cm above the screen flame holder was selected to avoid regions of high temperature and concentration gradients found in axial probing. These results are shown in Figures 4.5-4.8. Where available, prevaporized/premixed limit results are also shown as data points at zero droplet diameter. For these premixed experiments, liquid fuel was vaporized in an evaporator and the fuel vapor was mixed with the dispersion air before entering the combustion facility. In all cases, a general trend was observed in which both NO and NO_x decreased with reducing droplet diameter, reaching minima around 43-58 μm, and then increasing to fairly constant levels with any further decrease in the droplet diameter. The equivalence ratio and fuel type appeared to only affect the absolute levels of NO_x measured, without appreciably affecting the observed droplet behavior. However, NO_x reductions were larger for rich mixtures with increased number densities and droplet interactions. For these tests at an air temperature of 24°C, the NO_x minima occurred at 43, 49, 54, and 58 μm initial droplet diameters for n-octane, n-heptane, isopropanol, and methanol, respectively.

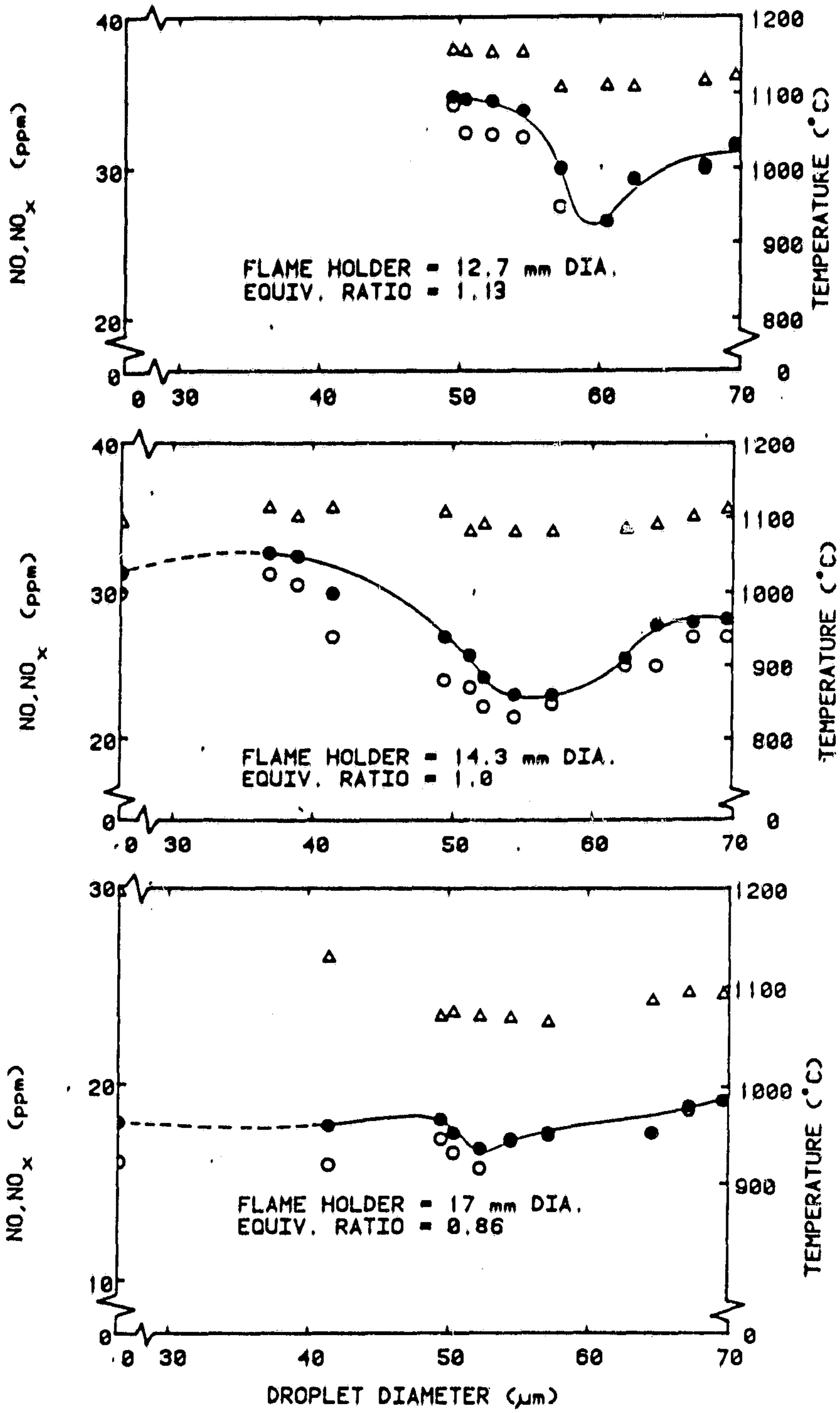

Figure 4.5. Droplet size effect on post flame temperature, NO and NO_x, for isopropanol at various equivalence ratios. o – NO; • – NO_x; Δ – Temperature.

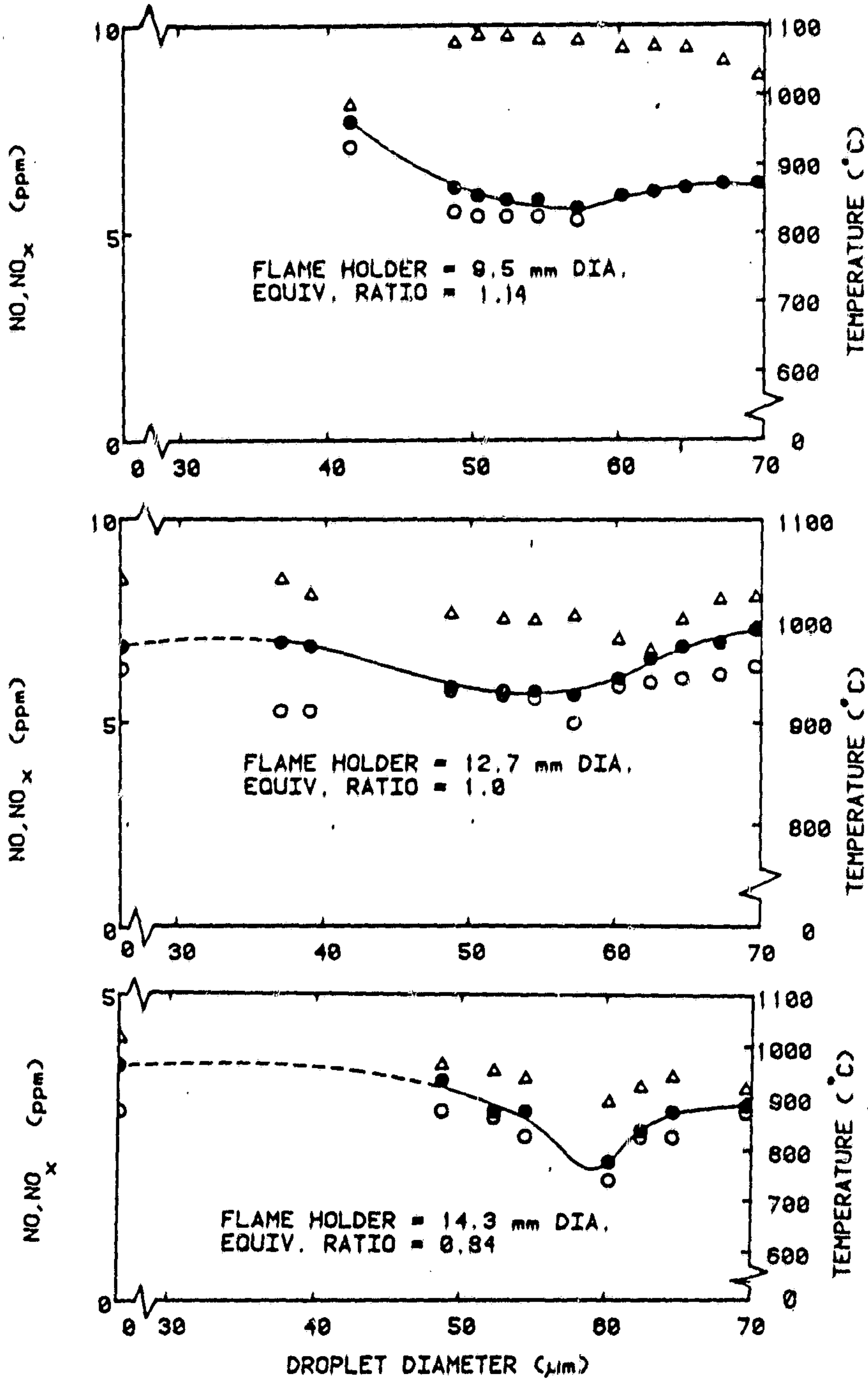

Figure 4.6. Droplet size effect on post flame temperature, NO and NO_x, for methanol at various equivalence ratios. o – NO; • – NO_x; Δ – Temperature.

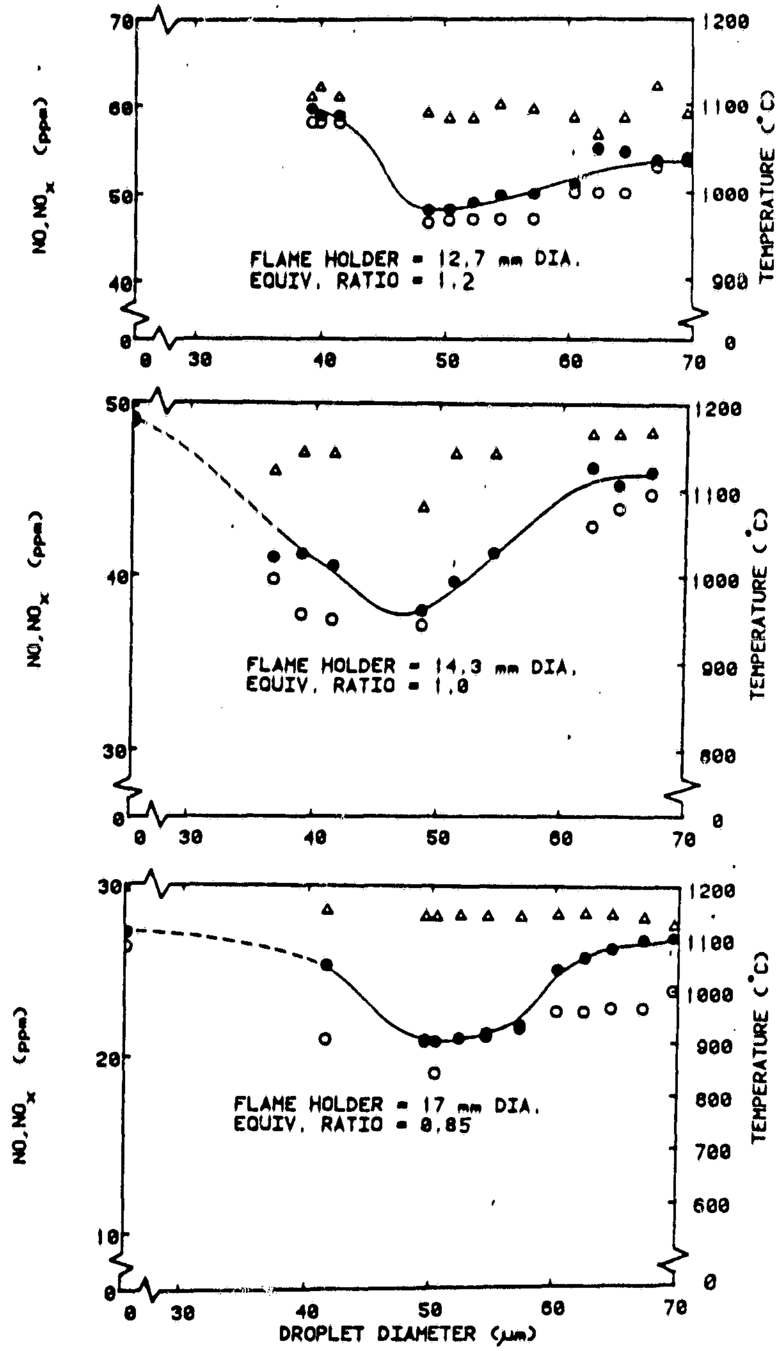

Figure 4.7. Droplet size effect on post flame temperature, NO and NO_x, for n-heptane at various equivalence ratios. o – NO; • – NO_x; Δ – Temperature.

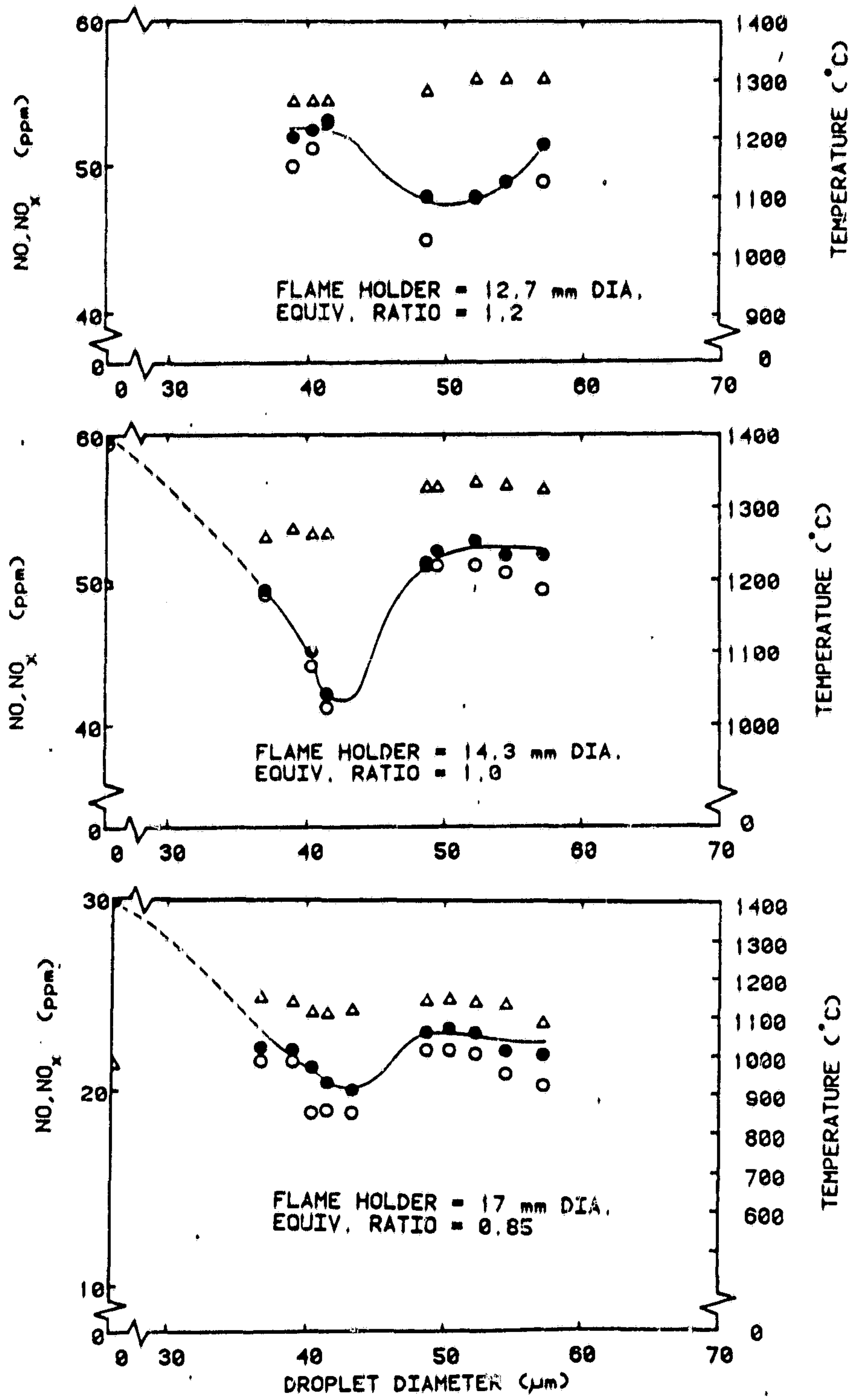

Figure 4.8. Droplet size effect on post flame temperature, NO and NO_x, for n-octane at various equivalence ratios. o – NO; • – NO_x; Δ – Temperature.

Similar trends in the experimental data were also found by Nizami et al. (1978-82) who hypothesized the following mechanism to explain the observed behavior. Decreasing the droplet diameter at a constant fuel feed rate increases the droplet number density and, hence, droplet interactions, leading to depletion of the local oxygen concentration around the burning droplets and a suppression of the local flame temperature and NO_x formation. This analysis is also consistent with the results of Nuruzzaman et al. (1971), Kesten (1972), and Bracco (1973). Continued reduction in droplet size further increases number density, but enhanced vaporization brings about increased droplet spacings, mitigates droplet interactions, increases burning rates and flame temperature, and eventually reverses the decreasing NO_x trend as the situation approaches the premixed case.

The variations in NO_x minima appear to be governed by the differences in the physical properties of the individual fuels. Larger initial droplet diameters are needed for high volatility fuels, such as methanol, to overcome rapid prevaporization and to give some level of droplet interactions in the flame. By the same argument, lower volatility fuels like n-octane, can achieve the optimum conditions at smaller droplet diameters.

In the next two sections, additional experimental results on the effect of extent of prevaporization and droplet interactions are presented. These phenomena have been incorporated into an analytical model that is described in Chapter 5.

4.4 Air Preheating and Prevaporization

In the previous section the shifts in the NO_x minimum points for the test fuels were found to be consistent with the differences in their evaporation and combustion characteristics. In this section, the importance of enhanced prevaporization in addition to droplet size effects on NO_x formation were investigated by air preheating experiments.

Air preheating was accomplished by wrapping heating tapes around the upper and lower housing assemblies (Figure 3.1) and controlling the temperature by a variac. For a constant setting, there were only small variations in temperature (less than one degree centigrade) throughout the combustor. The water flow rate in the cooling jacket was also adjusted to keep the exit water temperature from the jacket equal to that of the preheated air. For this study, measurements were made at a height of 10 cm above the screen flame holder (the adjustment in sampling location was made to reduce potential catalytic $NO_2 \rightarrow NO$ conversion reactions in the uncooled sampling probe).

The effect of air preheating and initial droplet diameter on temperature, NO, and NO_x for the various fuels are shown in Figures 4.9–4.12. Air preheating results in enhanced vaporization of droplets, shifting the minimum NO_x point towards larger initial droplet sizes and mitigating the reduction in NO_x levels at the NO_x minimum point. These effects are believed to result from a balancing of two phenomena: (1) a requirement for larger initial droplet sizes to maintain some optimum extent of prevaporization, since air preheating increases prevaporization and local fuel

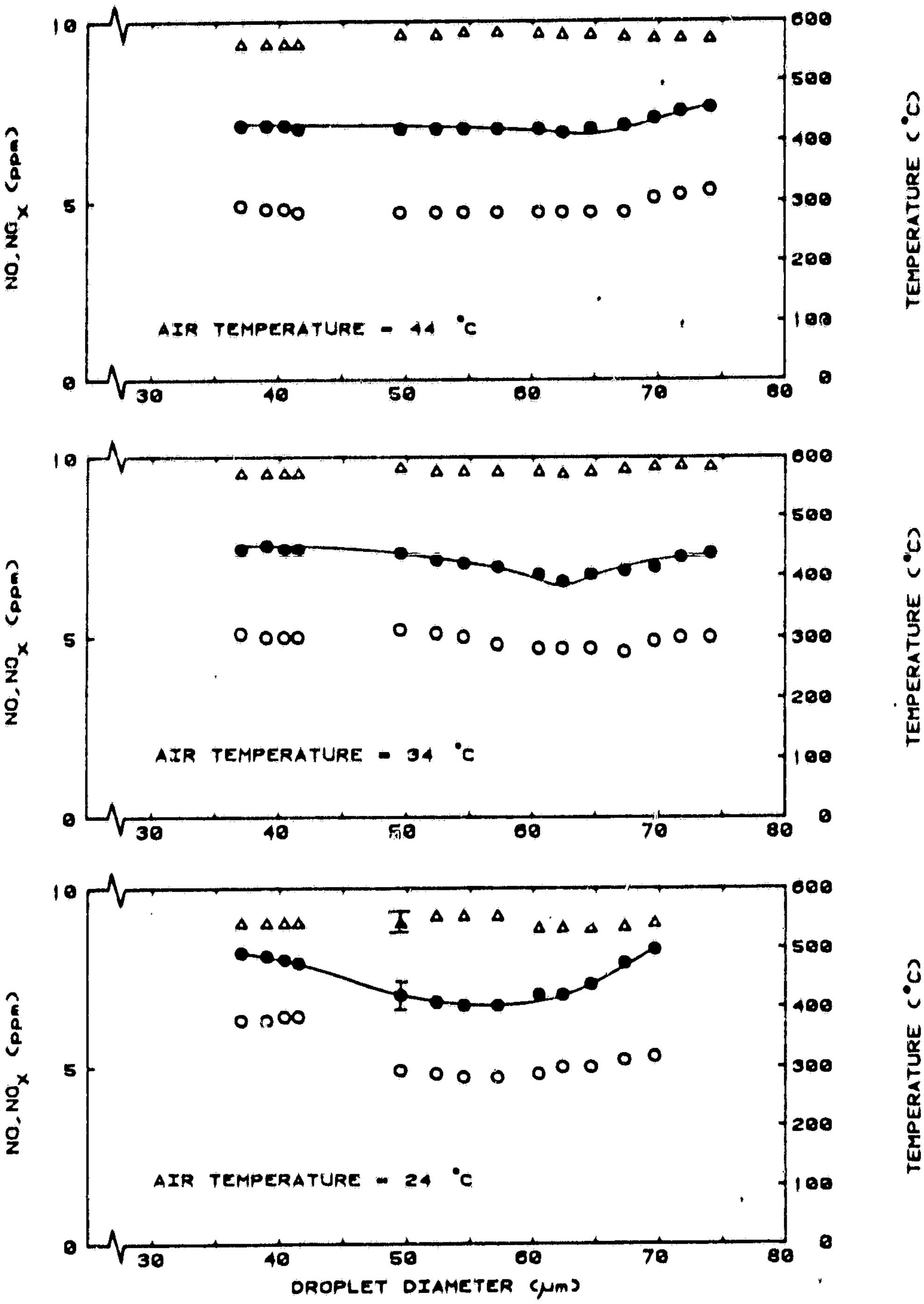

Figure 4.9. Air preheating and droplet size effects on post flame temperature, NO and NO_X, for methanol at $\phi = 1.0$. o – NO; ● – NO_X; Δ – Temperature.

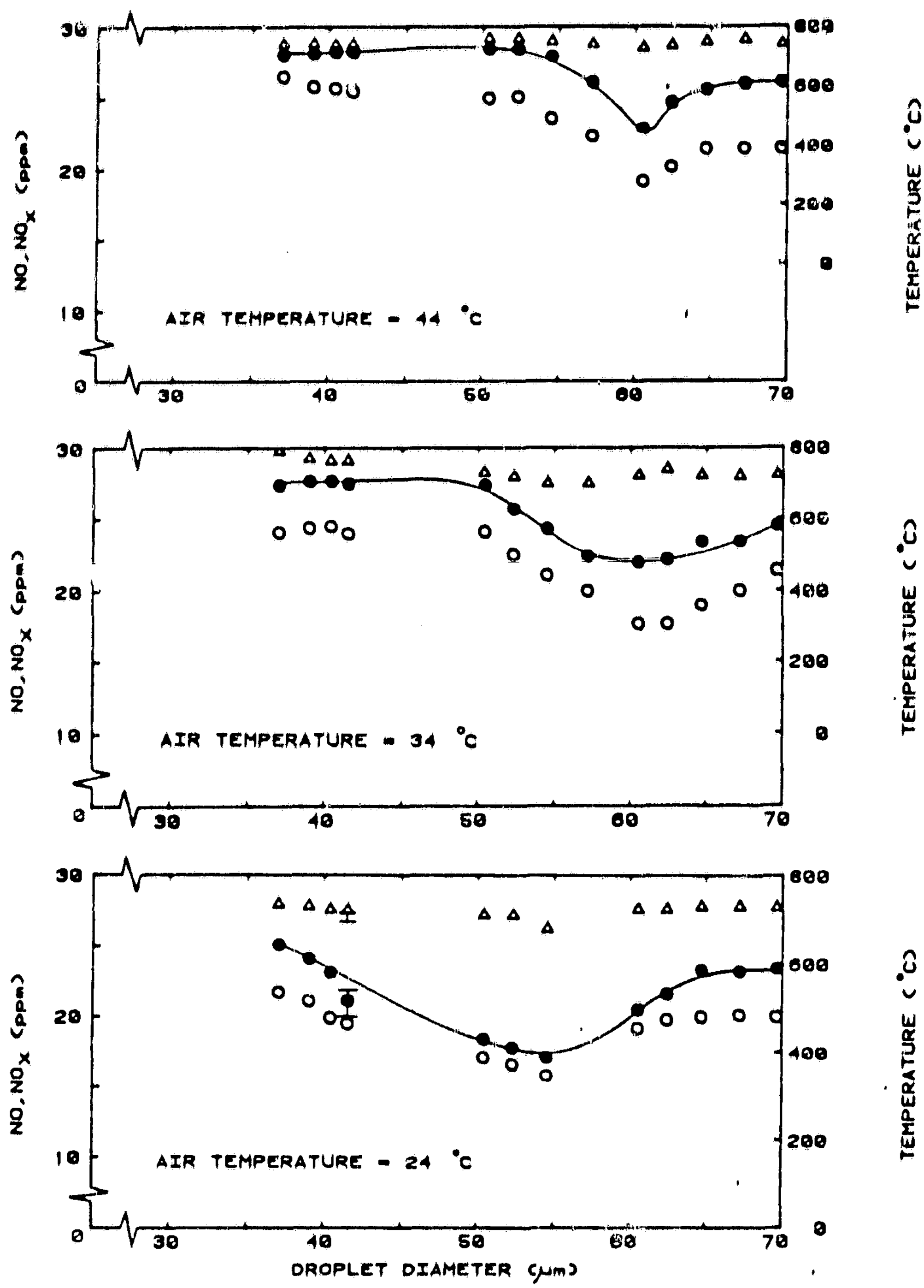

Figure 4.10. Air preheating and droplet size effects on post flame temperature, NO and NO_X, for isopropanol at $\phi = 1.0$. o – NO; • – NO_X; Δ – Temperature.

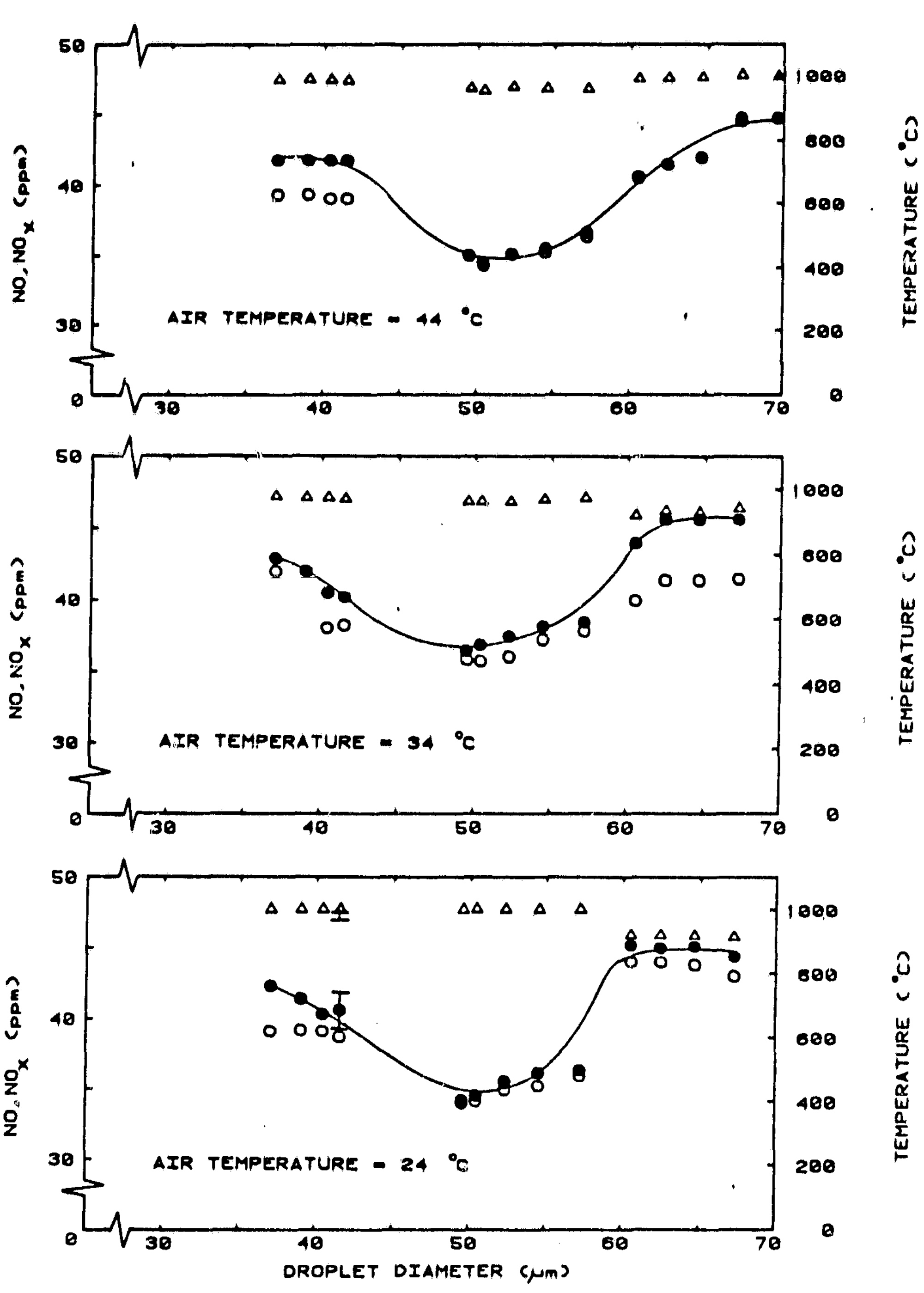

Figure 4.11. Air preheating and droplet size effects on post flame temperature, NO and NO_x, for n-heptane at $\phi = 1.0$. o – NO; • – NO_x; Δ – Temperature.

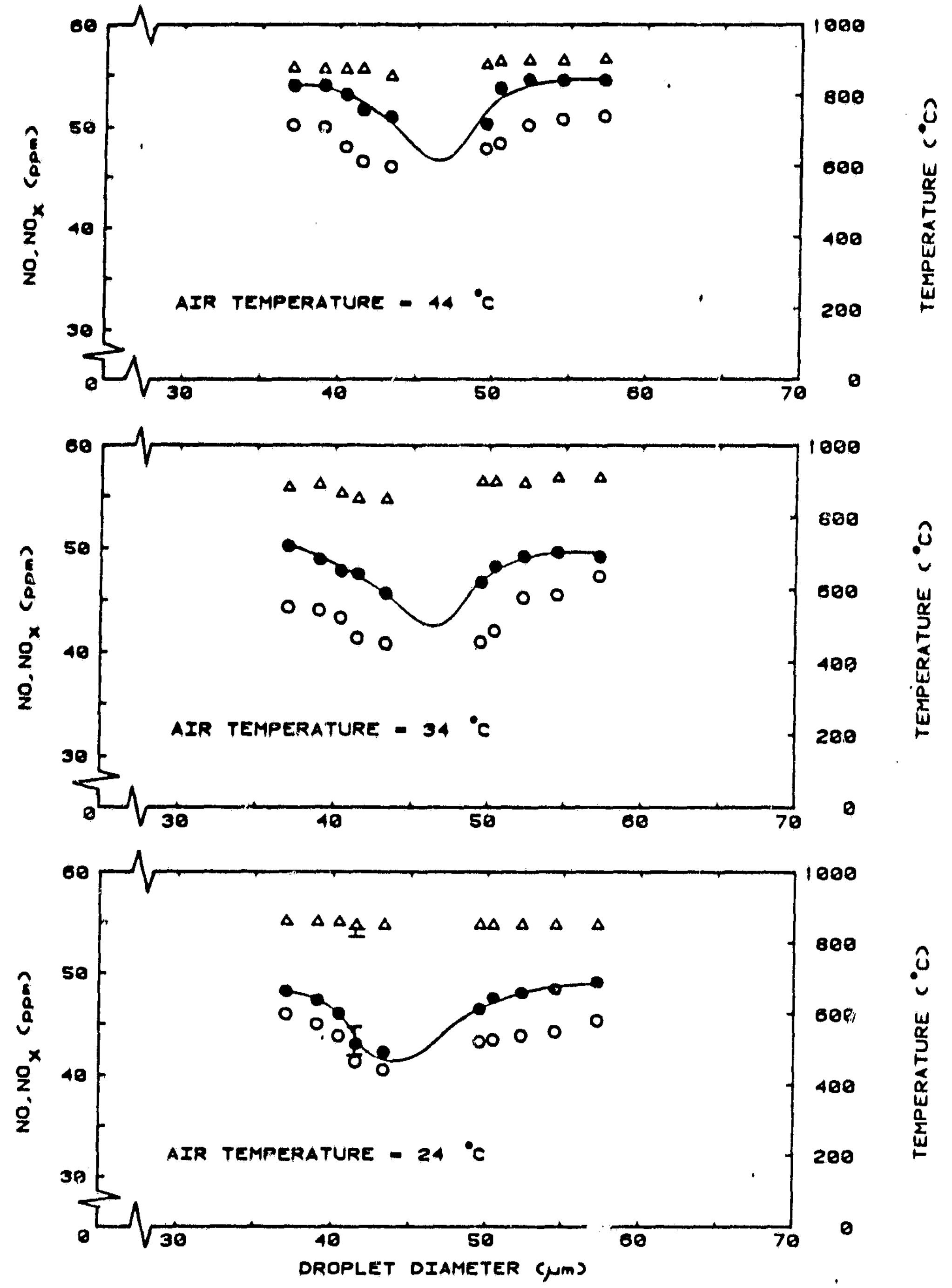

Figure 4.12. Air preheating and droplet size effects on post flame temperature, NO and NO_x, for n-octane at $\phi = 1.0$. o – NO; • – NO_x; Δ – Temperature.

vapor concentrations as well as droplet spacings; and (2) fewer droplets and reduced droplet interactions as the size is increased. This tradeoff is particularly pronounced in the case of methanol (Figure 4.9), where the NO_x reduction phenomena almost disappears with preheating.

In order to adequately interpret these results, it is important to realize that the effectiveness of air preheating on fuel vaporization relies upon the droplet travel time as well as the specific fuel properties. At a constant equivalence ratio and fuel feed rate, the air flow requirement increases with increasing fuel molecular weight, which consequently reduces the droplet travel time. For instance, NO_x minima for methanol, having the highest volatility and droplet travel time among the test fuels, quickly moved towards larger initial droplet diameters and the NO_x levels began to reach a constant value at elevated air temperatures. These effects were somewhat retarded for isopropanol due to its lower volatility and shorter droplet residence time.

For n-heptane, there is a relatively shorter droplet residence time. Thus, preheat temperature increases primarily affected the small droplet sizes and their associated NO_x values, with some smoothing in the large droplet region. N-octane, with the lowest volatility and shortest droplet travel time, seemed relatively unaffected by the increases in temperature. Air preheating temperatures above 44 °C are required to cause a significant shift in NO_x minima for n-octane. These factors are discussed in more detail as part of the analytical studies in Chapter 5.

4.5 Synthetic Oxidizers

Results of the parametric fuel studies and air preheating experiments indicated the importance of parameters such as fuel properties and temperature on droplet diameter and interactions. In spray combustion, changes in flame temperature affect the droplet lifetime, interactions with neighboring droplets, and the formation of NO_x. These effects were studied by a series of experiments in which air was partly replaced by a mixture of oxygen and argon, keeping all other operating conditions the same.

Air, oxygen, and argon were individually metered, then mixed in a cross, and later divided into the usual dispersion/dilution proportions before entering the combustion facility. In all cases the volumetric ratio of oxygen to the inert gas (nitrogen plus argon) was kept at 21/79.

The experimental results shown in Figure 4.13 demonstrate the effect of droplet size and fraction of synthetic oxidizer on NO, NO_x, and temperature at a sampling height of 10 cm above the flame holder. Since argon is a monatomic gas with a lower heat capacity than nitrogen, its substitution for nitrogen increases the flame temperature and flame speed. For this reason, different size flame holders had to be used (as indicated on the Figure) to stabilize the flame.

Compared to air, the NO_x minimum point moves towards larger initial droplet diameters as the fraction of the synthetic oxidizer increases in the gas phase. Lesser NO_x reductions and higher NO_x levels (relative to air) can also be observed from the

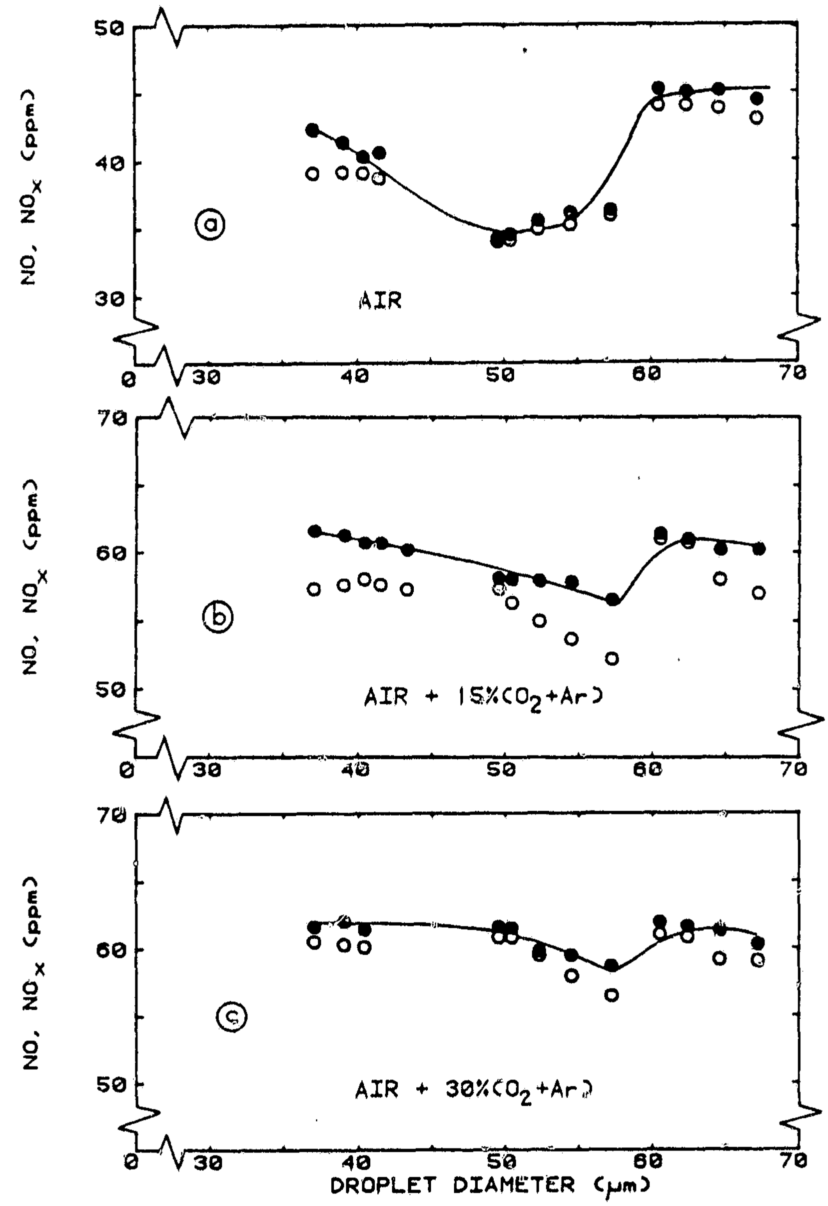

Figure 4.13. Synthetic oxidizer and droplet size effects on post flame NO, NO_x and temperature for n-heptane at $\phi = 1.0$. Flame holder I.D. (mm): a – 14.3; b and c –12.7.

data.

All of the above observations are due to changes in flame temperature. An increase in temperature reduces the droplet lifetime and diminishes the droplet interactions in flame. As a consequence, the minimum NO_x point occurs with larger droplets which burn for a longer time. However, shifts towards larger droplet diameters are accompanied by a lower droplet number density and reduced interactions. Therefore, at very high temperatures, the effect of droplet interactions on NO_x production is minimal.

4.6 Fuel-Nitrogen Additives

A series of experiments with simulated synthetic fuels were conducted in order to investigate the effect of droplet size on the conversion of fuel-nitrogen to NO_x. In general, synthetic fuels contain traces of nitrogen-containing organic compounds including pyridines, nitriles, quinolines, pyrroles, indoles and carbazoles (Chan et al., 1984). These compounds undergo thermal decomposition in the reaction zone, producing radicals such as HCN, N, CN, and NH which can either oxidize to NO_x or recombine to form molecular nitrogen.

N-heptane was doped with pyridine (C_5H_5N) and pyrrole (C_4H_4NH) to give a 0.1-1.0 % nitrogen content by weight in the fuel (typically found in synthetic fuels from shale oil).

The experimental data collected at a sampling position of 10 cm above the burner (Figures 4.14 and 4.15), indicate that the optimum droplet diameter for minimizing NO_x (which was observed

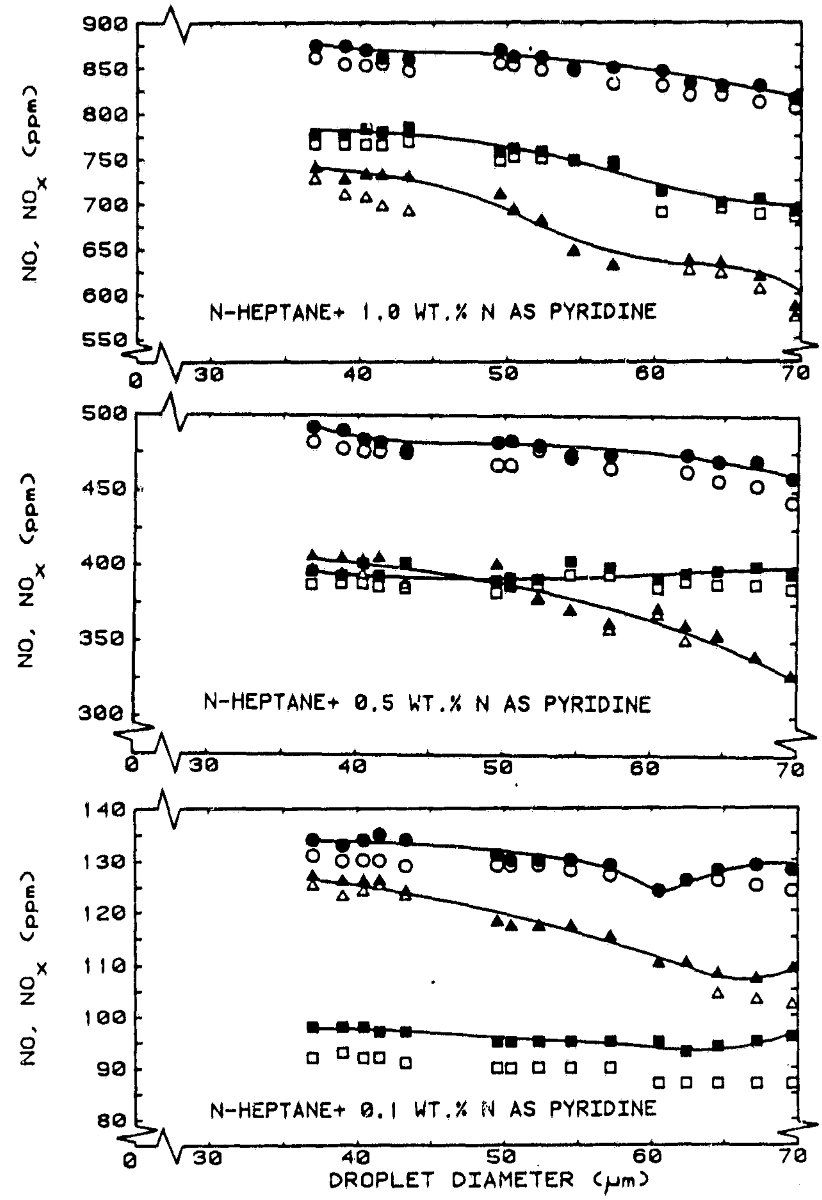

Figure 4.14. Effect of fuel-N content and droplet size on NO and NO_x for n-heptane doped with pyridine.
□-ϕ= 0.85; o -ϕ= 1.0; △-ϕ= 1.2.

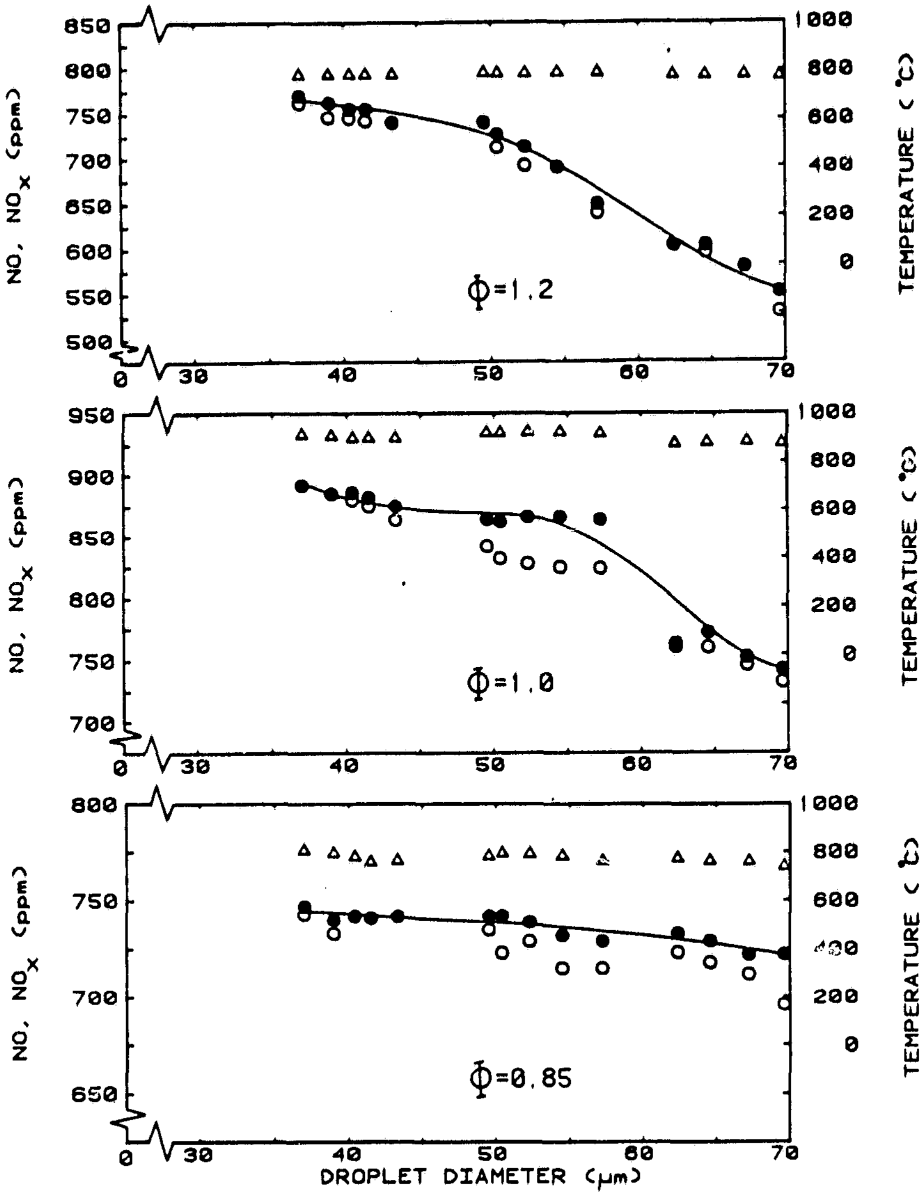

Figure 4.15. Effect of droplet size on NO, NO_x and temperature for n-heptane doped with pyrrole (1%N by weight). o - NO; • - NO_x; Δ - Temperature.

previously with pure n-heptane) disappears with increases in the fuel-N concentration. Also, it was noticed that more fuel-N is converted to NO_x at small droplet diameters.

Appleton and Heywood (1973) suggested that the degree of air/fuel mixing and the availability of oxygen atoms control the oxidation of the nitrogenous species. In their investigation, maximum conversion efficiencies were found for fuel-lean and well atomized cases. The present results show that under stoichiometric and rich conditions, reducing the droplet size improves the oxidation of the pyrolysis fragments of the additives to NO_x by better oxygen penetration through the droplet flame zones. The abundance of oxygen for lean mixtures made this process less dependent on the size of droplets as shown in Figures 4.14 and 4.15. Changing the dopant from pyridine to pyrrole with a different molecular structure did not change the results. The fact that the type of nitrogen-bearing additive does not change the NO_x yield has also been addressed in a number of other studies (Fenimore, 1976a; Foster and Keck, 1980; Sapre and Quader, 1983).

It should be pointed out that the presented results include the thermal NO_x contribution. However, for fuel-N, the dependence of nitric oxide yield on flame temperature is not as strong as it is for the oxidation of molecular nitrogen (De Soete, 1974; Fenimore, 1976a). Therefore, temperature changes resulting from droplet interactions become unimportant as the concentration of the nitrogen-containing compounds in the fuel increases.

The conversion efficiency of the fuel nitrogen to NO_x (determined from a nitrogen balance and subtracting the thermal NO_x

contribution) for the 37 μm droplets are given in Table 4.1. The fraction of fuel-N that was not recovered as NO_x presumably appeared mostly as N_2 in the products. Foster and Keck (1980) measured high HCN concentrations in fuel-rich turbulent diffusion flames as far as five burner diameters downstream of the fuel nozzle, constituting a large portion of the nitrogenous species ($HCN+NO+NH_3$).

In the following section, inflame and post flame measurements of NO, NO_x, and temperature are presented.

4.7 NO_x Structure in Flame

4.7.1 Pure (Nitrogen Free) Fuels

Axial temperature, NO and NO_x concentrations were measured for various fuels and droplet sizes by traversing the gas sampling/ thermocouple probe along the burner centerline inside a 27 cm long Pyrex tube. Figure 4.16–4.19 represent the measurements for stoichiometric combustion of methanol, isopropanol, n-heptane, and n-octane aerosols, respectively. In general, temperature, NO and NO_x concentrations increase rapidly in the flame zone, with NO and NO_x reaching their maximum values slightly above the temperature peak and then decreasing gradually to relatively constant levels.

The effect of sampling probe on the measured NO and NO_x values was also studied using the water cooled probe. The probe was cooled to 50°C during all measurements. Figures 4.20–4.22 show the concentration profiles of NO and NO_x sampled by both cooled and uncooled probes. The results indicate minor differences between the NO_x values for each condition while a higher NO_2 yield

Table 4.1. Conversion efficiency* of fuel-N to NO_x from the combustion of 37 μm n-heptane droplets doped with pyridine.

% N By Weight of Fuel	ϕ=0.85	ϕ=1.0	ϕ=1.2
0.1	73 (70)	74 (69)	69 (55)
0.5	70 (67)	80 (70)	59 (48)
1.0	70 (67)	76 (66)	59 (48)

* Calculations are based on the maximum NO_x concentration measured along the burner centerline. Values inside the parentheses are calculated based on the steady state NO_x concentration at 10 cm above the burner.

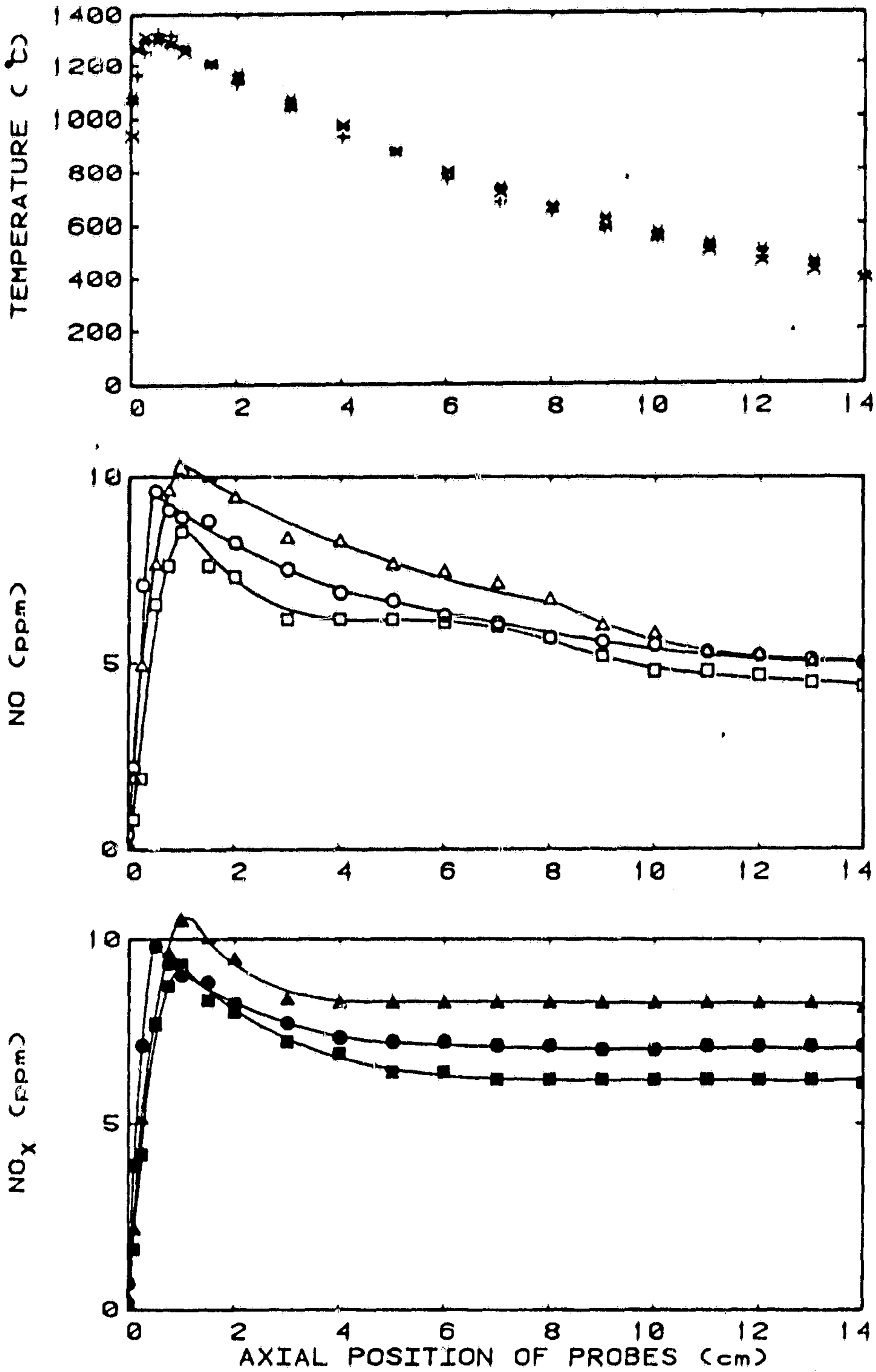

Figure 4.16. Centerline NO, NO_x and temperature profiles for combustion of methanol at $\phi = 1.0$. o , •,* - D = 37.0 µm; □,■,x - D = 57.2 µm; △,▲,+ - D = 69.6 µm.

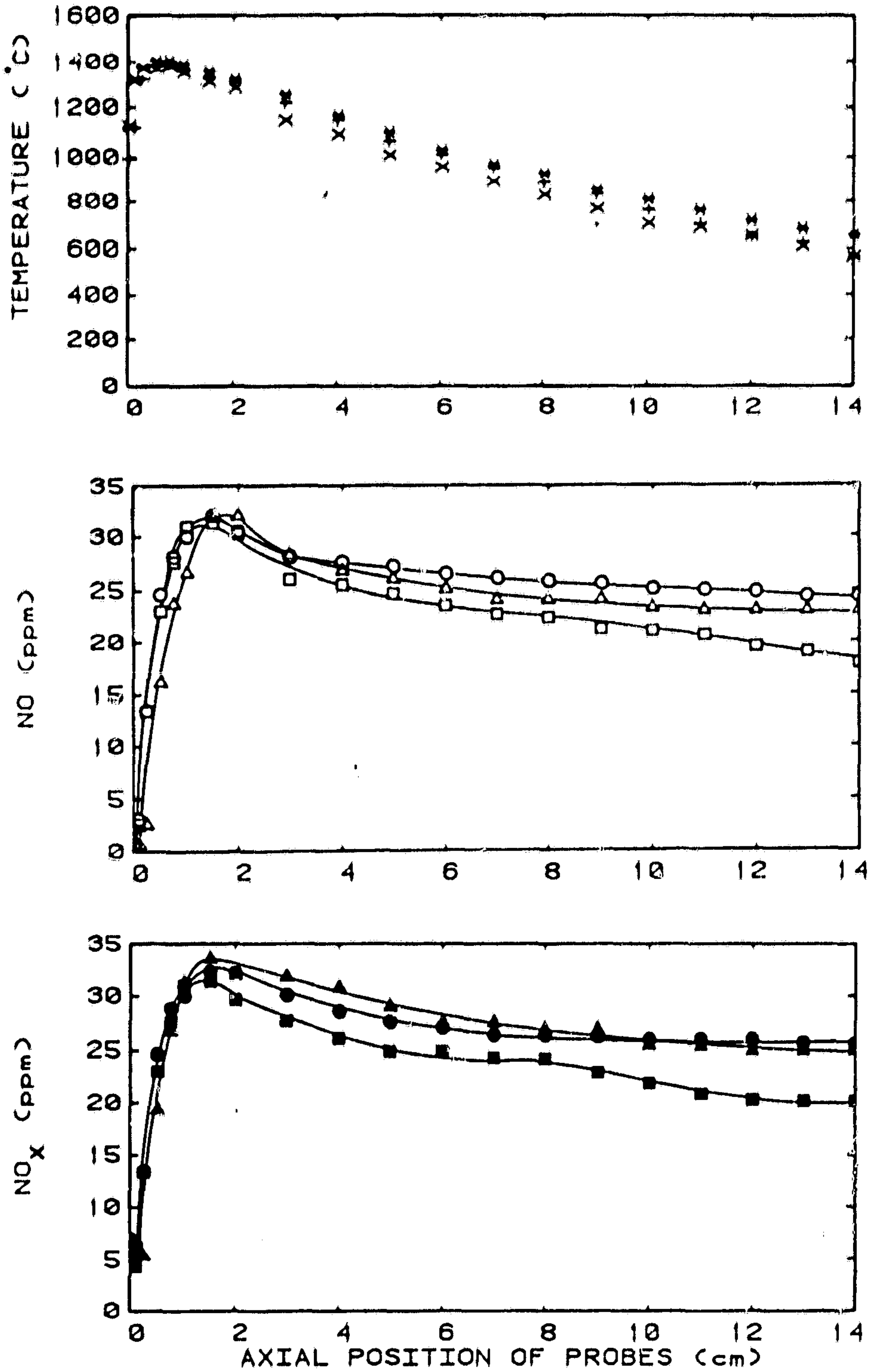

Figure 4.17. Centerline NO, NO_x and temperature profiles for combustion of isopropanol at $\phi = 1.0$. o , ●,* - D = 37.0 μm; □,■,x - D = 54.5 μm; △,▲,+ - D = 69.6 μm.

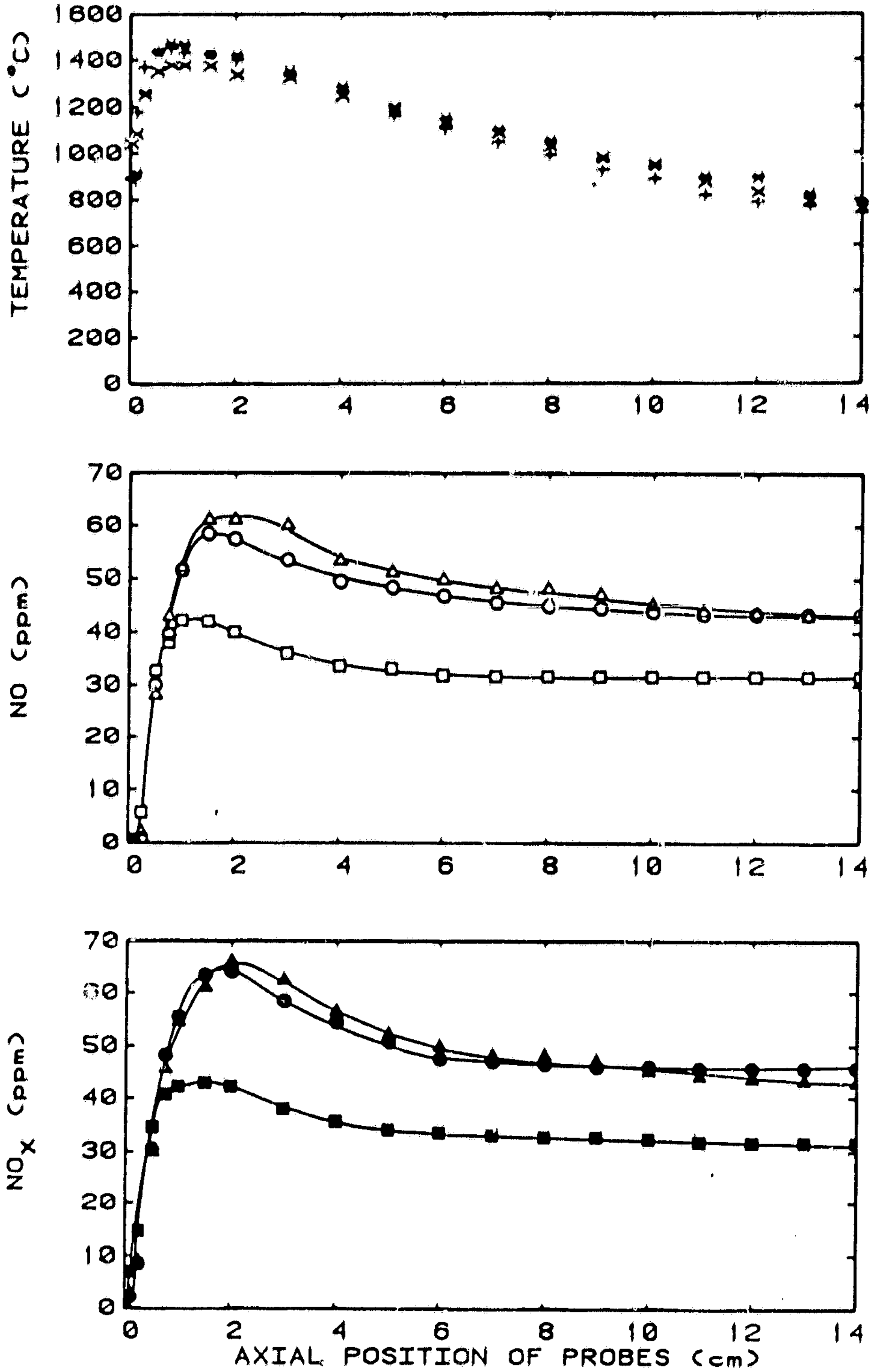

Figure 4.18. Centerline NO, NO_X and temperature profiles for combustion of n-heptane at $\phi = 1.0$. o , •,* - D = 37.0 µm; □,■,x - D = 49.5 µm; △,▲,+ - D = 67.2 µm.

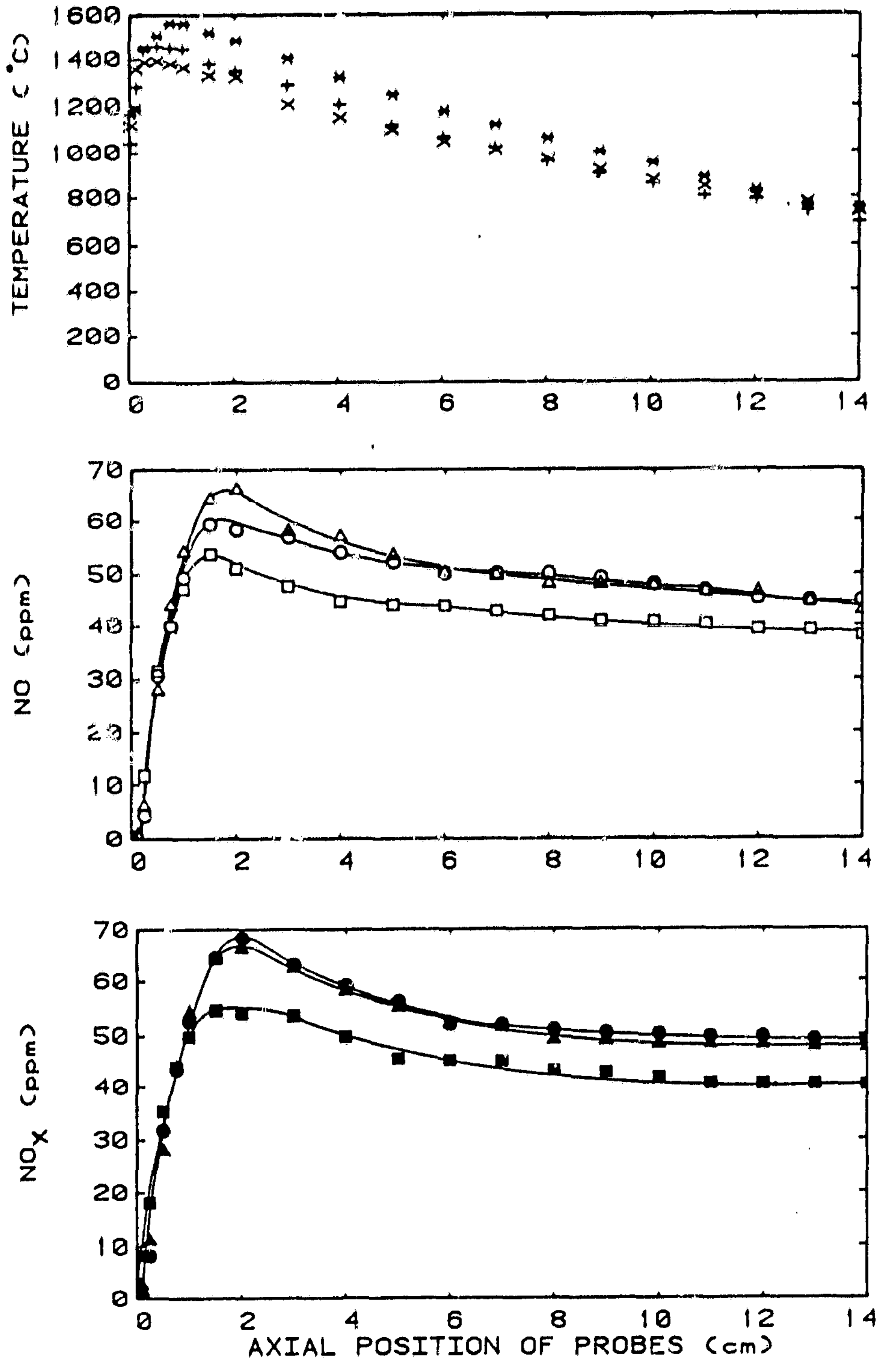

Figure 4.19. Centerline NO, NO_X and temperature profiles for combustion of n-octane at $\phi = 1.0$. o , ●,* - D = 37.0 μm; □,■,x - D = 43.3 μm; △,▲,+ - D = 57.2 μm.

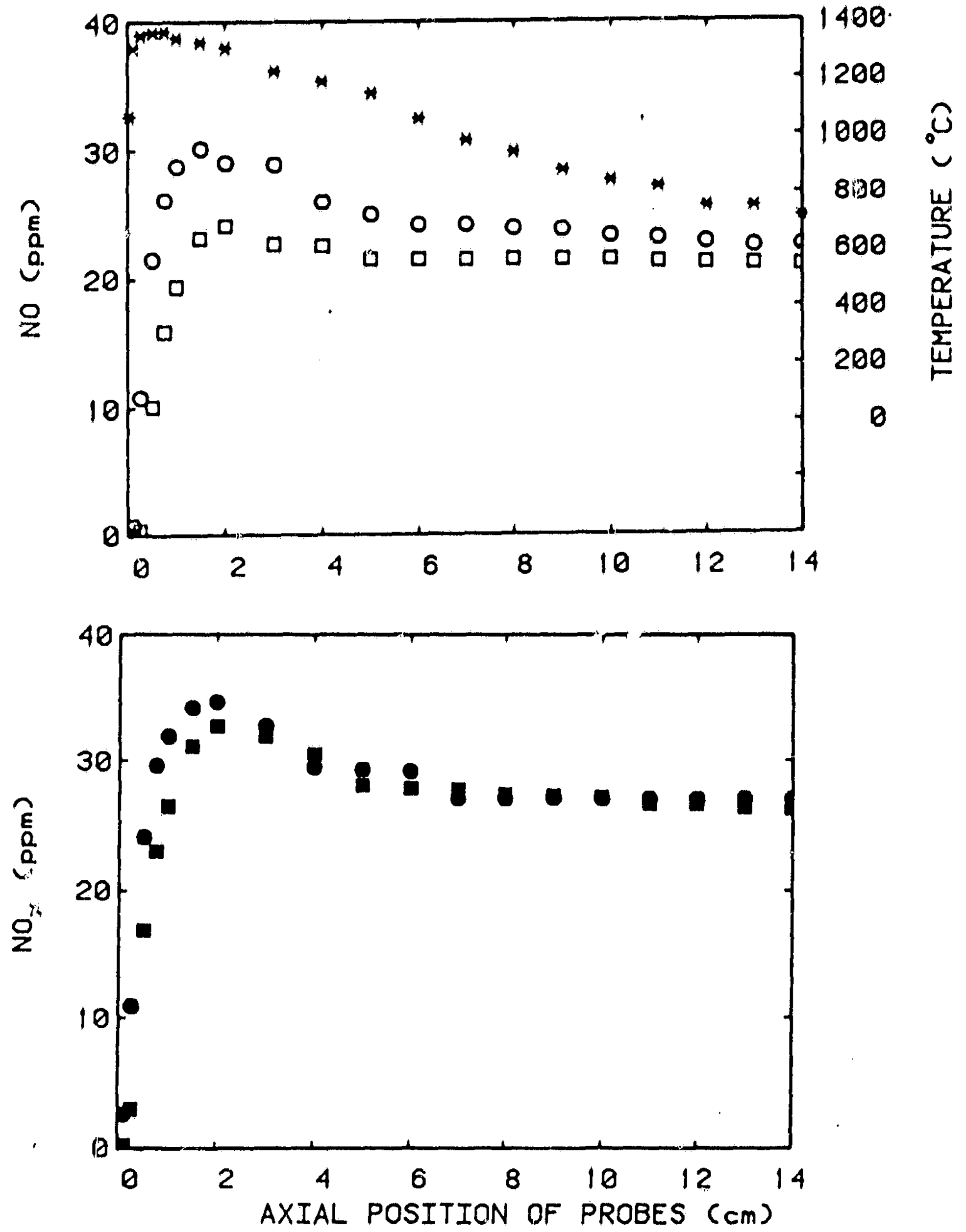

Figure 4.20. Sampling probe effects on centerline measurements of NO and NO_x for 37 μm n-octane droplets at $\phi = 0.85$. o , • - uncooled probe; □, ■ - water cooled probe.

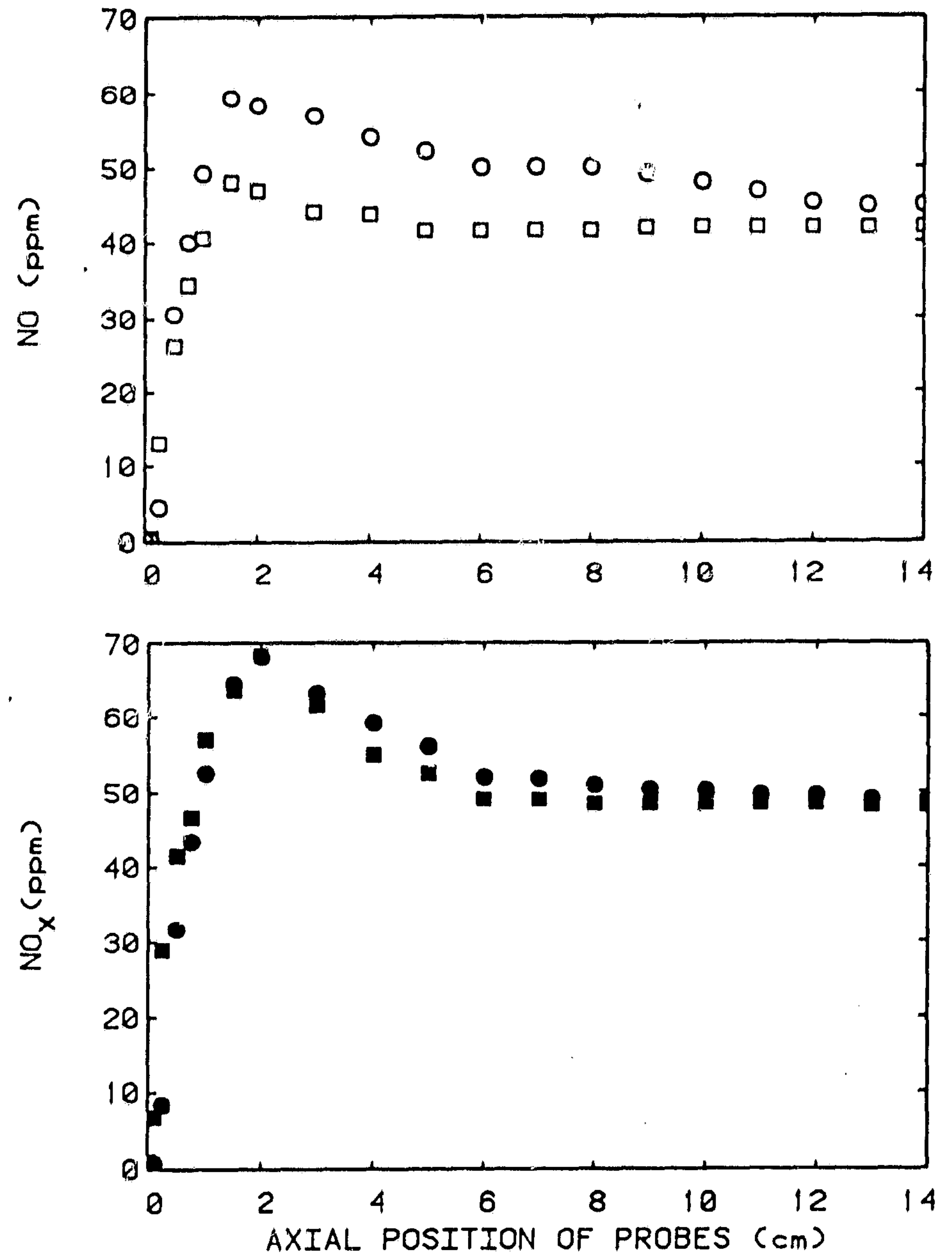

Figure 4.21. Sampling probe effects on centerline measurements of NO and NO_x for 37 μm n-octane droplets at $\phi = 1.0$. o , • – uncooled probe; □, ■ – water cooled probe.

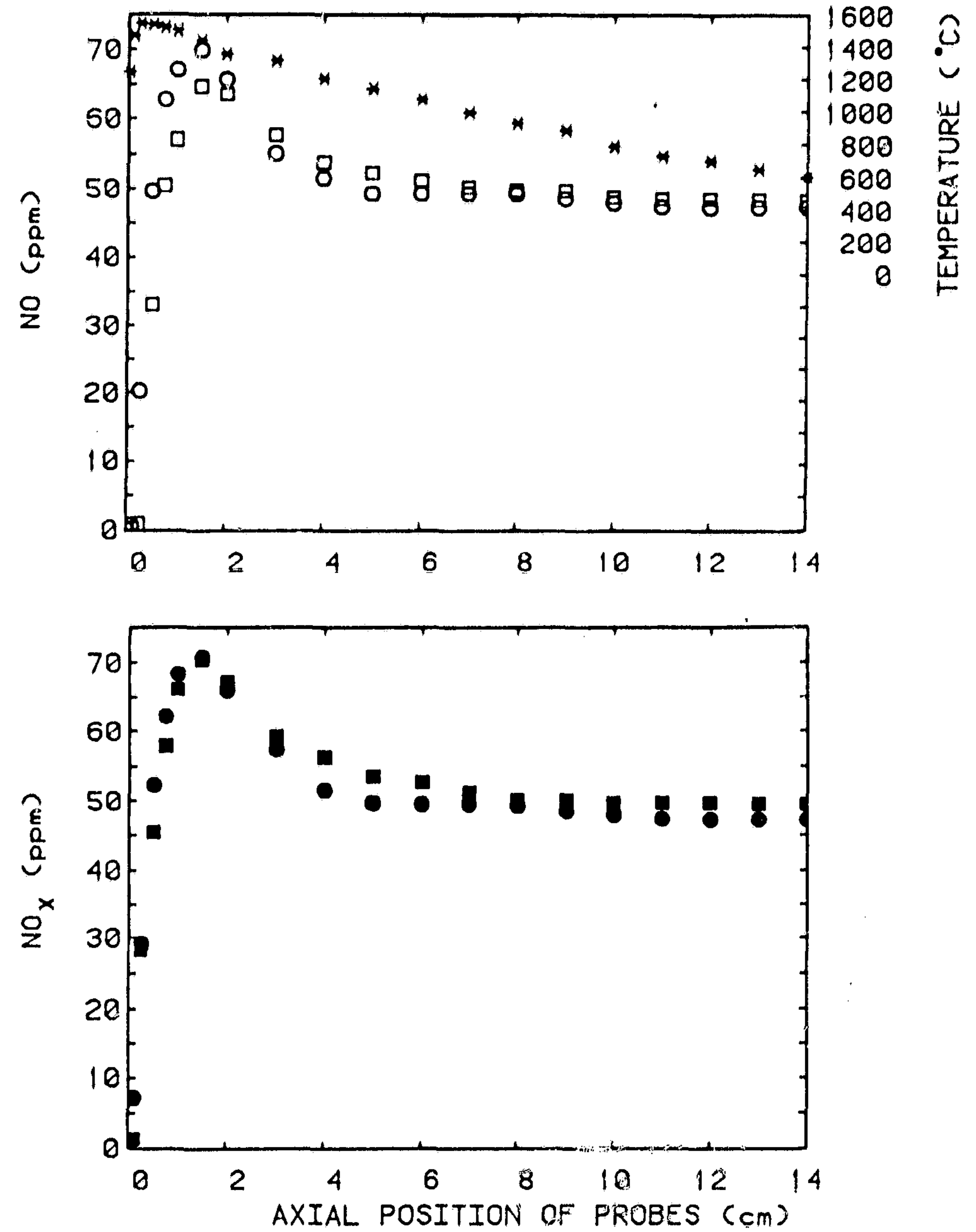

Figure 4.22. Sampling probe effects on centerline measurements of NO and NO_x for 37 μm n-octane droplets at $\phi = 1.2$. o , ● - uncooled probe; □, ■ - water cooled probe.

is observed when gases were sampled with the cooled probe. This occurs as a result of the oxidation of NO by HO_2 which is formed under rapid quenching in the sampling probe (Cernansky, 1977; Hori, 1980; Duterque et al., 1981).

In these flames, nitric oxide originates from the molecular nitrogen in air according to the Zeldovich mechanism (described elsewhere; e.g., Bowman, 1972). Some "prompt" NO formation is observed near the flame front at a few millimeters above the flame holder (considered as the main reaction zone). This is particularly noticed in fuel-rich cases where the Zeldovich mechanism cannot account for the measured NO_x levels. Several plausible reaction schemes for the prompt NO formation in rich flames involving the attack of hydrocarbon fragments on N_2 and the conversion of the products to NO have been suggested (Fenimore, 1971; Bachmaier et al., 1973; Haynes; 1977b; Hayhurst and Vince, 1983). In spray combustion, the presence of liquid droplets increases hydrocarbon cracking and thus intensifies the prompt NO production.

The consumption of NO_x in the post flame regions appears to be independent of the fuel type or stoichiometry. Equivalence ratio seemed to only affect the NO_x reduction rates. For 37 μm n-octane droplets, this accounted for a drop of 22, 27, and 31% at ϕ=0.85, 1.0, and 1.2, respectively. Duterque et al. (1981) reported similar behavior in a stirred reactor.

Changes in flame temperature were also found to affect the removal rate of NO_x in the post flame regions. Experiments with synthetic oxidizers were carried out at an equivalence ratio of

1.0 (see section 4.5 for the experimental details). Figure 4.23 compares the axial NO_x and temperature profiles obtained for 37 μm n-heptane droplet combustion with various oxidizers. The data show that raising the flame temperature increases the NO_x formation markedly, but also augments its downstream decay to constant levels.

A possible explanation for the axial NO_x reduction is the removal of NO by nitrogen atoms which are generated from the molecular nitrogen at high temperatures. Other reactions that can also contribute to the consumption of NO_x are discussed in the following section.

4.7.2 Nitrogen-Containing Fuels

Several operating conditions were selected to study the NO_x formation in spray combustion from fuel-N. Centerline NO, NO_x and temperature measurements for stoichiometric combustion of n-heptane doped with 1% nitrogen by weight as pyridine, are shown in Figure 4.24. Effect of equivalence ratio for a fixed droplet diameter of 37 μm is demonstrated in Figure 4.25. Again, in the flame zone, NO and NO_x rise quickly with temperature to their maximum values, and then fall slowly to a plateau in the post flame regions. Both NO and NO_x peak faster at higher fuel-N contents and stoichiometries, indicating a strong dependence on O_2 concentration but a weak dependence on flame temperature for fuel-N transformation. Similar results for different fuel-N concentrations are shown in Appendix B.

Surprisingly, in each case, a lower percentage of the measured

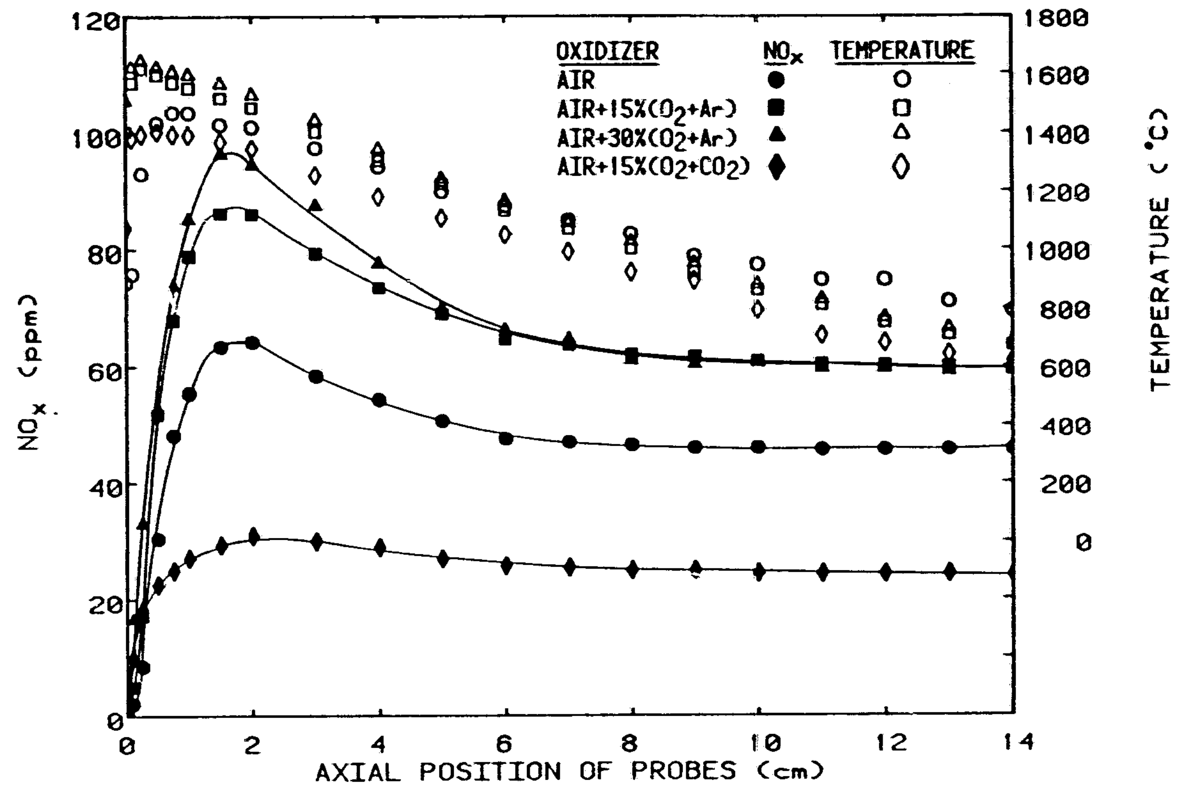

Figure 4.23. Effect of synthetic oxidizers on centerline NO, NO_x and temperature for 37 μm n-heptane droplets at $\phi = 1.0$.

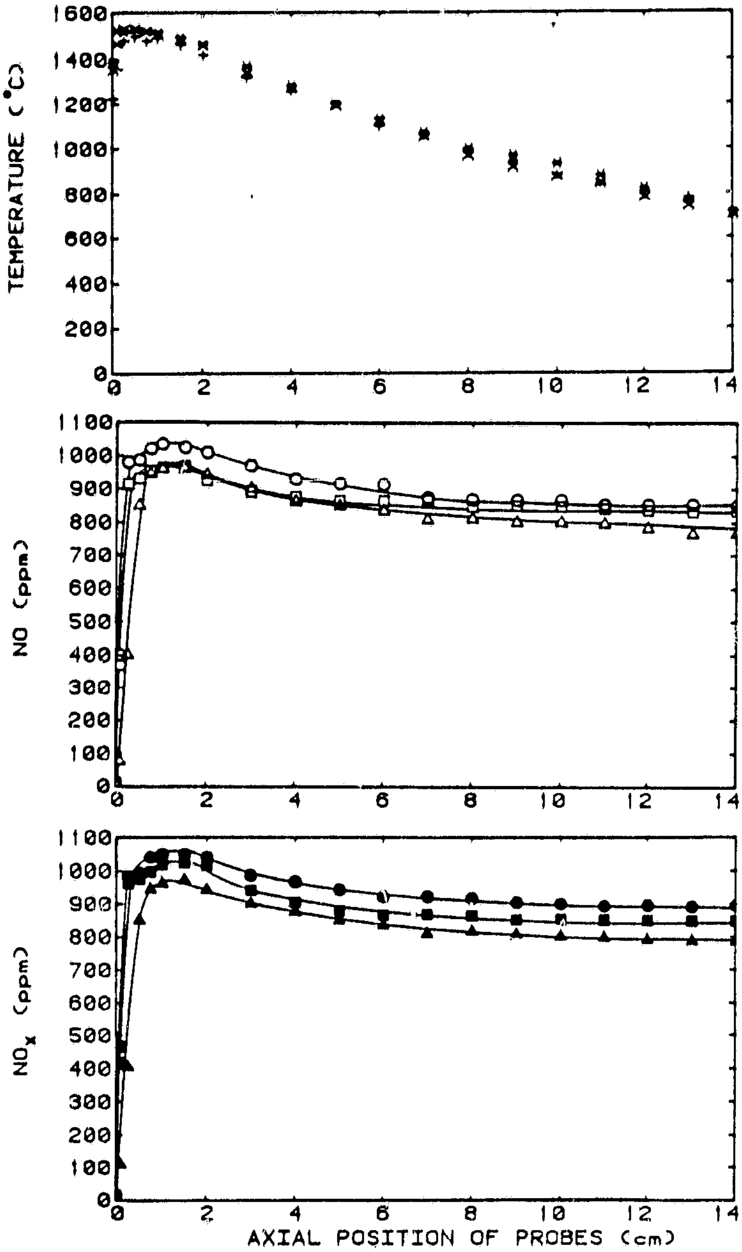

Figure 4.24. Centerline NO, NO_X and temperature profiles for n-heptane doped with pyridine (1% N by weight). o , ●,* - D = 37.0 μm; □,■,x - D = 49.5 μm; △ ,▲,+ - D = 69.6 μm.

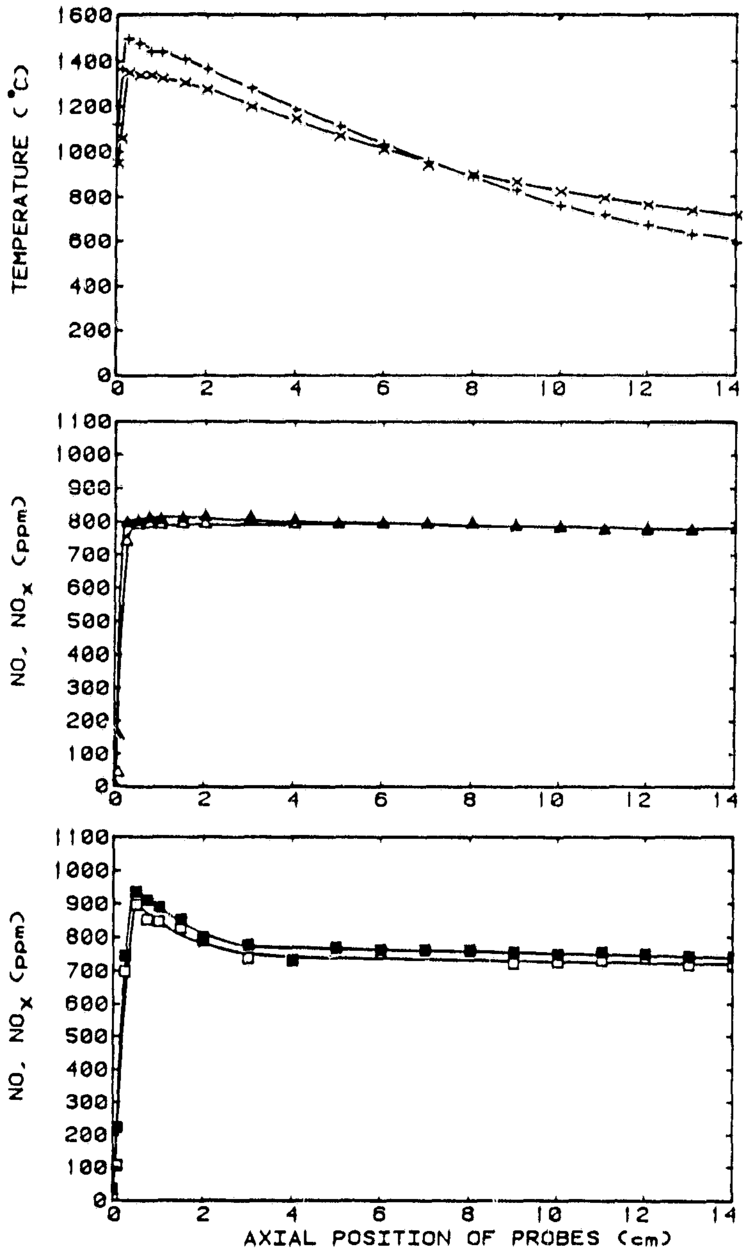

Figure 4.25. Centerline NO, NO_x and temperature profiles for 37 μm n-heptane droplets doped with pyridine (1% N by weight). □,■,x − ϕ = 0.85; △,▲,+ − ϕ = 1.2.

peak NO_x was consumed far from the burner, as compared to the results with nitrogen-free fuels. Table 4.2 summarizes the reduction percentages for the conditions studied. One may reason that the NO_x generated from the fuel-N is far greater than the thermal NO_x and therefore its removal by the flame radicals is less efficient.

At this point a closer look at some of the processes that control the NO_x formation from fuel-nitrogen may help the interpretation of the results. It is generally believed that, in fuel rich flames, the overall reaction mechanism for fuel-N conversion to NO_x occurs according to the following path (Fenimore, 1976b; Haynes 1977a; Chen and Malte, 1984):

$$\text{Fuel-N} \rightarrow HCN \rightarrow NH_i \left. \begin{array}{l} \xrightarrow{O+} NO \\ \xrightarrow{NO} N_2 \end{array} \right.$$

Among different reactions that can lead to the oxidation of the NH_i species (N, NH, NH_2, NH_3) and NO formation, the reaction:

$$N+OH \rightarrow NO+H$$

is considered to be the most important (Haynes, 1977a). The unoxidized NH_i species can react with NO as it forms to generate N_2 by any of the following reactions:

$$N+NO \rightarrow N_2+O$$

$$NH+NO \rightarrow N_2+OH$$

$$NH_2+NO \rightarrow N_2+H_2O$$

For lean mixtures, due to the abundance of O_2 and the presence of O atoms, the fuel-N transformation to NO_x is much easier. The

Table 4.2. Percent NO_x consumed in the post flame gases of 37 μm n-heptane droplets doped with pyridine.

% N By Weight of Fuel	ϕ=0.85	ϕ=1.0	ϕ=1.2
0.0	19	28	20
0.1	9	18	20
0.5	5	15	20
1.0	4	15	20

likely reactions are perhaps those suggested by Appleton and Heywood (1973), by which radicals such as NH and CN oxidize to NO according to:

$$NH+O \rightarrow NO+H$$

$$NH+O \rightarrow OH+N$$

$$N+O_2 \rightarrow NO+O$$

and,

$$CN+O \rightarrow NO+C$$

$$CN+O \rightarrow CO+N$$

$$N+O_2 \rightarrow NO+O,$$

In ammonia oxidative systems, NO can also form when nitroxyl hydride (HNO) which is a product of amine species oxidation, is stripped from its hydrogen (Dasch and Blint,1984). This can happen as a consequence of radical termination reactions:

$$HNO+NH_2 \rightarrow NO+NH_3$$

$$HNO+O_2 \rightarrow NO+HO_2$$

or, the radical branching reaction:

$$HNO+M \rightarrow NO+H+M.$$

Other routes for NO formation and destruction in these flames involve OCN radicals (Crowhurst and Simmons, 1983, 1985a, 1985b)

$$OCN+O \rightleftharpoons CO+NO$$

$$OCN+NO \rightleftharpoons N_2+CO_2,$$

as well as

$$CN+NO \rightleftharpoons N_2+CO.$$

CHAPTER 5

Analytical Studies

5.1 Introduction

So far, it has been shown that, in spray combustion, variations in fuel properties, air preheating temperature and oxidizer constituents affect the NO_x production. These parameters are examined by an analytical model which is described in this chapter.

The model is in two parts and consists of spray vaporization and spray combustion. First, droplet diameter and extent of vaporization before the flame are evaluated by the fuel spray vaporization model. Then, the calculated results are used as initial conditions in the spray combustion model that also considers droplet interactions and the Zeldovich mechanism of NO formation. Temperature and fuel, oxidizer and NO mass fractions around the burning droplets are determined from this analysis. Single component nitrogen free fuels are studied; therefore, atmospheric nitrogen is the only source of NO_x formation.

Details of the assumptions and the governing equations as well as the comparison between the experimental and computed results are discussed in the following sections. Calculations of the thermophysical properties are given in Appendix C.

5.2 Spray Vaporization

Given the initial state of a monodisperse fuel spray at the aerosol generator, this model predicts the final droplet diameter and the extent of vaporization of the spray prior to the flame. Various equations describing the motion of droplets in the gas flow field, as well as energy and mass conservation equations, were considered. A stepwise droplet tracking technique was used to estimate the local vaporization parameters within the spray and to solve the coupled equations.

Starting with the equation of motion (Beer and Chigier, 1983), the forces acting on a droplet travelling in a gas flow field are balanced according to

$$4/3\,\pi \rho_f r_s^3 \frac{dU}{dt} = 4/3\,\pi \rho_f r_s^3 g - 4/3\,\pi \rho_g r_s^3 g + C_D \pi r_s^2 \rho_g \frac{U'^2}{2} \quad . \qquad (5\text{-}1)$$

The droplet acceleration term on the left side of equation (5-1), which is determined from the rate of change of spray velocity due to divergence, is balanced by the gravity, buoyancy, and drag force terms on the right side. Considering a drag coefficient of $C_D = 24/Re_D$ (Re_D<1), U', the relative velocity between the droplet and the surrounding gas can be determined from equation (5-1)

$$U' = \frac{4 r_s^2 \left[g(\rho_g - \rho_f) + \frac{dU}{dt} \rho_f \right]}{18 \mu_g} \qquad (5\text{-}2)$$

or

$$Re_D = \frac{8 r_s^3 \left[\rho_f \frac{dU}{dt} + g(\rho_g - \rho_f) \right] \rho_g}{18 \mu_g^2} \quad . \qquad (5\text{-}3)$$

Since equation (5-1) is one dimensional, its use in the model requires some justification. From visual observations of the spray pattern in the experimental setup (Figure 3.1), it was found that the droplets are contained within an inverted cone created by the dispersion jet. The spray cone is diluted by rapid dilution air entrainment near the baffle plate and diverges gradually to a maximum spread of about 1.5 cm along the 17.8 cm path to the flame holder. Because of the small cone angle, the radial variation of droplet size is expected to be negligible. Therefore, a one dimensional model should adequately describe the droplet motion in the preflame regions. Furthermore, the entrainment effect was determined experimentally (Cernansky and Sarv, 1983) and used to calculate the droplet travel time. This was done by integrating the ratio of the unit volume of the spray cone to the volumetric flow rate of the combined dispersion and dilution air flows (described empirically as a function of axial distance). Also, the gas phase temperature in the model was adjusted based on the dilution air entrainment results.

At any given time, the total mass of fuel is constant. This can be expressed as

$$m_f + m_F = m_{f_o} + m_{F_o} \quad . \tag{5-4}$$

Assuming that the heat and mass transfer rates around the droplets are sufficiently fast to rapidly modify the local properties of the gas phase, the mass fraction of fuel vapor, Y_F , is given by (Law, 1977)

$$Y_F = \frac{Y_{F_o} + \epsilon Y_{f_o}}{1 + \epsilon Y_{f_o}} \tag{5-5}$$

where, Y_{F_o} and Y_{f_o} are the initial mass fractions of vapor and liquid fuel in the combined vapor/gas system, and ϵ is the fraction of liquid vaporized defined as

$$\epsilon = \frac{m_{f_o} - m_f}{m_{f_o}} \tag{5-6}$$

or

$$\epsilon = 1-(r_s/r_{s_o})^3 . \tag{5-7}$$

For a control volume of aerosol containing both liquid and vapor, the energy balance is given by

$$m_f c_{p_f} T_f + m_{g_o} c_{p_g} T_g + (m_{f_o} - m_f) L + (m_{f_o} - m_f) c_{p_f} T_f + (m_{f_o} - m_f) c_{p_f} (T_g - T_s)$$
$$= m_{f_o} c_{p_f} T_{f_o} + (m_{g_o} + m_{F_o}) c_{p_g} T_{g_o} . \tag{5-8}$$

Solving for T_g from the above equation, the gas temperature can be expressed as

$$T_g = \frac{Y_{f_o} c_{p_f} [T_{f_o} - (1-\epsilon) T_f] + c_{p_g} T_{g_o} - \epsilon Y_{f_o} [L + (c_{p_f} - c_{p_g}) T_s]}{c_{p_g} (1 + \epsilon Y_{f_o})} . \tag{5-9}$$

The evaporation rate for a droplet influenced by the relative gas phase motion is given by (Rao and Lefebvre, 1981)

$$\dot{m} = 4 \pi r_s \frac{k_g}{c_{p_g}} \ln (1+B) (1 + 0.25 Re^{0.5}) \tag{5-10}$$

where, k_g and C_{p_g} are the conductivity and specific heat of the gas surrounding a droplet of radius r_s, and B is the vaporization mass transfer number given by the following expressions

$$B = \frac{Y_F - Y_{F_s}}{Y_{F_s} - 1} \, . \tag{5-11}$$

Assuming that the fuel mass fraction at the droplet surface is that corresponding to the saturated vapor pressure, one can integrate the Clausius-Clapeyron equation and use Dalton's law to obtain

$$Y_{F_s} = \left\{ 1 - \frac{W_g}{W_f} \left(1 - \exp\left[\frac{L}{R^\circ} (1/T_s - 1/T_b) \right] \right\}^{-1} . \tag{5-12}$$

$\dot{m}$ can also be expressed as

$$\dot{m} = -4 \pi r_s^2 \rho_f \frac{dr_s}{dt} . \tag{5-13}$$

Substituting equation (5-3) into equation (5-10), and using the equality between equations (5-10) and (5-13), we get

$$r_s \frac{dr_s}{dt} = -C_2 \left(1 + C_1 r_s^{3/2}\right) \tag{5-14}$$

where

$$C_1 = 0.25 \left\{ \frac{8\left[\rho_f \frac{dU}{dt} + 9(\rho_g - \rho_f)\right] \rho_g}{18 \mu_g^2} \right\}^{0.5} \tag{5-15}$$

and

$$C_2 = \frac{k_g}{\rho_g C_{p_g}} \ln(1 + B) . \tag{5-16}$$

The parameters in the equations given for C_1 and C_2 are temperature dependent. However, the gas phase and the droplet surface temperature are also related by

$$B = \frac{c_{p_g}(T_g - T_s)}{L + c_{p_f}(T_s - T_f)} \qquad (5\text{-}17)$$

and T_s is solved using the equality between equations (5-11) and (5-17) (Lewis Number = 1).

The droplet temperature must be determined prior to the gas phase temperature calculations. Since the temperature inside a droplet varies both radially and with time, the heat conduction equation takes the form

$$\frac{\partial T_f}{\partial t} = \frac{\alpha_f}{r^2}\frac{\partial}{\partial r}\left(r^2 \frac{\partial T_f}{\partial r}\right) \qquad (5\text{-}18)$$

with initial conditions

$$T_f(r,0) = T_{f_o}(r) \qquad (5\text{-}19)$$

and boundary conditions

$$\left(\frac{\partial T_f}{\partial r}\right)_{r=0} = 0 \qquad (5\text{-}20)$$

$$T_f(r_s, t) = T_s \qquad (5\text{-}21)$$

which has to be solved to get the temperature distribution within the droplet. A dimensionless radial coordinate, $\tilde{r} = r/r_s$ is used to include changes of droplet size during heating or cooling. Substitution of $\tilde{r}$ into equations (5-18) to (5-21) yields

$$\frac{\partial T_f}{\partial t} = \frac{\alpha_f}{r_s^2 \tilde{r}^2}\frac{\partial}{\partial \tilde{r}}\left(\tilde{r}^2 \frac{\partial T_f}{\partial \tilde{r}}\right) \qquad (5\text{-}22)$$

with $T_f(\tilde{r},0) = T_{f_0}(\tilde{r})$ (5-23)

$$\left(\frac{\partial T}{\partial \tilde{r}}\right)_{\tilde{r}=0} = 0 \quad (5\text{-}24)$$

and $T_{f_{\tilde{r}=1}} = T_S$. (5-25)

The above differential equation can be easily replaced by a finite difference equation. In the explicit form as described by Law and Sirignano (1977), droplet temperature can be determined by simple marching. This technique requires small time steps to avoid instability. On the other hand, the implicit procedure is unconditionally stable and, therefore, is a more appropriate choice. Using $\Delta\tilde{r}$ and Δt to denote the radial and time intervals, the implicit finite difference approximation of equation (5-22) becomes

$$T'_{f_{i-1}}(\beta-\gamma)+T'_{f_i}(1+2\gamma)+T'_{f_{i+1}}(-\beta-\gamma)=T_{f_i} \quad (5\text{-}26)$$

with $T'_{f_{0}i} = T_{f_{0}i}$, (5-27)

$T'_{f_1} = T'_{f_2}$, (5-28)

where,

$$\beta = \frac{\alpha_f \Delta t}{\tilde{r}\, r_S^2 \Delta\tilde{r}}, \quad (5\text{-}29)$$

and

$$\gamma = \frac{\alpha_f \Delta t}{r_S^2 (\Delta\tilde{r})^2}. \quad (5\text{-}30)$$

The superscript prime specifies the new value of temperature determined at the end of a time step and the subscript i designates the radial index for N_r meshes. Equation (5-26) represents a system of linear equations wich can be written in matrix form with $(\beta-\gamma)$, $(1+2\gamma)$ and $(-\beta-\gamma)$ becoming the coefficients of a tridiagonal matrix. Knowing the initial and boundary conditions as given by equations (5-27) and (5-28), the simultaneous system of equations is solved for N_r-1 unknowns, T'_{f_i}. Once the radial temperature distribution has been determined, the average droplet temperature can be evaluated by spatial integration.

$$T_f = \frac{\int_0^{\tilde{r}=1} T_f' (4\pi\tilde{r}^2) d\tilde{r}}{4/3\,\pi (1)^3} . \tag{5-31}$$

Substituting for T_f from equation (5-31) into equation (5-9) gives the gas phase temperature, T_g.

Equation (5-14) can now be integrated as a function of time, subject to $r_s\,(t=0) = r_{s_o}$. Dividing the total droplet travel time into time steps, the local temperatures, mass fractions, gas properties and droplet diameter can be evaluated at the end of each time step. The calculated values are then used as the initial conditions for the next step. This procedure is continued until the total travel time is reached.

5.3 Spray Combustion

It was noted that, in the present experimental setup, the fuel spray enters a self-supporting, one dimensional flame, stabilized on a screen flame holder. Due to vaporization along the spray path and droplet impactions on the screen wires, part of the fuel is prevaporized and premixed with the oxidizer. The prevaporization due to simple evaporation is calculated by the vaporization model just described, while the screen impaction contribution to prevaporization must be determined experimentally and entered manually.

After the fuel spray enters the combustion zone, solution involves a transient-diffusive-convective problem. The basic formulation is similar to that of Botros et al. (1980) in their numerical treatment of a single fuel droplet burning in a reactive gaseous system.

With assumption of uniform pressure, zero relative velocity, and one-step reaction kinetics for fuel oxidation, the governing equations in a spherically symmetric system reduce to

continuity :

$$\frac{\partial \rho_g}{\partial t} + \frac{1}{r^2}\frac{\partial}{\partial r}(\rho_g v r^2) = 0 \tag{5-32}$$

fuel :

$$\rho_g\left(\frac{\partial Y_F}{\partial t} + v\frac{\partial Y_F}{\partial r}\right) - \frac{1}{r^2}\frac{\partial}{\partial r}\left(\rho_g \mathcal{D} r^2 \frac{\partial Y_F}{\partial r}\right) = -\nu_F W_F \omega \tag{5-33}$$

oxidizer :

$$\rho_g\left(\frac{\partial Y_O}{\partial t} + v\frac{\partial Y_O}{\partial r}\right) - \frac{1}{r^2}\frac{\partial}{\partial r}\left(\rho_g \mathcal{D} r^2 \frac{\partial Y_O}{\partial r}\right) = -\nu_O W_O \omega \tag{5-34}$$

energy :

$$\rho_g c_{p_g}\left(\frac{\partial T_g}{\partial t} + v\frac{\partial T_g}{\partial r}\right) - \frac{1}{r^2}\frac{\partial}{\partial r}\left(K_g r^2 \frac{\partial T_g}{\partial r}\right) = \nu_F W_F \Delta H \omega \tag{5-35}$$

state :

$$P = \rho_g R^o T_g \sum_{j=1}^{N'} \frac{Y_j}{W_j} \tag{5-36}$$

where

$$\omega = A \exp\left(-\frac{E}{R^o T_g}\right)\left(\frac{X_F P}{R^o T_g}\right)^{0.25}\left(\frac{X_O P}{R^o T_g}\right)^{1.5}, \tag{5-37}$$

$\mathcal{D}$ is the mass diffusivity, v is the convective velocity due to droplet vaporization and temperature variations in the gas phase, ν is the stoichiometric coefficient, A is the pre-exponential term and E is the activation energy (for n-octane, $A=4.6\times10^{11}$, $E=30{,}000$ and for methanol, $A=3.2\times10^{12}$, $E=30{,}000$ cal/mole; Westbrook and Dryer, 1984).

Boundary conditions at the droplet surface ($r=r_s$) are

$$\frac{d}{dt}\left(\frac{4}{3}\pi r_s^3 \rho_f\right) = -4\pi r_s^2 \rho_{g_s}\left(v_s - \frac{dr_s}{dt}\right) \tag{5-38}$$

$$\left(\rho_g \mathcal{D} \frac{\partial Y_F}{\partial r}\right)_s + \rho_{g_s}\left(v_s - \frac{dr_s}{dt}\right)(1 - Y_{F_s}) = 0 \tag{5-39}$$

$$\left(\rho_g \mathcal{D} \frac{\partial Y_O}{\partial r}\right)_s - \rho_{g_s}\left(v_s - \frac{dr_s}{dt}\right) Y_{O_s} = 0 \tag{5-40}$$

$$\left(K \frac{\partial T}{\partial r}\right)_s - \rho_{g_s}\left(v_s - \frac{dr_s}{dt}\right) L = 0 \tag{5-41}$$

$$T(r=r_s) = T_s \,. \tag{5-42}$$

At the midpoint between the droplet centers, the ambience boundary conditions are

$$\left(\frac{\partial Y_F}{\partial r}\right)_\infty = \left(\frac{\partial Y_O}{\partial r}\right)_\infty = \left(\frac{\partial T_g}{\partial r}\right)_\infty = 0 \,. \tag{5-43}$$

The initial conditions at t=0 are given as radial profiles

$$T_g(r,0) = T_{g_o}(r) \tag{5-44}$$

$$Y_F(r,0) = Y_{F_o}(r) \tag{5-45}$$

$$Y_O(r,0) = Y_{O_o}(r) \tag{5-46}$$

$$v(r,0) = v_o(r) \tag{5-47}$$

with $$r_s(0) = r_{s_o} \,. \tag{5-48}$$

Applying the dimensionless coordinate, $\tilde{r}$, the governing equations (5-32) to (5-35) as well as the boundary and initial conditions (Eqs. 5-38 to 5-48) can be represented as

$$\frac{\partial \rho_g}{\partial t} + \frac{1}{\tilde{r}\, r_s^2} \frac{\partial}{\partial \tilde{r}} \left(\rho_g v \tilde{r}^2 \right) = 0 \qquad (5\text{-}32)'$$

$$\rho_g \left(\frac{\partial Y_F}{\partial t} + \frac{v}{r_s} \frac{\partial Y_F}{\partial \tilde{r}} \right) - \frac{1}{\tilde{r}\, r_s^2} \frac{\partial}{\partial \tilde{r}} \left(\rho_g \mathcal{D} \tilde{r}^2 \frac{\partial Y_F}{\partial \tilde{r}} \right) = -\nu_F W_F \omega \qquad (5\text{-}33)'$$

$$\rho_g \left(\frac{\partial Y_O}{\partial t} + \frac{v}{r_s} \frac{\partial Y_O}{\partial \tilde{r}} \right) - \frac{1}{\tilde{r}\, r_s^2} \frac{\partial}{\partial \tilde{r}} \left(\rho_g \mathcal{D} \tilde{r}^2 \frac{\partial Y_O}{\partial \tilde{r}} \right) = -\nu_O W_O \omega \qquad (5\text{-}34)'$$

$$\rho_g c_{p_g} \left(\frac{\partial T_g}{\partial t} + \frac{v}{r_s} \frac{\partial T_g}{\partial \tilde{r}} \right) - \frac{1}{\tilde{r}\, r_s^2} \frac{\partial}{\partial \tilde{r}} \left(K_g \tilde{r}^2 \frac{\partial T_g}{\partial \tilde{r}} \right) = \nu_F W_F \Delta H \omega \qquad (5\text{-}35)'$$

$$\frac{d}{dt} \left(\frac{4}{3} \pi r_s^3 \rho_f \right) = -4\pi r_s^2 \rho_{g_s} \left(v_s - \frac{dr_s}{dt} \right) \qquad (5\text{-}38)'$$

$$\frac{\rho_g \mathcal{D}}{r_s} \left(\frac{\partial Y_F}{\partial \tilde{r}} \right)_{\tilde{r}=1} + \rho_{g_s} \left(v_s - \frac{dr_s}{dt} \right) (1 - Y_{F_s}) = 0 \qquad (5\text{-}39)'$$

$$\frac{\rho_g \mathcal{D}}{r_s} \left(\frac{\partial Y_O}{\partial \tilde{r}} \right)_{\tilde{r}=1} - \rho_{g_s} \left(v_s - \frac{dr_s}{dt} \right) Y_{O_s} = 0 \qquad (5\text{-}40)'$$

$$\frac{K_{g_s}}{r_s} \left(\frac{\partial T_g}{\partial \tilde{r}} \right)_{\tilde{r}=1} - \rho_{g_s} \left(v_s - \frac{dr_s}{dt} \right) L = 0 \qquad (5\text{-}41)'$$

$$T_{\tilde{r}=1} = T_s \qquad (5\text{-}42)'$$

$$\left(\frac{\partial Y_F}{\partial \tilde{r}} \right)_{\tilde{r}=\infty} = \left(\frac{\partial Y_O}{\partial \tilde{r}} \right)_{\tilde{r}=\infty} = \left(\frac{\partial T_g}{\partial \tilde{r}} \right)_{\tilde{r}=\infty} \qquad (5\text{-}43)'$$

$$T_g(\tilde{r}, 0) = T_{g_o}(\tilde{r}) \qquad (5\text{-}44)'$$

$$Y_F(\tilde{r}, 0) = Y_{F_o}(\tilde{r}) \qquad (5\text{-}45)'$$

$$Y_O(\tilde{r},0) = Y_{O_o}(\tilde{r},0) \tag{5-46)'$$

$$v(\tilde{r},0) = v_o(\tilde{r},0) \tag{5-47)'$$

$$r_s(0) = r_{s_o}\,. \tag{5-48)'$$

A finite difference approximation scheme was used to solve these governing partial differential equations. For better resolution in the high gradient regions around the droplet surface, the radial spacing was ramped according to

$$\tilde{r}_i = \tilde{r}_{i-1} + 0.2 + 0.06(i-2), \qquad i \geq 2. \tag{5-49}$$

Also, in order to apply this model to sprays, the burning rate was corrected to account for droplet interactions. Since the droplet surface regression rate, $v_s - \frac{dr_s}{dt}$ is directly proportional to the mass burning rate, such correction was accommodated by adjusting the velocity term in the model. Calculations of the correction factor are discussed in the next section.

5.4 Droplet Interactions

A mathematical procedure has been developed to transform the quasi-steady transport equations describing the Stephan flow field around the interacting droplets to the Laplace equation. Details of the analysis as well as the underlying assumptions have been given by Labowsky (1976-1980) and therefore, will not be repeated here. However, the following discussion should provide some insight to the development of the model.

The combined fuel/oxidizer conservation equation can be written as

$$\nabla \cdot \left[\rho_g v \left(Y_F - Y_O \frac{\nu_F W_F}{\nu_O W_O} \right) - \rho_g \mathcal{D} \nabla \left(Y_F - Y_O \frac{\nu_F W_F}{\nu_O W_O} \right) \right] = 0. \tag{5-50}$$

Defining the velocity potential, ψ, as

$$\psi = \frac{\ln\left[\left(1-Y_F+Y_O\frac{\nu_F W_F}{\nu_O W_O}\right)/\left(1+Y_{O,\infty}\frac{\nu_F W_F}{\nu_O W_O}\right)\right]}{\ln(1+B)}, \tag{5-51}$$

the mass averaged gas velocity, v, can be expressed according to

$$v = -\mathcal{D}\ln(1+B)\nabla\psi \tag{5-52}$$

where B is the combustion transfer number given by

$$B = \frac{Y_{F_S}+Y_{O,\infty}\frac{\nu_F W_F}{\nu_O W_O}}{1-Y_{F_S}}. \tag{5-53}$$

Equation (5-52) together with the mass conservation equation ($\nabla.\rho v=0$) yields the Laplace equation

$$\nabla^2\psi = 0. \tag{5-54}$$

From the definition of ψ (Eq. 5-51), the boundary conditions become

$$\psi = \begin{cases} 1 & \text{on the surface of droplets} \\ 0 & \text{far away from the droplets.} \end{cases}$$

The above equation is solved using a superposition technique called the method of images. Briefly, in order to solve for the fields, a series of point sources and sinks are placed inside every droplet in the array which satisfy the boundary conditions.

The burning rate of the droplet k in an array is determined by integrating the mass flux over its surface area

$$\dot{m}_k = \iint \rho_g v_k . dS. \tag{5-55}$$

Substitution for v from equation (5-52), gives

$$\dot{m}_k = 4\pi r_s \rho_g \mathcal{D} \ln (1+B) \frac{1}{4\pi r_s} \iint \nabla \psi_k . dS. \tag{5-56}$$

The right hand side of equation (5-56) can be rewritten as

$$\dot{m}_k = \dot{M}_k \eta_k , \tag{5-57}$$

where $\dot{M}_k$ is the burning rate of droplet k if it were burning as an isolated droplet and η_k is the burning rate correction factor for droplet interactions defined as

$$\eta_k = - \frac{1}{4\pi r_s} \iint \nabla \psi_k . dS. \tag{5-58}$$

For an array of N interacting droplets, η_k can also be shown as (Labowsky, 1980b)

$$\eta_k = \sum_{\ell=1}^{N} \alpha'_{k,\ell} \psi_\ell \tag{5-59}$$

where $\alpha'_{k,\ell}$ designates elements of an NxN matrix representing the transfer rates of droplet k, when it is in the field of a unity potential droplet, ℓ, with the rest of the array being at zero potential. Using the method of images, these elements can be determined by adding the images source strengths inside the k-th particle that are associated with the ℓ field.

As it appears, the calculations of the combustion rate correction factor are independent of the fuel or oxidizer properties and only depend on array configuration.

5.5 Array Geometry

In this work, the correction factor is computed for an evenly dispersed configuration inside the flame holder. The droplets are divided into geometrically similar planar arrays separated by the interdroplet spacing, as shown in Figure 5.1. Except for the droplets near the burner wall, every droplet is encircled by six immediate neighbors placed at the corners of a hexagon. For a burner diameter, d, and center-to-center droplet spacing, $\mathcal{L}$, the number of droplets that can be placed on a layer is equal to

$$\text{number of droplets per layer} = \frac{\pi\, d^2/4}{\mathcal{L}^2/2\ \sin 60} \quad . \tag{5-60}$$

The total number of droplets per unit volume or number density is given by

$$\text{droplet number density} = \frac{\left(1+\frac{h}{\mathcal{L}}\right)\left(\frac{\pi\,\frac{d^2}{4}}{\mathcal{L}^2\ \sin 60}\right)}{\pi\, h\, d^2/4} \quad . \tag{5-61}$$

Since the burner dimensions are large compared to the droplet spacings (i.e. $h/\mathcal{L} >> 1$), the above expression simplifies to

$$\text{droplet number density} = \frac{2}{\mathcal{L}^3\ \sin 60} \quad . \tag{5-62}$$

Usually, droplet number density is measured by optical counters or determined from the operating conditions (as in well-characterized sprays). Thus, droplet spacing in a uniformly distributed monodisperse spray, can be calculated from equation

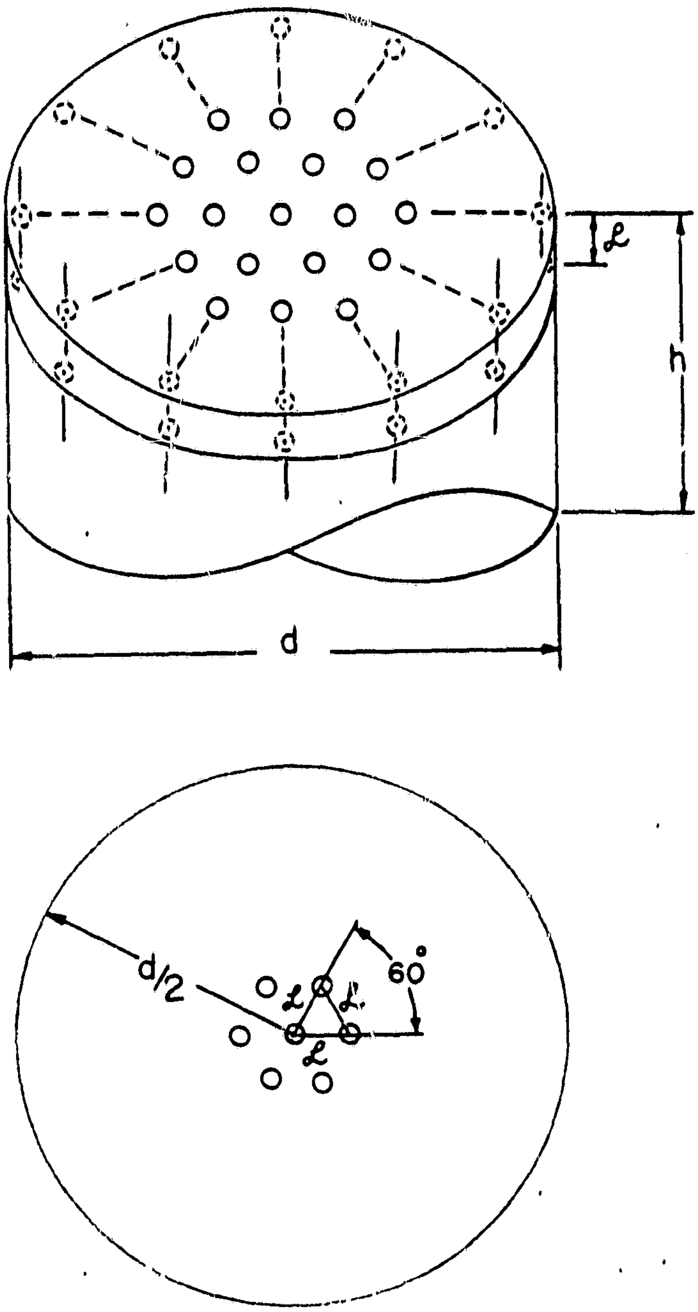

Figure 5.1. Monodisperse droplet arrangement used in the numerical calculations.

(5-61).

5.6 NO Kinetics

Nitric oxide formation reactions involving the oxidation of atmospheric nitrogen (Zeldovich mechanism) are considered. These reactions and their rate data are listed below (Bracco, 1973; Bowman, 1975; Peterson and Laurendeau, 1982; Dasch and Blint, 1984).

	Forward rate constant	Backward rate constant
$O + N_2 \rightleftharpoons NO + N$	$1.36 \times 10^{14} \exp(-75{,}400/\mathring{R}T)$	$3.1 \times 10^{13} \exp(-334/\mathring{R}T)$
$N + O_2 \rightleftharpoons NO + O$	$6.4 \times 10^{9}\ T \exp(-6260/\mathring{R}T)$	$1.5 \times 10^{9}\ T \exp(-38{,}640/\mathring{R}T)$
$O_2 + N_2 \rightleftharpoons O + O + N_2$	$6.0 \times 10^{13}\ (118{,}000/\mathring{R}T) \times \exp(-118{,}000/\mathring{R}T)$	1.0×10^{14}

The rate constants for the bimolecular and termolecular reactions are in units of cm^3/mole sec and $cm^6/mole^2$ sec, respectively. In view of the fact that NO transformation to NO_2 is not considered, these reactions account for the total NO_x production.

Assuming steady-state N atom concentration and equilibrium concentration for O atom with respect to O_2, concentrations of N_2 and NO are determined as their species conservation equations are solved simultaneously with the energy, fuel and oxidizer equations. The initial and boundary conditions are similar to those for oxygen as discussed in section 5.3.

5.7 Representative Results

5.7.1 Preflame Spray Vaporization

Calculated results for stoichiometric sprays of methanol and

C-2

n-octane are presented in Figures 5.2 and 5.3 for an initial droplet diameter of 50 μm and droplet and gas temperatures of 24 °C. These plots show changes in droplet diameter, gas phase and droplet temperatures, extent of prevaporization and the mass transfer number during vaporization. The last point on each curve corresponds to conditions at the end of the droplet travel time in the preflame regions of the combustor.

After vaporization is initiated, the droplet surface temperature drops to its lowest value. Then, as illustrated in Figure 5.4, it increases gradually and approaches the falling gas and droplet temperatures. The reduced gas temperature and increased fuel vapor concentration decrease the rate of vaporization substantially, inhibiting further droplet size reduction. This is also demonstrated in the plots of the mass transfer number versus droplet travel time, where B number decreases continuously and nears zero as the fuel vapor concentration reaches its saturated value.

When vaporization occurs adiabatically, heat is extracted from the liquid fuel as well as the gas phase to vaporize the droplets. Among the fuels used in this study, methanol and isopropanol require higher heat of vaporization than n-heptane and n-octane. At the same time, the air to fuel mass ratio for a fixed stoichiometry is less for the alcohols as compared to the alkanes, leading to a more effective cooling and enrichment of the gas phase by droplet vaporization. Under such conditions, the vapor pressure at the surface of the fuel droplets decreases and thus hinders further changes in the evaporation characteristics of the

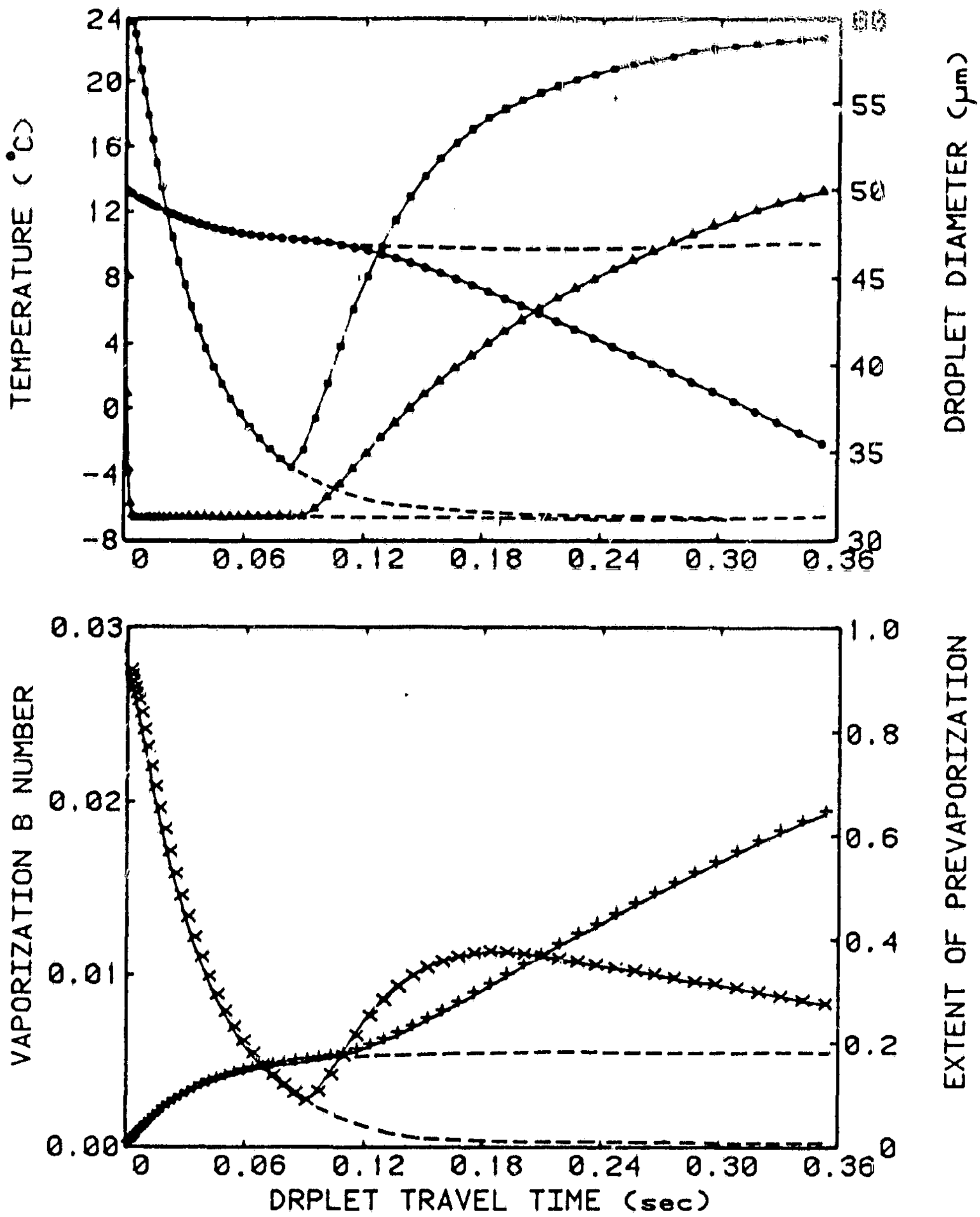

Figure 5.2. Calculated evaporation characteristics of a 50 µm diameter droplet in a monodisperse spray of methanol. ● - Droplet diameter; ▲ - Droplet temperature; ■ - Gas phase temperature; x - Mass transfer number; + - Extent of prevaporization. Dotted lines represent adiabatic vaporization.

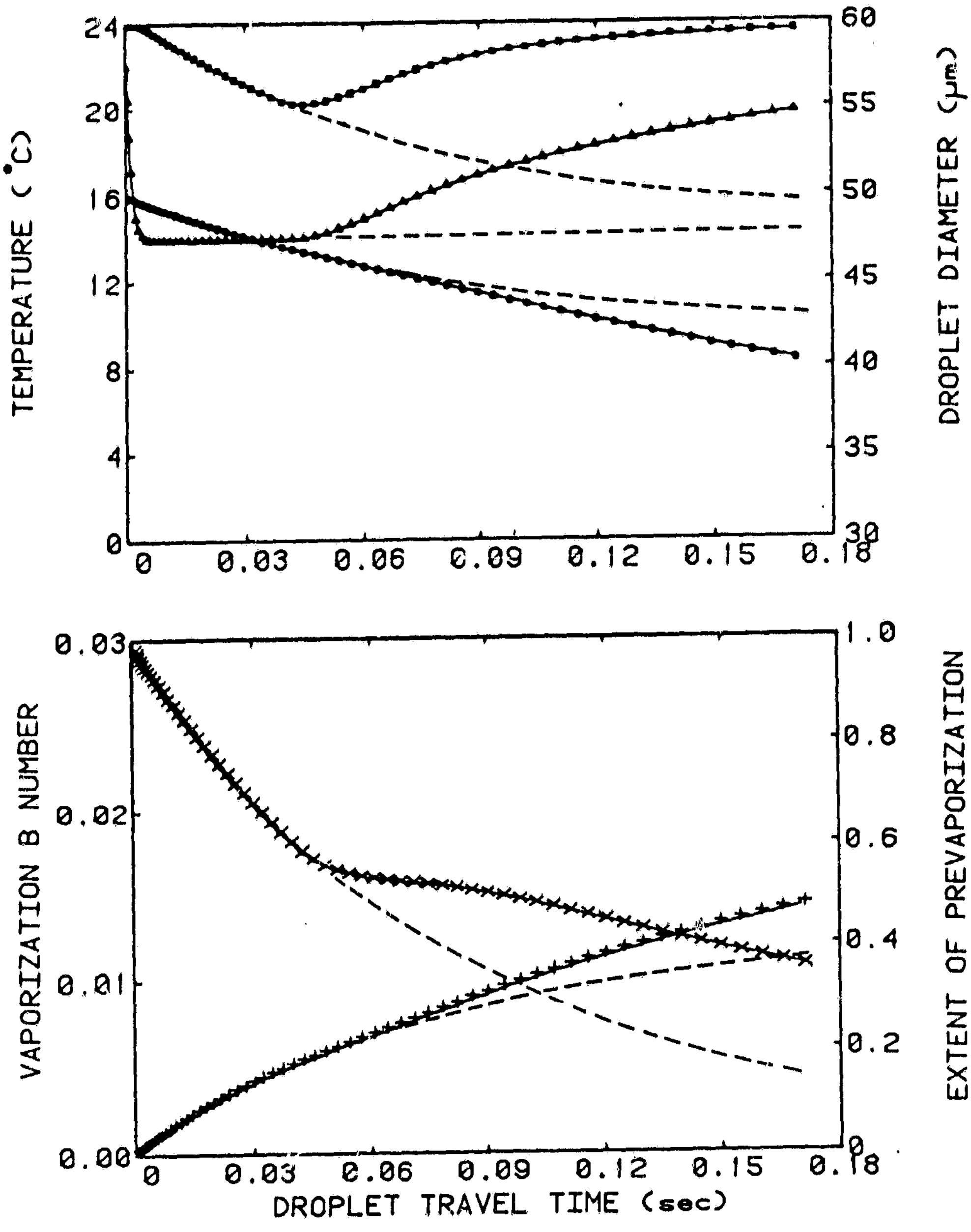

Figure 5.3. Calculated evaporation characteristics of a 50 μm diameter droplet in a monodisperse spray of n-octane. ● - Droplet diameter; ▲ - Droplet temperature; ■ - Gas phase temperature; x - Mass transfer number; + - Extent of prevaporization. Dotted lines represent adiabatic vaporization.

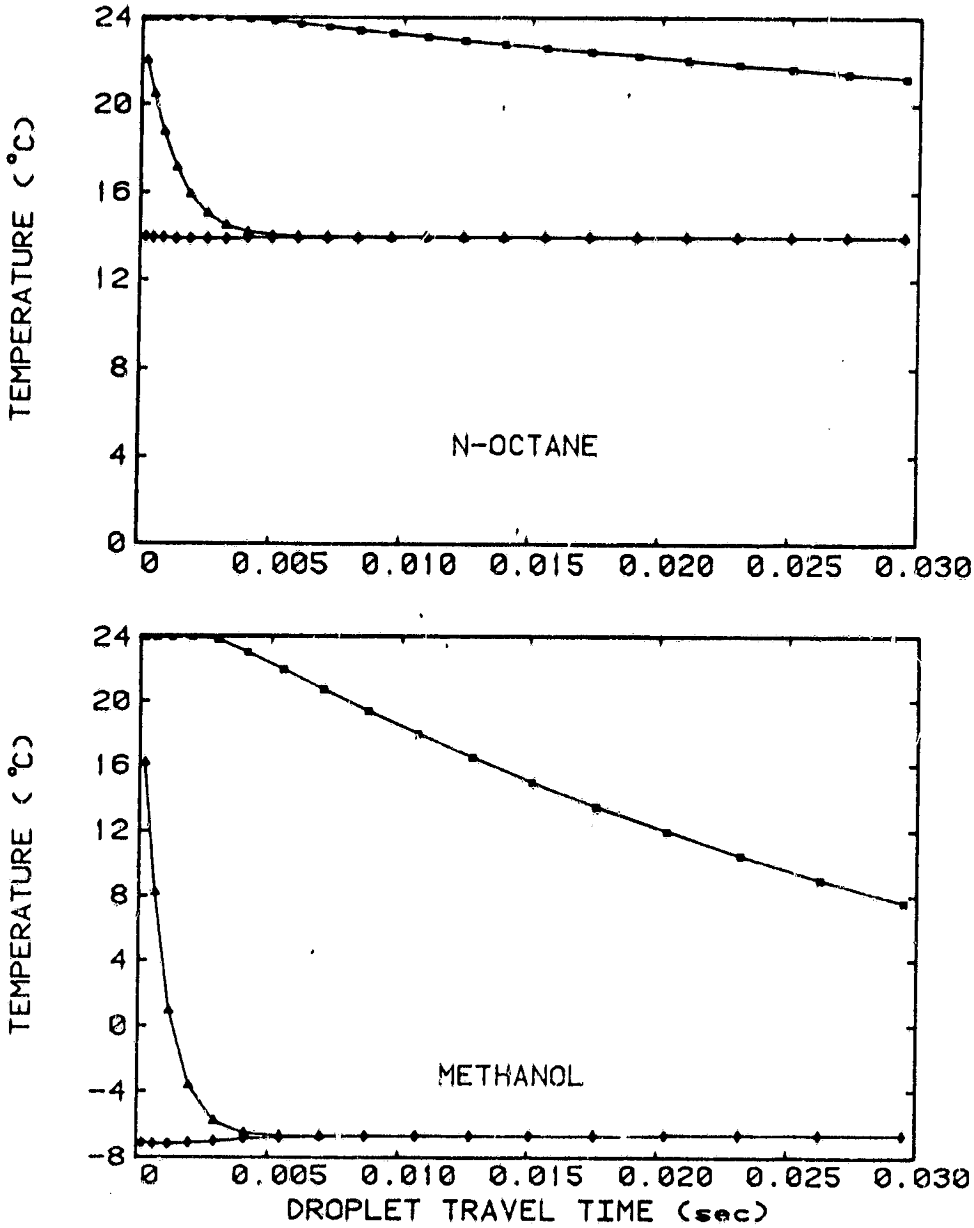

Figure 5.4. Calculated temperatures for early stage vaporization of monodisperse methanol and n-octane aerosols. ▲ - Droplet temperature; ♦ - Droplet surface temperature; ■ - Gas phase temperature.

fuel spray, even for long droplet residence times.

In these calculations, the spray is considered to vaporize adiabatically while travelling inside the upper and lower housing assemblies. But, as the fuel aerosol enters the flow reducing sections, additional heat is transferred to the cold spray from the combustor walls which are kept at the air preheat temperature. Heating of the aerosol by constant temperature walls is treated as a thermal-entry length problem. This results in an increase in the gas and droplet temperatures and a decrease in droplet size as shown in Figures 5.2 and 5.3. In the absence of the wall heating, adiabatic spray vaporization continues for the entire droplet travel time as shown by the dotted lines.

Table 5.1 summarizes the calculated vaporization parameters for the fuel sprays tested in this study, based on an initial droplet diameter of 50 μm and different air preheating temperatures. As expected, the final droplet size and the extent of prevaporization are strongly influenced by fuel volatility and ambient temperature. These predictions are used later as initial conditions in the spray combustion model.

Figure 5.5 compares the predicted results of the aerosol temperature with the actual measurements made along the spray centerline. Since droplet impaction and agglomeration on the thermocouple tip was unavoidable, it is assumed that the measurements represent the average of the droplet, gas phase and droplet surface (wet bulb) temperatures. Both measured and calculated values correspond to initial droplet diameters equal to the NO_x minima, air temperature at 22°C and overall stoichiometry

Table 5.1. Computed parameters for preflame spray vaporization of 50 μm droplets at various air preheat temperatures. Droplet temperature is initially at 24°C.

Air Temperature (°C)	Droplet Diameter at the Flame Holder (μm)			
	Methanol	Isopropanol	N-heptane	N-octane
24	35.0	40.0	33.4	40.0
34	25.6	34.1	24.6	33.3
44	0.0	25.2	3.2	22.4

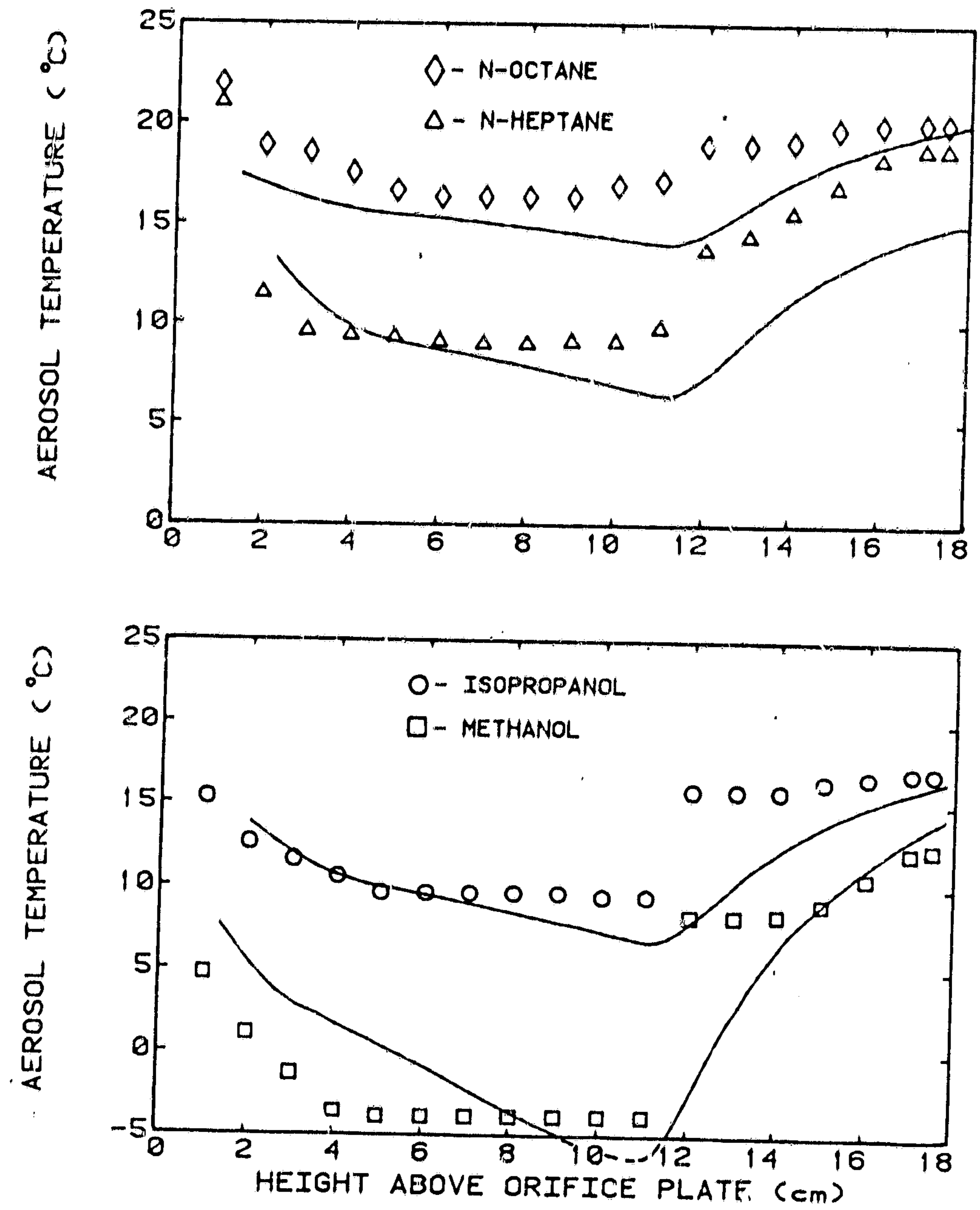

Figure 5.5. Comparison of calculated and measured aerosol temperatures. Solid lines represent the calculated values.

of 1.0. In spite of the uncertainties in the measurements and the model predictions, the trends are similar.

5.7.2 Burning Rate Correction Factor

Effects of droplet number density and interdroplet spacings on spray burning rate are examined for evenly dispersed arrays of monosized droplets (similar to the one shown in Figure 5.1). In such configuration, droplets that are located around the array center experience a stronger interaction than those located close to the outer edge.

Computed burning rate correction factors for three arrays of interacting droplets are listed in Table 5.2. The calculations were done for a fixed interdroplet distance of 20 droplet diameters (ℓ=40). In all cases, the burning rate correction factor, η, for any given droplet is less than unity, indicating slower burning compared to that of an isolated droplet of the same size. η increases as one moves away from the center of the array and decreases with increasing number of droplets.

For closely packed arrays or those that contain large number of droplets (>37), the accurate determination of η by Labowsky's droplet superposition procedure becomes exceedingly tedious. Thus, A second superposition method was used to extend his technique to cases that involve a great number of droplets. This development is based on the fact that any monodisperse array can be constructed by superimposing arrays of six droplets around a primary array of seven. For instance, a 55 droplet array can be composed of eight consecutive arrays spaced about the center of

TABLE 5.2 Computed burning rate correction factors for three monodisperse arrays of droplets with $\mathcal{L}$ =40.

Number of Droplets Per Array	η		
	Center Droplet	Edge Droplet	Array Average
7	0.865	0.897	0.892
13	0.813	0.872	0.847
19	0.772	0.835	0.815

the primary array, as demonstrated in Figure 5.6. With every addition, the burning rate of the entire configuration reduces by a factor which is equivalent to the burning rate correction factor of the superimposed array. Figure 5.7 shows the calculated average burning rate correction factor as a function of droplet spacing for various monodisperse arrays. The data points and the solid lines represent the results obtained from the droplet and array superposition techniques, respectively. The results are in good agreement with a maximum difference of 1.0% for the studied cases.

When droplet interactions are considered in a spray combustion model, the burning rate correction factor has to be reevaluated as the interdroplet spacing changes. However, successive application of the droplet interaction model could add up to a considerable increase in the computation time. To overcome this problem, the dependence of the burning rate correction factor on $\mathcal{L}$ is expressed as a functional relationship. Computed values of η are used to determine the 'best fit' in the form of four degree polynomials. These expressions are utilized in the spray combustion model to facilitate the evaluation of η.

5.7.3 Spray combustion and NO formation

Computations were performed for stoichiometric sprays of n-octane and methanol. In all cases, the initial conditions at t=0 were determined by the spray vaporization model. The time domain was set equal to the duration, after which, the calculated results were at their steady state values.

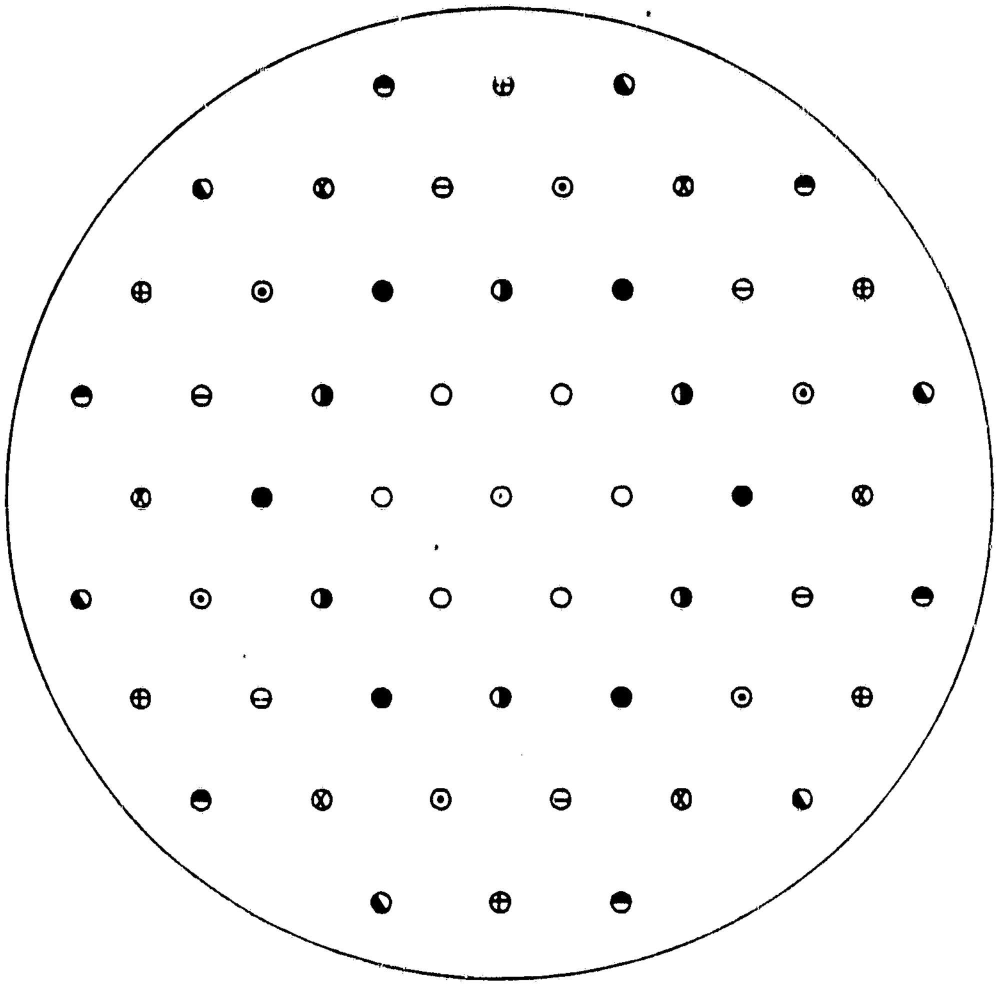

Figure 5.6. Droplet configuration for a 55 droplet array.

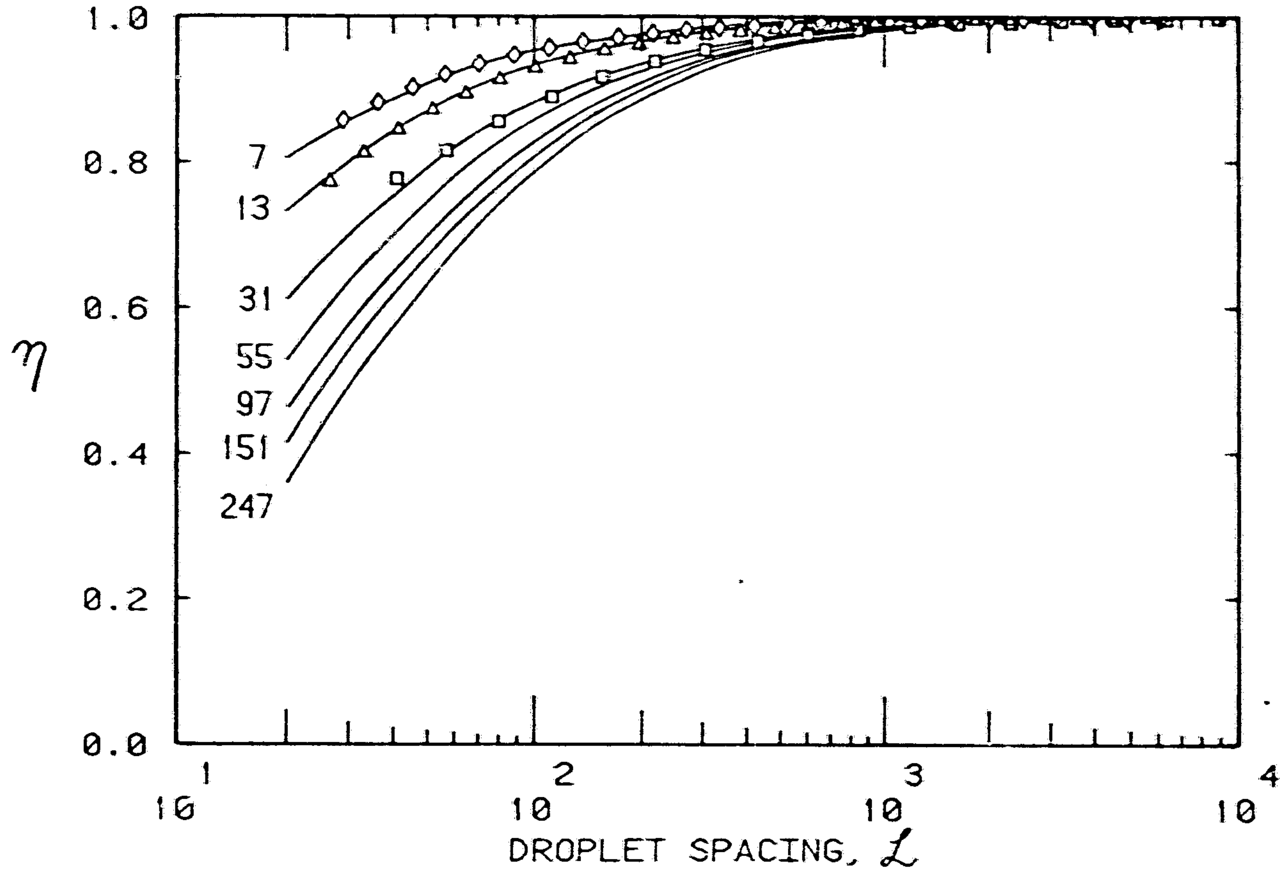

Figure 5.7. Calculated burning rate correction factor as a function of droplet spacing for various numbers of interacting droplets. Data points represent the calculated results based on droplet superposition procedure. Solid lines are determined by the array superposition method.

To initiate combustion, the gas phase temperature was raised to 1100°K by reacting a part of the fuel vapor and the oxidizer. Further fuel and oxidizer consumption as well as the temperature rise due to the heat release are determined by the spray combustion model. The continous increase in the gas phase temperature eventually leads to droplet ignition which is seen as a bulge in the temperature profiles. Figure 5.8 to 5.10 show the development of temperature and species profiles for 27.0, 33.2 and 47.7 μm n-octane droplets, corresponding to initial droplet diameters of 37.0, 43.3 and 57.5 μm, respectively. The time dependence of the profiles are noted on the plots. Followed by a rapid reduction in the fuel vapor concentration, the flame temperature reaches its maximum value close to the droplet surface. The location of the maximum temperature coincides with the crossing of the fuel and oxidizer profiles and moves with changes in droplet vaporization rate and oxygen concentration during combustion. For small droplets, gas phase combustion and droplet ignition are intensified by the high preflame extent of vaporization. Much of the NO is formed in the hot gases surrounding the burning fuel droplets, where premixed type of burning appears to dominate. In the case of large droplets, temperature rises slowly as the reactions occur in a relatively narrow zone. This is attributed to a lower droplet vaporization before the flame front and the slow propagation of the fuel vapor emerging from the surface of the burning droplets. After the initial temperature rise, diffusional burning is also observed near the droplet surface, as indicated by the peak in temperature

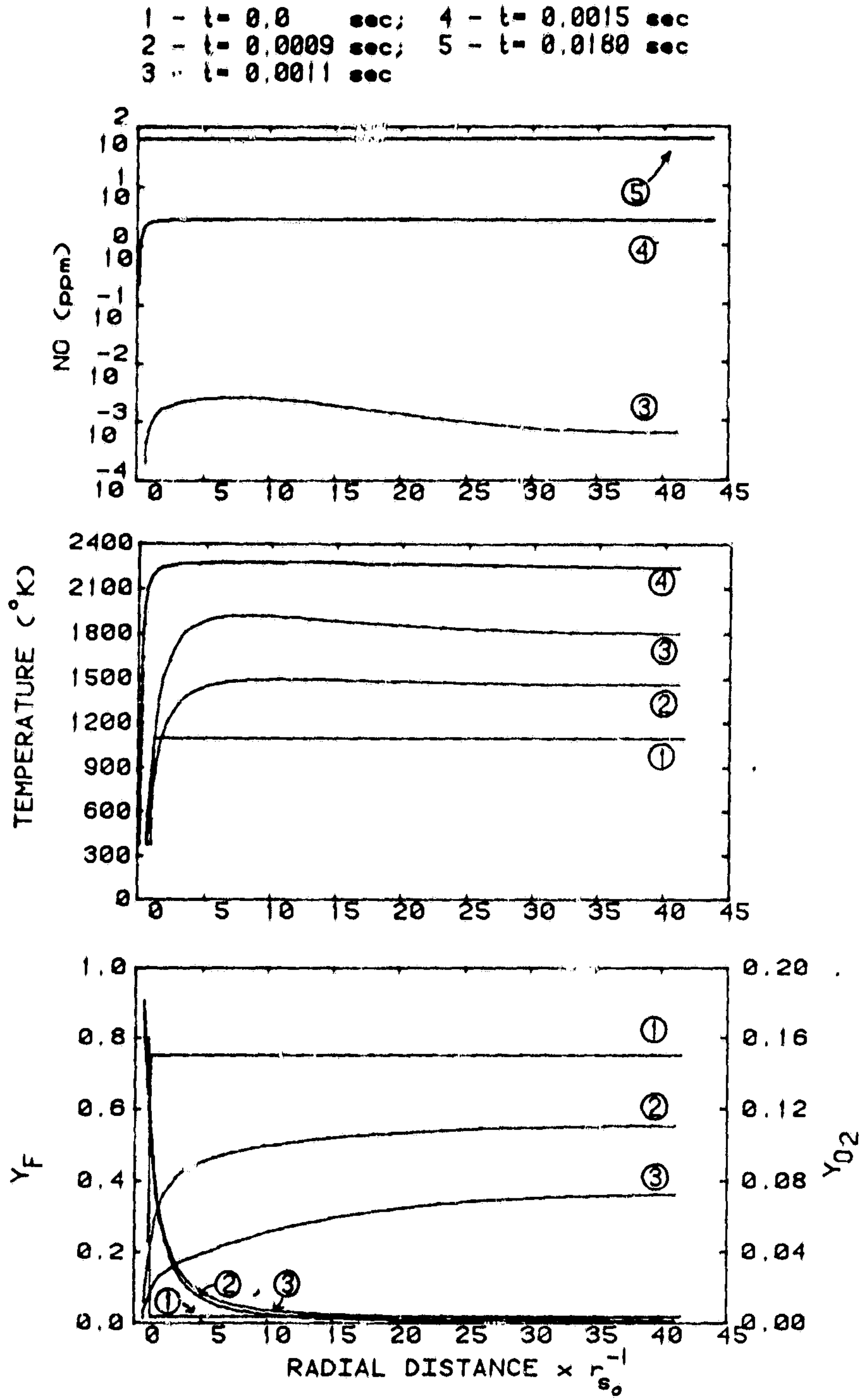

Figure 5.8. Evolution of temperature and mass fraction profiles for a 27.0 μm droplet in a monodisperse spray of n-octane at $\phi = 1.0$ and $\epsilon_o = 0.61$.

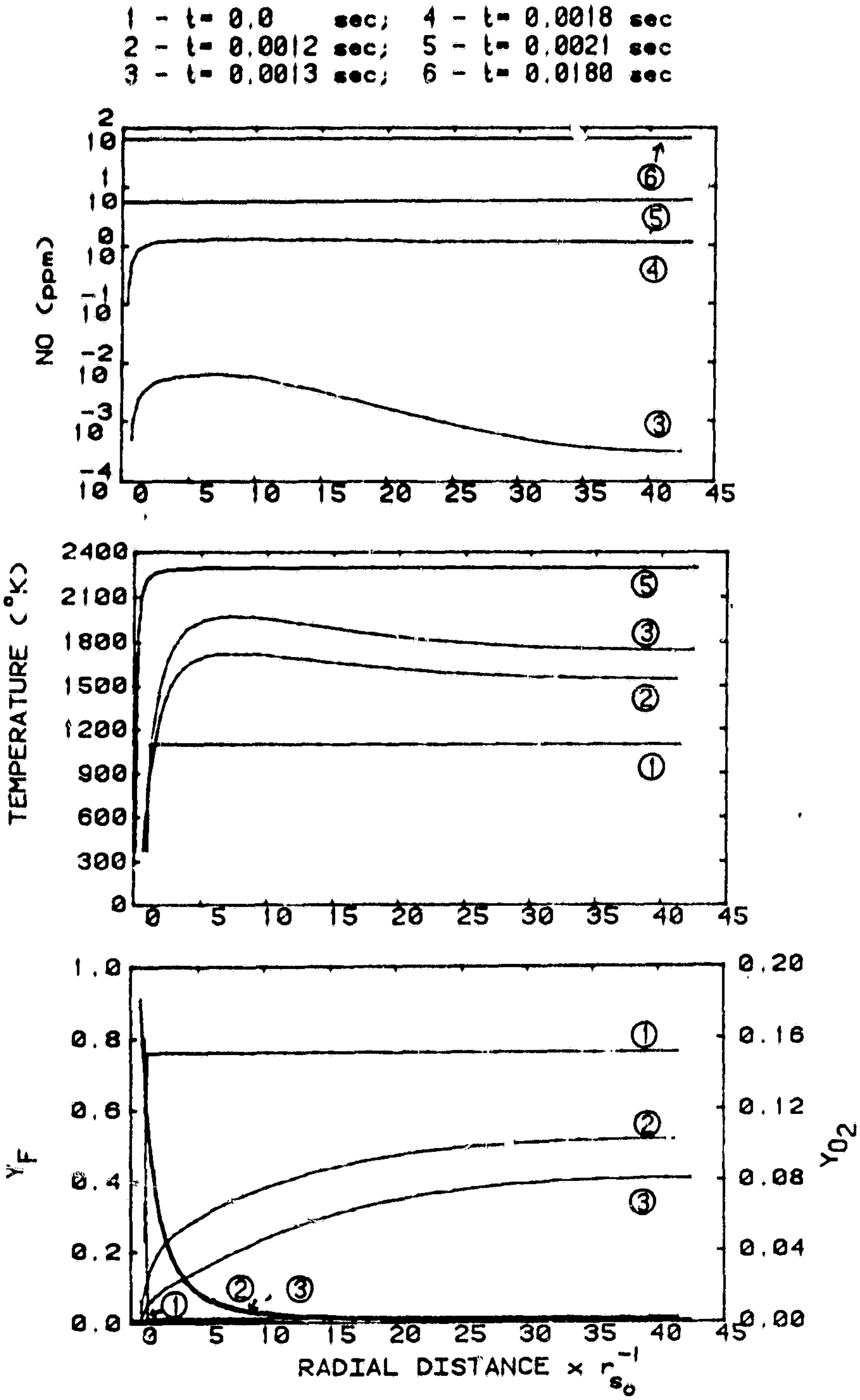

Figure 5.9. Evolution of temperature and mass fraction profiles for a 33.2 μm droplet in a monodisperse spray of n-octane at $\phi = 1.0$ and $\epsilon_o = 0.55$.

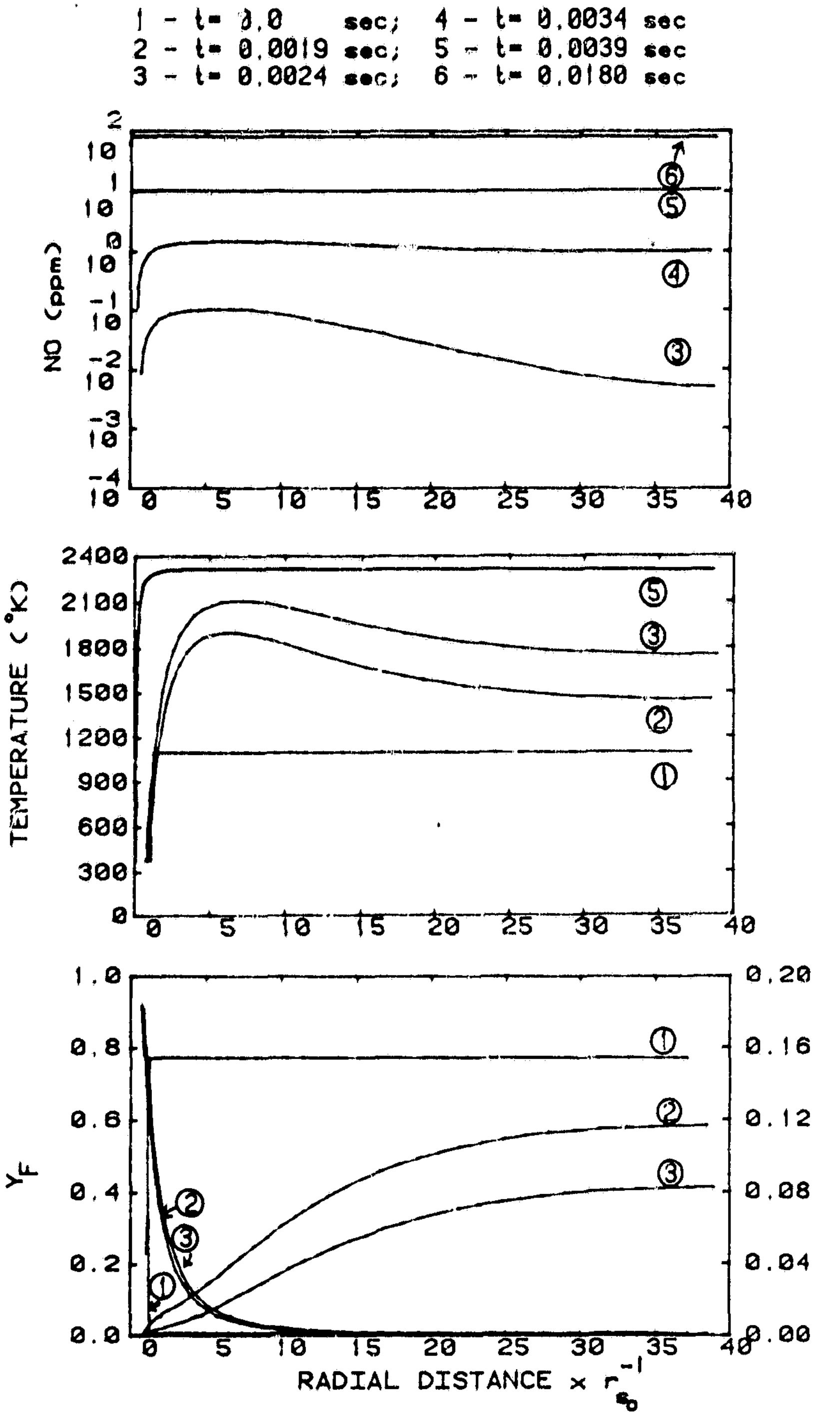

Figure 5.10. Evolution of temperature and mass fraction profiles for a 47.7 μm droplet in a monodisperse spray of n-octane at $\phi = 1.0$ and $\epsilon_o = 0.43$.

profiles. However, NO production for large droplets increases as they achieve elevated flame temperatures due to their higher Damkohler number. At some intermediate size, where minimum NO_x is predicted, the flame temperature and the fuel vapor concentration in the gas phase fall in between the values observed for the small and large droplets. Under this situation, droplet interactions reduce the burning rate and lower NO formation by confining its production to a thin reaction zone.

In these plots, there is little change in the nitrogen profiles as a very small amount of it reacts to form nitric oxide. A slight but gradual decline in the N_2 levels is noticed as the product gases move out radially and change the nitrogen mass fractions. Since, nitrogen is always in abundance, nitric oxide formation is primarily influenced by the gas phase temperature and oxygen concentration. The location of maximum NO formation is in the vicinity of the peak temperature, but it moves outward to regions of higher oxygen concentration as the temperature peak begins to diminish.

Similar profiles were also obtained for methanol sprays. The main difference between the methanol and n-octane results is in the relative location and the magnitude of the flame temperature. For methanol, the flame front stays very close to the droplet surface due to its high heat of vaporization. This phenomenon has also been recognized by Kesten (1972). Relative to n-octane, methanol has a lower heat of combustion which gives a lower flame temperature. These two events result in a lower NO formation for methanol. In addition, inclusion of the prompt NO formation mechanism can be expected to increase the difference, by predicting a higher contribution for n-octane.

Predicted and experimental results for n-octane, showing the effects of droplet size and air preheating temperature on NO_x formation, are compared in Figures 5.11. Although the calculated results are higher than the measured values, the general trends are in reasonable agreement. As the air preheat temperature increases, more fuel is vaporized before the flame front, leading to a rapid increase in the flame temperature and the weakening of the droplet interactions. The model also predicts the shifts of the NO_x minimum point towards larger droplet diameters with increased air preheating temperatures. In these analyses, the contribution to the total extent of preflame vaporization due to screen impaction was not considered. Such consideration requires experimental measurements of fuel droplet losses. Inclusion of this effect is expected to reduce the skewness of the predicted NO_x trends on both sides of the minimum NO_x point, thereby improving the agreement between the model and experiment.

In summary, the computed results indicate the importance of the extent of prevaporization and droplet interactions on NO_x production. Gas phase stoichiometry has a significant effect on the volume of the hot gases surrounding a fuel droplet, where NO is formed. On the other hand, the release of fuel vapor from the droplet to the reaction zone is controlled by droplet interactions which reduce the volume of the hot gases and NO production by bringing the flame closer to the droplet surface.

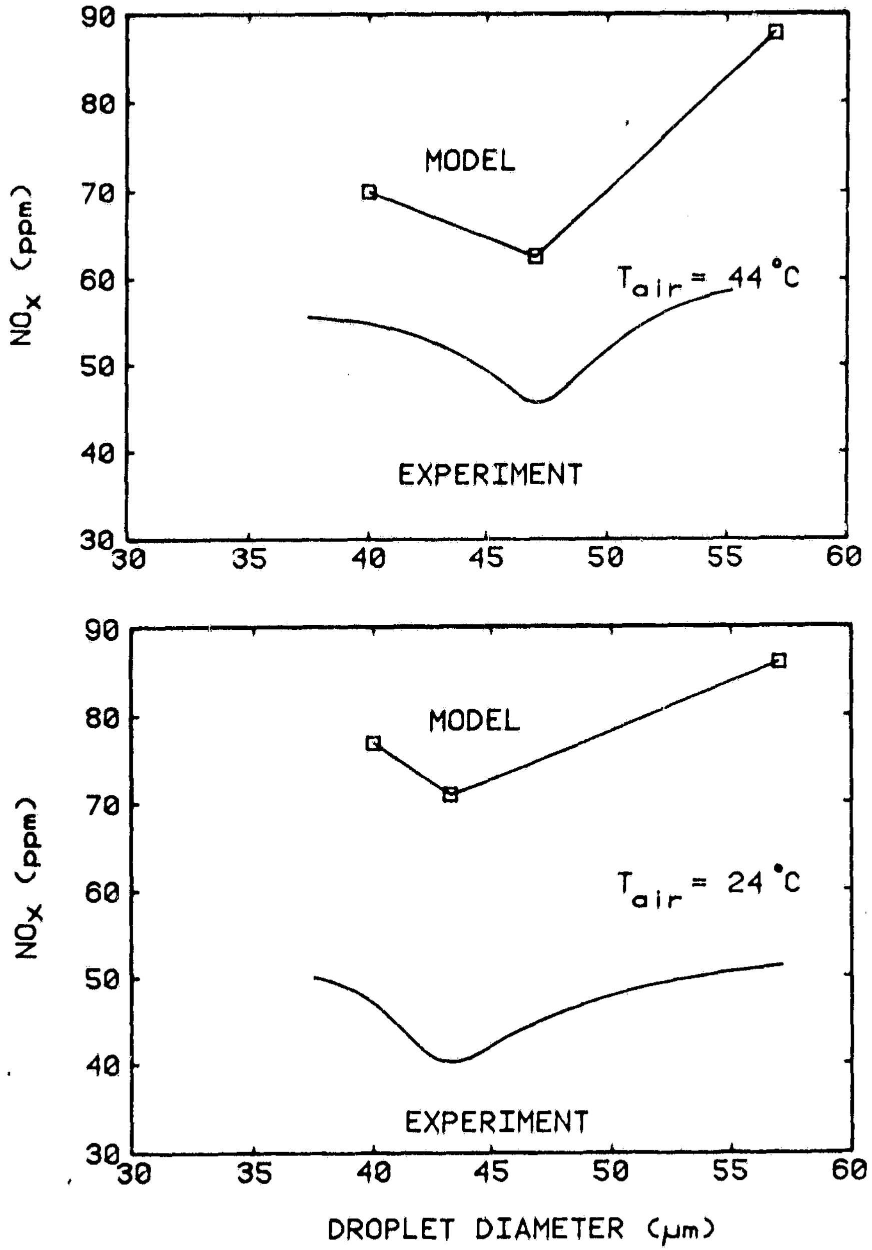

Figure 5.11. Comparison of measured and predicted NO_x concentrations at different droplet diameters and air preheat temperatures for n-octane sprays at $\phi = 1.0$.

While a qualitative agreement exists between the measurements and the predictions, the model overestimates the NO emission levels. Higher NO predictions are directly related to the greater flame temperatures computed in the model, using a single step fuel oxidation rate. The discrepancies can be remedied by the following considerations. Use of detailed kinetic mechanisms for the fuel oxidation and NO_x formation can improve the predictions significantly. An accurate determination of the actual droplet travel time in the preflame regions of the combustor is also desirable due to its importance in the evaluation of the initial conditions for this model. Also, the applicability of the spherico-symmetric governing equations is restricted to zero gravity or convection free situations. Convective effects distort the spherical flame shape which can bring about different droplet interactions and NO_x formation. A detailed analysis of the flow field around the burning droplets would be necessary in order to relax the restrictions imposed upon spherical flames.

These refinements should alleviate the differences and make the model a useful tool for defining the operating conditions at which NO_x formation is minimum.

CHAPTER 6

Conclusions and Recommendations

6.1 Conclusions

A one dimensional monodisperse fuel spray combustion facility was developed and used to study the formation of oxides of nitrogen under various operating conditions. Inflame and postflame measurements of temperature, NO and NO_x, and other emissions were made over a 26-74 μm droplet size range and different stoichiometries. Single component fuels including methanol, isopropanol, n-heptane and n-octane, as well as nitrogen-containing fuels were tested.

Postflame measurements of the exhaust gases from the combustion of nitrogen-free fuels indicated the existance of an optimum droplet diameter for lower NO_x production in the 43-58 μm droplet size range. Up to 30% reduction in the NO_x emissions, relative to the small droplet limit, was detected. The observed behavior was attributed to the effects of droplet size, gas phase stoichiometry and droplet interactions in the flame.

Extent of prevaporization determines the gas phase stoichiometry and affects the temperature and the volume of the hot gases surrounding the fuel droplets. The thickness of the reaction zone, however, is influenced further by droplet interactions which control the spray burning rate. All of these factors depend on the initial droplet diameter and the fuel evaporation characteristics. For small droplets, rapid vaporization before the flame front intensifies gas phase reactions, leading to a fast increase of temperature and NO_x production. Large droplets evaporate less, but form more NO_x as they attain higher flame temperatures during their lifetime.

Droplet interactions are weak for both small and large droplets. This is caused by rapid preflame vaporization and increased droplet spacings in the former case, and fewer interacting droplets in the case of large droplets. The optimum droplet diameter for minimum NO_x formation occurs at some intermediate size with relatively stronger interactions.

A mathematical model for the analysis of preflame droplet vaporization and NO_x formation in the combustion of nitrogen-free fuel sprays, was developed. The predicted results indicated a qualitative agreement with the measurements and demonstrated the importance of the evaporation and combustion characteristics on NO_x emissions.

With nitrogen-containing additives, the nitrogen transformation process to NO_x was less dependent on flame temperature and was influenced primarily by oxygen concentration. At high fuel-N contents, NO_x decreased continuously with increasing droplet size. For small droplets, oxidation of the pyrolysis fragments of the nitrogen additive improved as a result of higher prevaporization and better oxygen penetration through the droplet flame zone.

6.2 Recommendations for Future Work

While this study points out the potential for minimizing NO_x emissions from fuel spray combustors, further experimental and theoretical advancements are still needed before the acquired knowledge can be applied to such systems.

Suggested experimental studies and their objectives are listed below.

(a) In situ droplet sizing and number density measurements in the flame and prior to the flame is required to obtain valuable information on vaporization and burning rates of interacting fuel droplets. The number of interacting droplets that survive the screen impaction and the total extent of preflame vaporization can be determined from such measurements.

(b) Detailed analysis of combustion products and probe reactions are necessary to explain the observed NO_x consumption in the post flame regions.

(c) Polydispersed sprays and the effect of Sauter Mean Diameter on NO_x formation should be considered for their applicability to practical spray combustors.

(d) Inflame and postflame analyses of the nitrogenous species must be carried out to get a better understanding of nitrogen transformation and NO_x yield in fuel sprays that contain chemically bound nitrogen.

As far as the modeling aspect of spray combustion and NO_x formation is concerned, improvements can be achieved in several ways.

(e) A more detailed chemical model for fuel oxidation is needed to improve prediction of NO production.

(f) Flame shape distortion due to convective affects and its impact on droplet vaporization, droplet interactions and NO_x formation requires some consideration. An in-depth analysis of the flow field around the burning fuel droplets is needed to account for such phenomena.

(g) Fuel-N conversion to NO_x should be studied by implementing a comprehensive species transformation mechanism into the spray combustion model.

LIST OF REFERENCES

Appelton, J.P. and J.B. Heywood,
1973, "The Effects of Imperfect Fuel-Air Mixing in a Burner on NO Formation from Nitrogen in the Air and the Fuel," Fourteenth Symposium (International) on Combustion, p.777, The Combustion Institute, Pittsburgh, PA.

Bachmaier, F., K. H. Eberius and TH. Just,
1973, "The Formation of Nitric Oxide and the Detection of HCN in Premixed Hydrocarbon-Air Flames at 1 Atmosphere," Combustion Science and Technology 7, 77-84.

Beèr, J.M. and N.A. Chigier,
1983, Combustion Aerodynamics, Krieger, Malabar, FL.

Bellan, J. and R. Cuffel,
1983, "A Theory of Nondilute Spray Evaporation Based upon Multiple Drop Interactions," Combustion and Flame 51, 55-67.

Berglund R.N. and B.Y.H. Liu,
1973, "Generation of Monodisperse Aerosol Standards," Environmental Science and Technology 7, 147-153.

Bolt, J.A. and T.A. Boyle,
1956, "The Combustion of Liquid-Fuel Spray," Transactions of ASME, April, 609-615.

Botros, P., C.K. Law and W.A. Sirignano,
1980, "Droplet Combustion in a Reactive Environment," Combustion Science and Technology 21, 123-130.

Bowman, C.T.,
1975, "Kinetics of Pollutant Formation and Destruction in Combustion," Prog. Energy Combust. Sci. 1, 33-45.

Bracco, F.V.,
1973, "Nitric Oxide Formation in Droplet Diffusion Flames," Fourteenth Symposium (International) on Combustion, p.831, The Combustion Institute, Pittsburgh, PA.

Burgoyne, J.H. and L. Cohen,
1954, "The Effect of Drop Size on Flame Propagation in Liquid Aerosols," Proc. of The Royal Society: Series A: Mathematical and Physical Sciences 225, 375-392.

Cernansky, N.P.,
1977, "Sampling and Measuring for NO and NO_2 in Combustion Systems," Prog. in Astronautics and Aeronautics 53, AIAA, 83-102.

Cernansky, N.P. and H. Sarv,
1983, "Pollutant Formation in Monodisperse Fuel Spray Combustion," Final Report Prepared for NASA Lewis Research Center, Grant No. NAG 3-1, Drexel University, Philadelphia, PA.

Chan, L., J. Ellis and P.T. Crisp,
1984, "Determination of Nitrogen Compounds in Hydrotreated Shale Oils by Preparative High-Performance Liquid Chromatography and Gas Chromatography-Mass Spectrometry," J. Chromatography 292, 355-368.

Chan, K.K. and C.E. Polymeropoulos,
1981, "An Experimental Investigation of the Minimum Ignition Energy of Monodisperse Sprays," Paper No. 81-21, Eastern States Section, The Combustion Institute, November.

Chen, A.T. and P.C. Malte,
1984, "Influence of Fuel-N Compound Type and SO_2 on Nitrogen Reactions in Stirred Flames," Paper No. 84-86, Western States Section, The Combustion Institute, October 22-23.

Chigier, N.,
1983, "Group Combustion Models and Laser Diagnostic Methods in Sprays: A Review," Combustion and Flame 51, 127-139.

Chiu, H.H. and T.M. Liu,
1977, "Group Combustion of Liquid Droplets," Combustion Science and Technology 17, 127-142.

Chiu, H.H., H.Y. Kim and E.J. Croke,
1983, "Internal Group Combustion of Liquid Droplets," Nineteenth Symposium (International) on Combustion, p.671, The Combustion Institute, Pittsburgh, PA.

Colket, M. B. III, L. Chiappetta, R.N. Guile, M.F. Zabielski, and
1982, D.J. Seery, "Internal Aerodynamics of Gas Sampling Probes," Combustion and Flame 44, 3-14.

Crowhurst, D. and R.F. Simmons,
1983, "The Formation of NO_x From Nitrogen Containing Additives in Premixed Methane Flames," Combustion and Flame 51, 289-298.

Crowhurst, D. and R.F. Simmons,
1985a, "A Structural Study of Methane-Acetonitrile-Oxygen Diffusion Flames Diluted with Argon," Combustion and Flame 59, 167-176.

Crowhurst, D. and R.F. Simmons,
1985b, "A Structural Study of Acetonitrile-Oxygen Diffusion Flames Diluted with Argon," Twentieth Symposium (International) on Combustion, The Combustion Instititute, Pittsburgh, PA.

Dasch, C.J. and R.J. Blint,
1984, "A Mechanistic and Experimental Study of Ammonia Flames," Combustion Science and Technology 41, 223-244.

De Soete, G.G.,
1974, "Overall Reaction Rates of NO and N_2 Formation from Fuel Nitrogen," Fifteenth Symposium (International) on Combustion, p.1093, The Combustion Institute, Pittsburgh, PA.

Duterque, J., N. Avezard and R. Borghi,
1981, "Further Results on Nitrogen Oxides Production in Combustion Zones," Combustion Science and Technology 25, 85-95.

Faeth, G.M.,
1979, "Spray Combustion Models-A Review," AIAA Paper No. 79-0293, AIAA Seventeenth Aerospace Sciences Meeting, New Orleans, LA., January 15-17.

Fenimore, C.P.,
1971, "Formation of Nitric Oxide in Premixed Hydrocarbon Flames," Thirteenth Symposium (International) on Combustion, p.373, The Combustion Institute, Pittsburgh, PA.

Fenimore, C.P.,
1976a, "Effects of Diluents and Mixing on Nitric Oxide from Fuel-Nitrogen Species in Diffusion Flames," Sixteenth Symposium (International) on Combustion, p.1065, The Combustion Institute, Pittsburgh, PA.

Fenimore, C.P.,
1976b, "Reactions of Fuel-Nitrogen in Rich Flame Gases," Combustion and Flame 26, 249-256.

Foster, D.E. and J.C. Keck,
1980, "Factors Affecting NO_x Formation from Nitrogen-Containing Fuels," Combustion and Flame 38, 199-209.

Fristrom, R.M. and A.A. Westenberg,
1965, Flame Structure, McGraw-Hill, New York, NY.

Godsave, G.A.E.,
1953, "Studies of the Combustion of Drops in a Fuel Spray- The Burning of Single Drops of Fuel," Fourth Symposium (International) on Combustion, p.818, The Williams & Wilkins Co., Baltimore, MD.

Gustaferro, J.F.,
1982, "U.S. Energy for the Rest of the Century," Office of Competitive Assesment, Office of Economic Affairs, U.S. Department of Commerce, July 2.

Hayashi, S., S. Kumagai and T. Sakai,
1976, "Propagation Velocity and Structure of Flames in Droplet-Vapor-Air Mixtures," Combustion Science and Technology 15, 169-177.

Hayhurst, A.N. and I.M. Vince,
1983, "The Origin and Nature of "Prompt" Nitric Oxide in Flames," Combustion and Flame 50, 41-57.

Haynes, B.S.,
1977a, "Reactions of Ammonia and Nitric Oxide in the Burnt Gases of the Fuel-Rich Hydrocarbon-Air Flames," Combustion and Flame 28, 81-91.

Haynes, B.S.,
1977b, "Production of Nitrogen Compounds from Molecular Nitrogen in Fuel-Rich Hydrocarbon-Air Flames," Fuel 56, 199-203.

Hori, M.,
1980, "Effects of Probing Conditions on NO_2/NO_x Ratios," Combustion Science and Technology 23, 131-135.

Kanevsky, J.,
1956, "Interference During Burning in Air for Nine Stationary Fuel Droplets Arranged in a Body-Centered Cubic Lattice," Jet Propulsion 26, 788.

Kent, J.A.,
1970, "A Noncatalytic Coating for Platinum-Rhodium Thermocouples," Combustion and Flame 14, 279-282.

Kesten, A.S.,
1972, "Analysis of NO Formation in Single Droplet Combustion," Combustion Science and Technology 6, 115-123.

Koshland, C.P. and C.T. Bowman,
1983, "Combustion of Monodisperse Droplet Clouds in a Reactive Environment," Paper No. 83-43, Western States Section/ The Combustion Institute, October 17-18.

Koshland, C.P. and C.T. Bowman,
1985, "Combustion of Monodisperse Droplet Clouds in a Reactive Environment," Twentieth Symposium (International) on Combustion, The Combustion Institute, Pittsburgh, PA.

Kumagai, S. and H. Isoda,
1956, "Combustion of Fuel Droplets in a Falling Chamber," Sixth Symposium (International) on Combustion, P.726, Chapman and Hall, London.

Labowsky, M.,
1976, "The Effects of Nearest Neighbor Interactions on the Evaporation Rates of Cloud Particles," Chemical Engineering Science 31, 803-813.

Labowsky, M.,
1978, "A Formalism for Claculating the Evaporation Rates of Rapidly Evaporating Interacting Particles," Combustion Science and Technology 18, 145-151.

Labowsky, M.,
1980a, "Calculation of the Burning Rates of Interacting Fuel Droplets," Combustion Science and Technology 22, 217-226.

Labowsky, M.,
1980b, "Transfer Rate Calculations for Compositionally Dissimilar Interacting Particles," Chemical Engineering Science 35, 1041-1048.

Law, C.K.,
1977, "Adiabatic Spray Vaporization with Droplet Temperature Transient," Combustion Science and Technology 15, 65-74.

Law, C.K. and W.A. Sirignano,
1977, "Unsteady Droplet Combustion with Droplet Heating-II: Conduction Limit," Combustion and Flame 28, 175-186.

Lorell, J., H. Wise and R.E. Carr,
1956, "Steady-State Burning of a Liquid Droplet. II. Bipropellant Flame," J. of Chemical Physics 25, 2, 325-331.

Marberry, M., A.K. Ray and K. Leung,
1984, "Effect of Multiple Particle Interactions on Burning Droplets," Combustion and Flame 57, 237-245.

Mellor, A.M.,
1980, "Semi-Empirical Correlations for Gas Turbine Emissions, Ignition, and Flame Stabilization," Prog. Energy Combust. Sci. 6, 347-358.

Miyasaka, K. and C.K. Law,
1981, "Combustion of Strongly-Interactive Linear Droplet Arrays," Eighteenth Symposium (International) on Combustion, p.283, The Combustion Institute, Pittsburgh, PA.

Murphy, M.J. and G.L. Borman,
1979, "Oxides of Nitrogen Emission from a Burning Fuel Mist," Combustion Science and Technology 21, 53-63.

Nicholls, J.A., C.W. Kauffman, D.G. Pellaccio, D.R. Glass and
1980, J.F. Driscoll, "The Effect of Fuel Sprays on Emissions From a Research Gas Turbine Combustor," Combustion Science and Technology 23, 203-213.

Nizami, A.A. and N.P. Cernansky,
1978, "A Monodisperse Spray Combustion System and the Measurement of Oxides of Nitrogen," Paper No. 78-37, Western States Section, The Combustion Institute.

Nizami, A.A. and N.P. Cernansky,
1979, "NO_x Formation in Monodisperse Fuel Spray Combustion," Seventeenth Symposium (International) on Combustion, p.475, The Combustion Institute, Pittsburgh, PA.

Nizami, A.A., S. Singh and N.P. Cernansky,
1982, "Formation of Oxides of Nitrogen in Monodisperse Spray Combustion of Hydrocarbon Fuels," Combustion Science and Technology 28, 97-106.

Nuruzzaman, A.S.M., A.B. Hedley and J.M. Beer,
1971, "Combustion of Monosized Droplet Streams In Stationary Self-Supporting Flames," Thirteenth Symposium (International) on Combustion, p.787, The Combustion Institute, Pittsburgh, PA.

Opdyke, G. Jr.,
1983, "Private Communication," AVCO, Lycoming Division, Stratford, CT.

Perry, R.H. and C.H. Chilton (ed.),
1973, Chemical Engineer's Handbook, McGraw-Hill, New York, NY.

Peterson, R.C. and N.M. Laurendeau,
1982, "A Kinetic Mechanism for Fuel-Nitrogen Conversion in Lean to Rich Flames," Paper No. 82-15, Central States Section/ The Combustion Institute, March.

Polymeropoulos, C.E. and S. Das,
1975, "The Effect of Droplet Size on the Burning Velocity of Kerosene-Air Sprays," Combustion and Flame 25, 247-257.

Rao, K.V.L. and A.H. Lefebvre,
1981, "Spontaneous Ignition Delay Times of Hydrocarbon Fuel/Air Mixtures," Paper No. 81-03, Central States Section/ The Combustion Institute, March 23-24.

Sangiovanni, J.J. and M. Labowsky,
1982, "Burning Time of Linear Droplet Arrays: A Comparison of Experiment and Theory," Combustion and Flame 47, 15-30.

Sapre, A.R. and A.A. Quader,
1983, "Conversion of Fuel Nitrogen to NO in Automotive Engines," SAE Paper No.831675.

Sirignano, W.A.,
1983, "Fuel Droplet Vaporization and Spray Combustion Theory," Prog. Energy Combust. Sci. 9, 291-322.

Spalding, D.B.,
1953, "The Combustion of Liquid Fuels," Fourth Symposium (International) on Combustion, p.847, The Williams & Wilkins Co., Baltimore, MD.

Thermo Systems Inc.,
1977, Instruction Manual for Model 3050 Berglund-Liu Vibrating Orifice Monodisperse Aerosol Generator, St. Paul, MN.

Tuttle, J.H., M.B. Colket, R.W. Bilger and A.M. Mellor,
1976, "Characteristic Times for Combustion and Pollutant Formation in Spray Combustion," Sixteenth Symposium (International) on Combustion, p.209, The Combustion Institute, Pittsburgh, PA.

Umemura, A., S. Ogawa and N. Oshima,
1981a, "Analysis of the Interaction Between Two Burning Droplets," Combustion and Flame 41, 45-55.

Umemura, A., S. Ogawa and N. Oshima,
1981b, "Analysis of the Interaction Between two Burning Droplets with Different Sizes," Combustion and Flame 43, 111-119.

Westbrook, C. K. and F. L. Dryer,
1984, "Chemical Kinetic Modeling of Hydrocarbon Combustion," Prog. Energy Combust. Sci 10, 1-57.

Williams, A.,
1973, "Combustion of Droplets of Liquid Fuels: A Review," Combustion and Flame 21, 1, 1-31.

Williams, F.A.,
1965, Combustion Theory, Addison-Wesley, Reading, MA.

Xiong, T.Y., C.K. Law and K. Miyasaka,
1985, Interactive Vaporization and Combustion of Binary Droplet Systems," Twentieth Symposium (International) on Combustion, The Combustion Institute, Pittsburgh, PA.

APPENDIX A

Supporting Experimental Facility

A.1 Introduction

The major components of the experimental setup, i.e., the monodisperse aerosol generator and the temperature and NO_x measurement systems, were described in Chapter 3. This appendix provides a description of additional facilities including a fuel prevaporizer and other exhaust gas analyzers.

A.2 Fuel Prevaporizing System

In order to determine the small droplet size limit, a fuel/air heating arrangement was added to the experimental facility. This set up provided prevaporized/premixed fuel/air mixtures by combining the liquid fuel and air in a tee and heating the mixture in a stainless steel tube. The tube was formed into a vertical three-loop helix and wrapped with heating tape. The fuel vapor was heated to about 65°C before entering the burner through the normal dispersion air path. This heating was sufficient to keep the mixture above the dew point of the fuel and to avoid condensation of the fuel vapor on the combustor walls. Normal cooling of the fuel vapor in the combustor resulted in a mixture temperature of about 26°C at the flame holder exit.

A.3 Sampling and Measurements of Exhaust Gases (UHC, CO, CO_2 and O_2)

Inflame and postflame combustion gases were sampled and analyzed for hydrocarbons, carbon monoxide, carbon dioxide and oxygen concentrations. Hydrocarbons were measured as propane using a heated flame ionization detector (Beckman Model 402). CO and CO_2 were measured using nondispersive infrared analyzers (Horiba Models AIA-21-AS and AIA-21, respectively). O_2 concentration was measured using a polarographic analyzer (Teledyne Model 326AL). Due to the high flow requirements by the analyzers, the combustion gases were sampled under atmospheric pressure using a 3.17 mm (O.D.) stainless steel tube with a 2 mm opening at its tip.

APPENDIX B

Complementary Results

B.1 Introduction

This appendix reports experimental results taken in addition to those presented in Chapter 4. In particular, the effects of fuel nitrogen content and droplet size on the NO_x flame structure are demonstrated in section B.2, while the results of the exhaust emission measurements for a number of operating conditions are given in section B.3.

B.2 Axial NO, NO_x and Temperature Profiles for Fuel-N Additives

Representative results for the axial variations of temperature, NO and NO_x concentrations for n-heptane droplets doped with 1% nitrogen by weight as pyridine, were shown in Figures 4.24 and 4.25. Additional results at different fuel-N contents are shown in Figures B.1-B.5. After a rapid increase with temperature in the flame zone, NO and NO_x reduce gradually in the post flame regions to their steady state levels. Results for different size droplets indicate that more fuel-N converts to NO_x at smaller diameters. These general trends are similar to those discussed previously in sections 4.6 and 4.7.2.

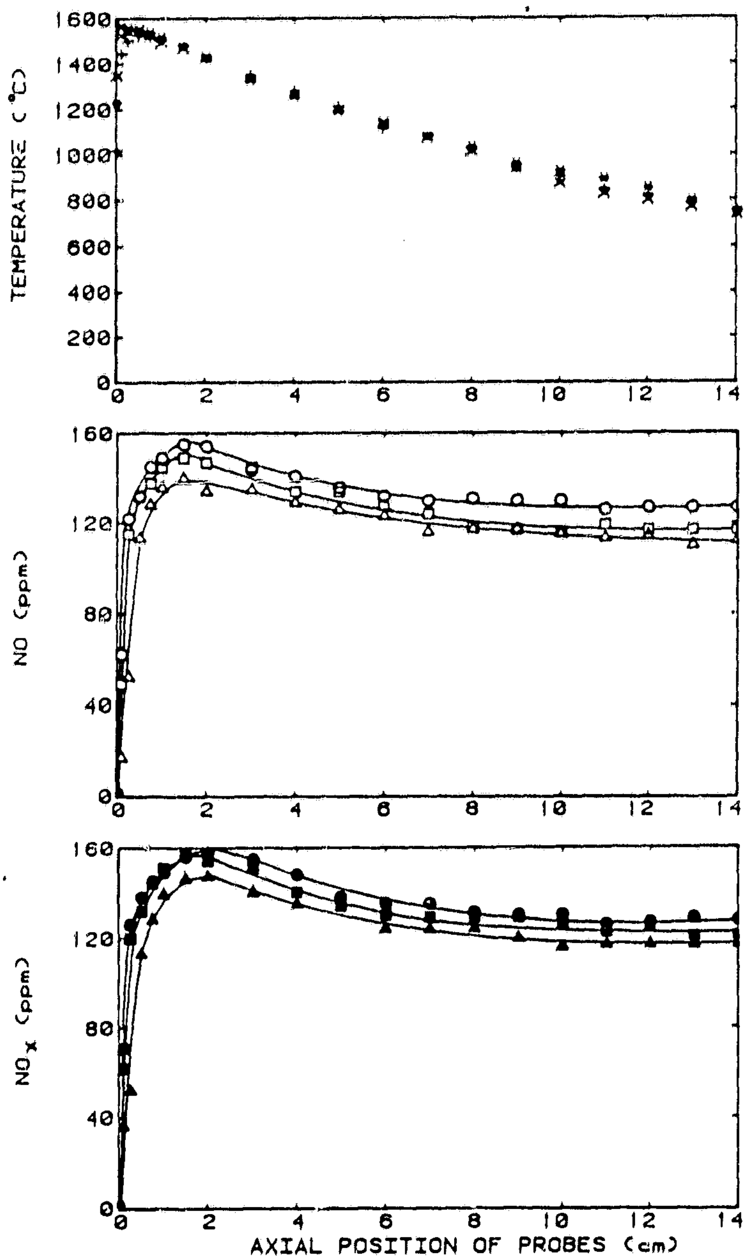

Figure B.1. Centerline NO, NO_x and temperature profiles for n-heptane doped with pyridine (0.1% N by weight). o , •,* - D = 37.0 μm; □,■,x - D = 49.5 μm; △ ,▲,+ - D = 69.6 μm.

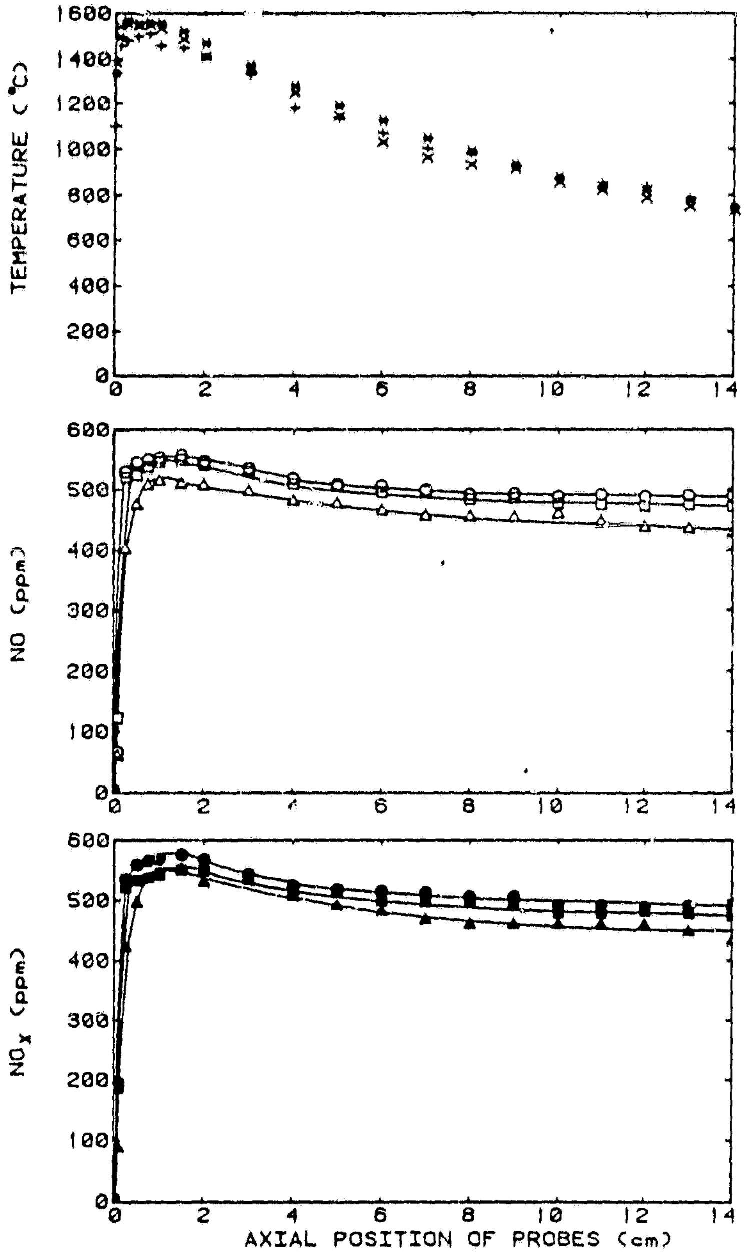

Figure B.2. Centerline NO, NO_x and temperature profiles for n-heptane doped with pyridine (0.5% N by weight). o, ●, * – D = 37.0 μm; □, ■, x – D = 49.5 μm; △, ▲, + – D = 69.6 μm.

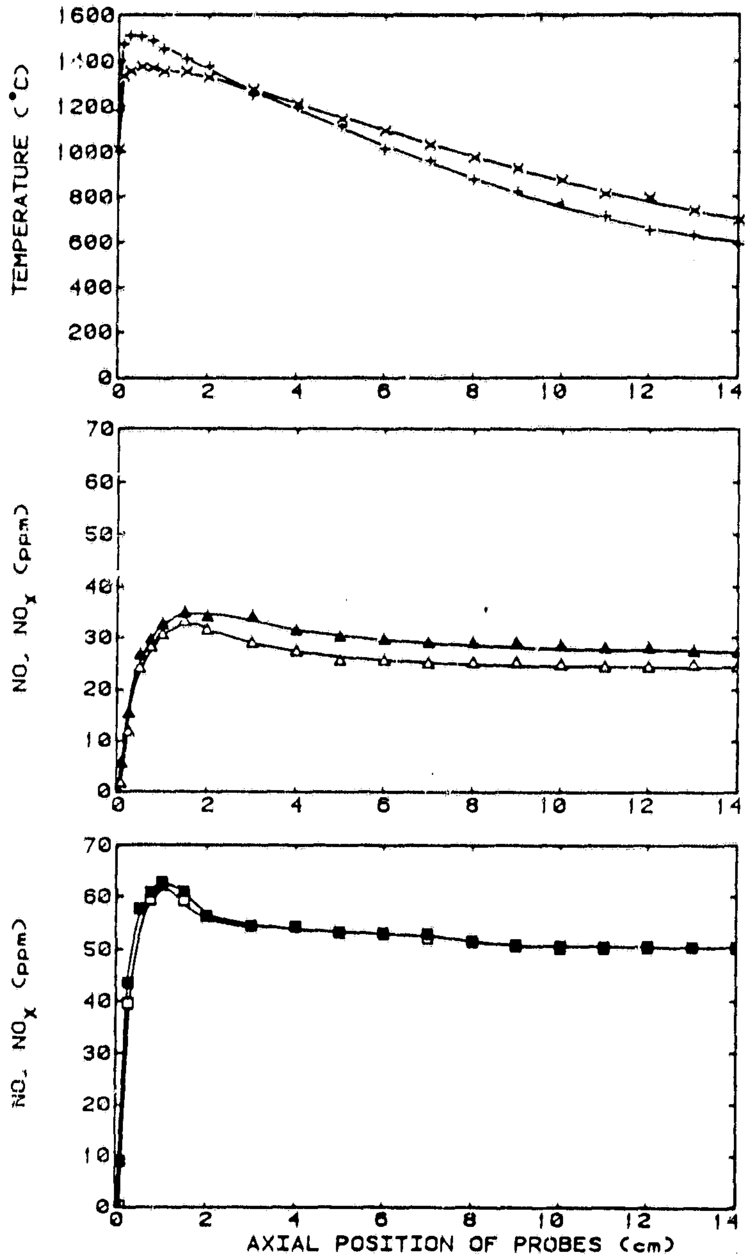

Figure B.3. Centerline NO, NO_X and temperature profiles for 37 μm n-heptane droplets. □,■,x – Φ = 0.85; △,▲,+ – Φ = 1.2.

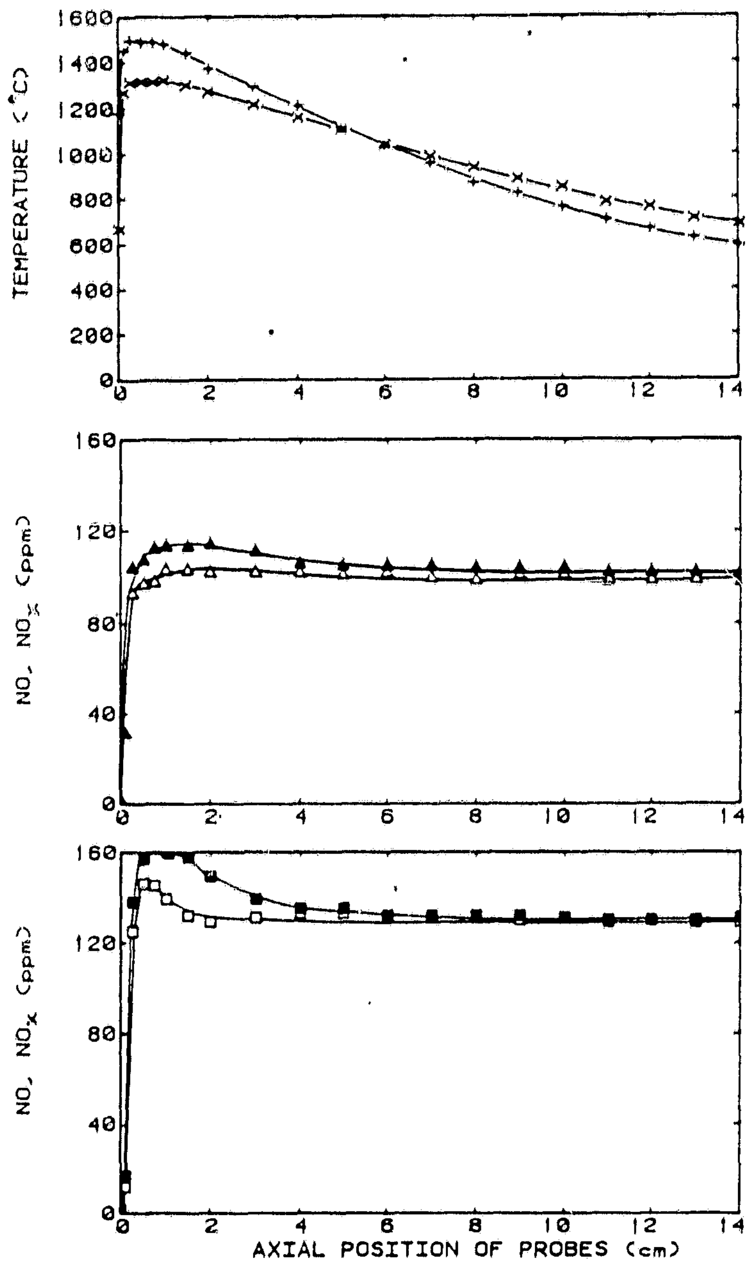

Figure B.4. Centerline NO, NO_x and temperature profiles for 37 μm n-heptane droplets doped with pyridine (0.1% N by weight). □,■,x $-\phi = 0.85$; △,▲,+ $- \phi = 1.2$.

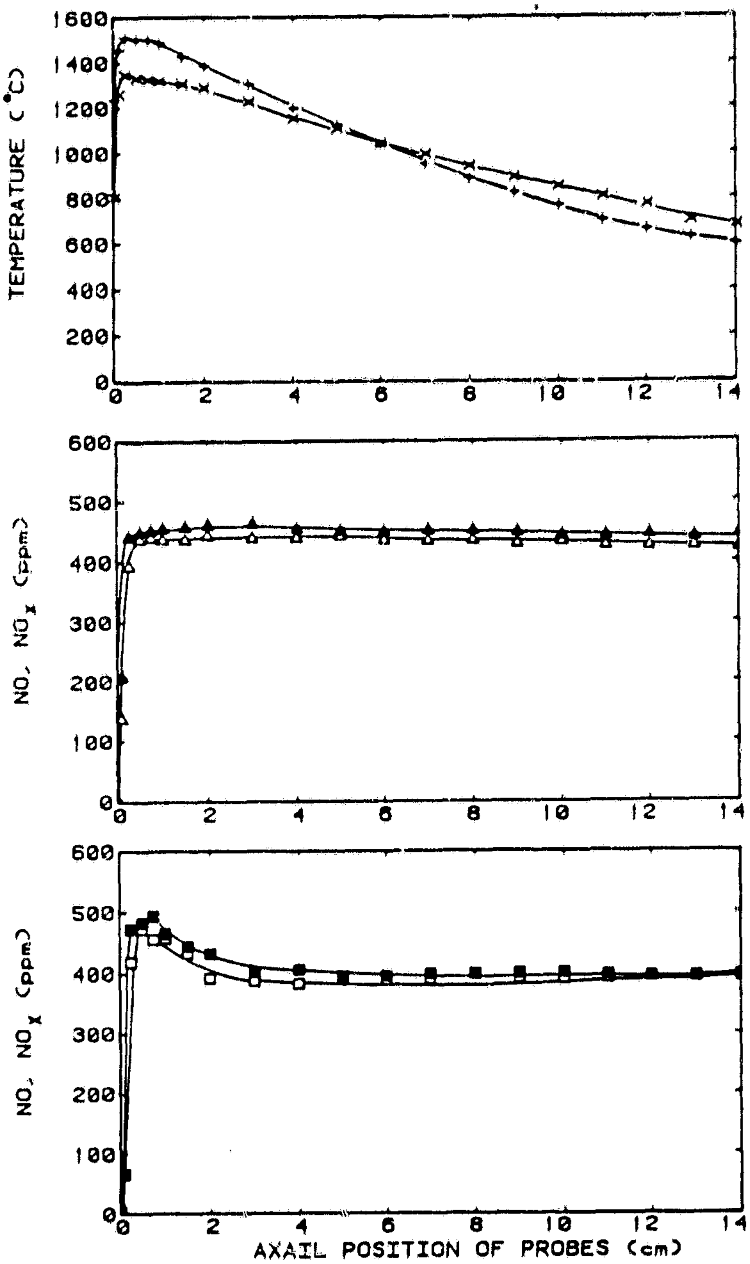

Figure B.5. Centerline NO, NO_x and temperature profiles for 37 μm n-heptane droplets doped with pyridine (0.5% N by weight). □,■,x $-\phi = 0.85$; △,▲,+ $-\phi = 1.2$.

B.3 Exhaust Emission Measurements

Exhaust gas analyses along the burner centerline were carried out in order to determine the local equivalence ratios and combustion efficiencies. Concentrations of major products and reactants including unburned hydrocarbons, CO, CO_2 and O_2 were determined from the combustion products of n-octane aerosols for different stoichiometries and droplet sizes. The hydrocarbon sampling line was heated and therefore, the measurements are on a wet basis. The CO, CO_2 and O_2 measurements, however, are on dry basis, since water was condensed and removed from the sampled gases before they were analyzed.

Figure B.6 and B.7 show the effect of equivalence ratio on the axial variations of UHC, CO, CO_2 and O_2 concentrations in a 37 μm aerosol of n-octane. The results demonstrate a rapid increase in CO and CO_2 with a substantial reduction in O_2 and UHC* concentrations in the flame zone. Further consumption of O_2, UHC and CO occurred in the post flame regions with CO_2 values reaching steady levels at about 5 cm above the flame holder. For lean and stoichiometric mixtures, the exit plane CO measurements were very low (order of ppm's), but increased for rich mixtures. On the other hand, the hydrocarbon emissions were consistently low for different equivalence ratios, indicating complete combustion for all cases.

---

* The UHC emission measurements are shown only for the post flame regions. Large fluctuations in the UHC readings were observed near the flame zone where fuel droplets were drawn into the sampling probe, due to the high sampling flow requirements by the hydrocarbon analyzer.

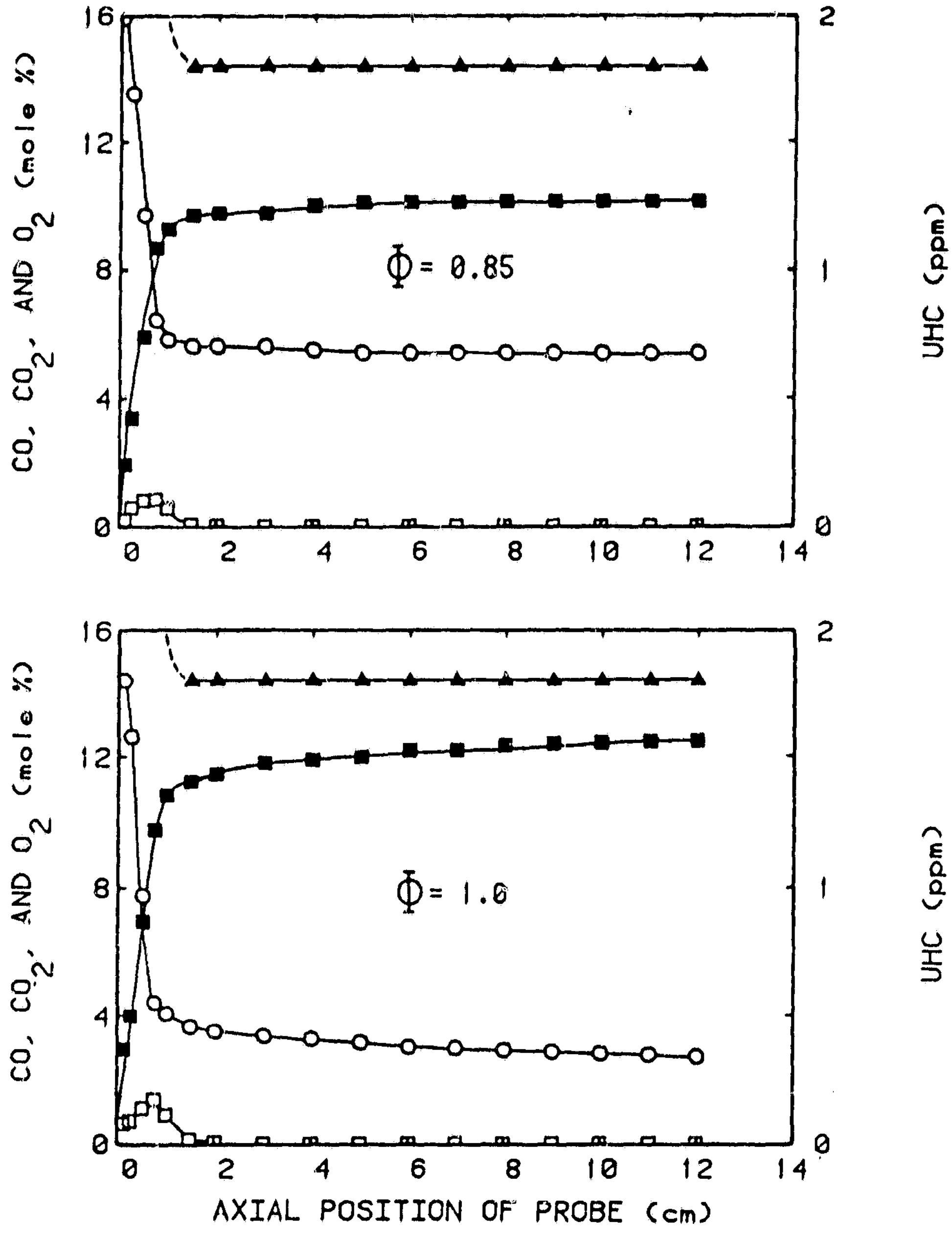

Figure B.6. Effect of equivalence ratio on centerline CO, CO_2, O_2 and UHC profiles for 37 μm n-octane droplets. □ - CO; ■ - CO_2; o - O_2; ▲ - UHC.

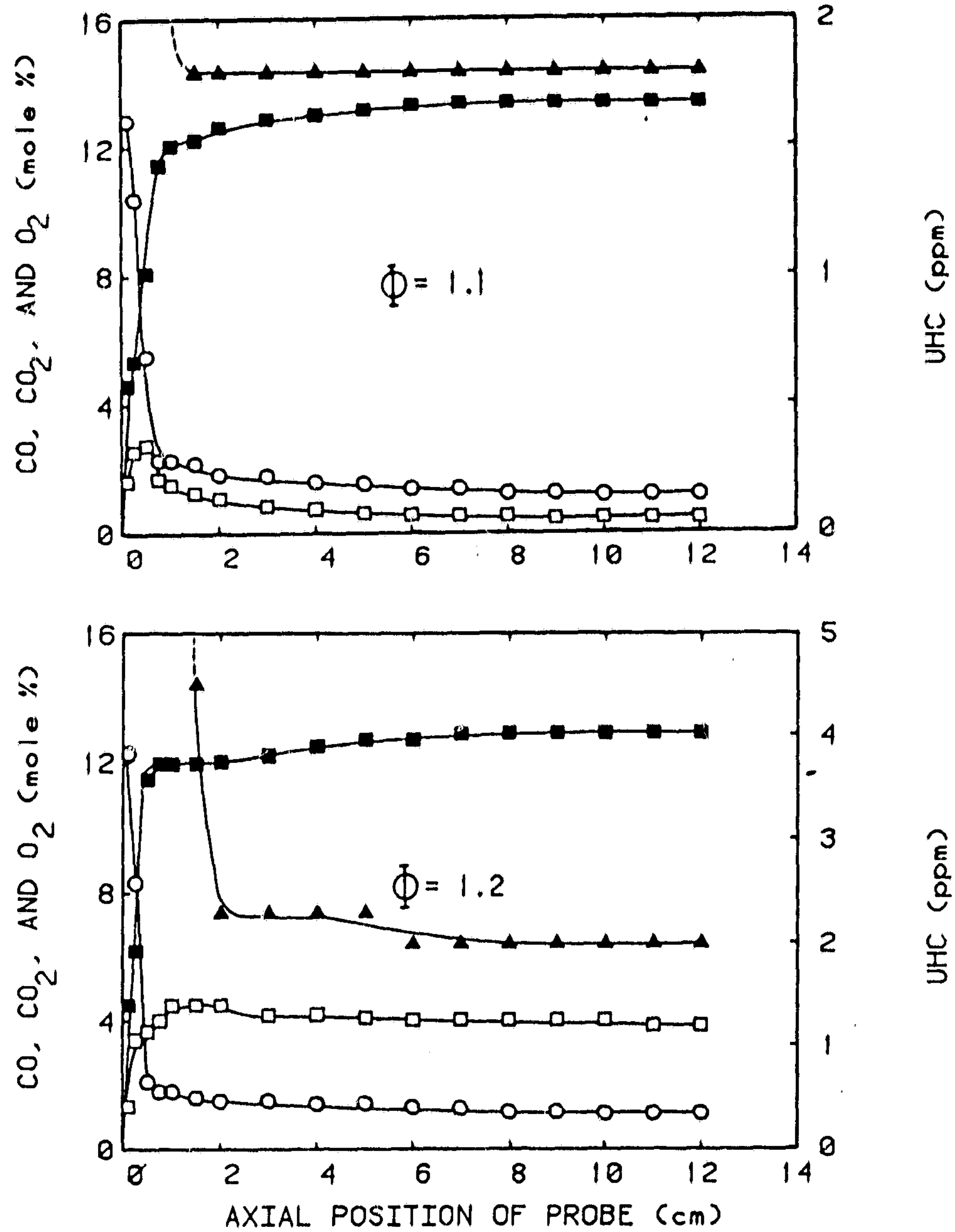

Figure B.7. Effect of equivalence ratio on centerline CO, CO_2, O_2 and UHC profiles for 37 μm n-octane droplets. □ - CO ; ■ - CO_2; o - O_2; ▲ - UHC.

The effect of droplet diameter on exhaust emissions was examined at an equivalence ratio of 1.0. Figure B.8 shows the UHC, CO, CO_2 and O_2 measurements at 10 cm above the flame holder. The highest CO and O_2 , and lowest CO_2 concentrations were observed around 43 μm droplet diameter (i.e., the observed NO_X minimum point for n-octane at ϕ=1.0). This behavior is caused as a result of increased droplet interactions and suppressed flame temperature which lead to reduced O_2 consumption and higher CO formation. Hydrocarbon concentrations appear to increase with increasing droplet diameter.

Computed equivalence ratios, based on the exhaust gas analysis, are about 12% leaner than the measured input values. However, gas chromatographic analyses of the exhaust gases for CO_2 and CO concentrations, revealed only a 3% difference in the overall stoichiometry relative to the measured input values, which is well within the accuracy of the measurments. The discrepancy in the measurements by the exhaust analyzer is due to instrumentation and calibration errors. However, this does not bias the above discussion, since, it is based solely on the relative changes of concentrations rather than the absolute values.

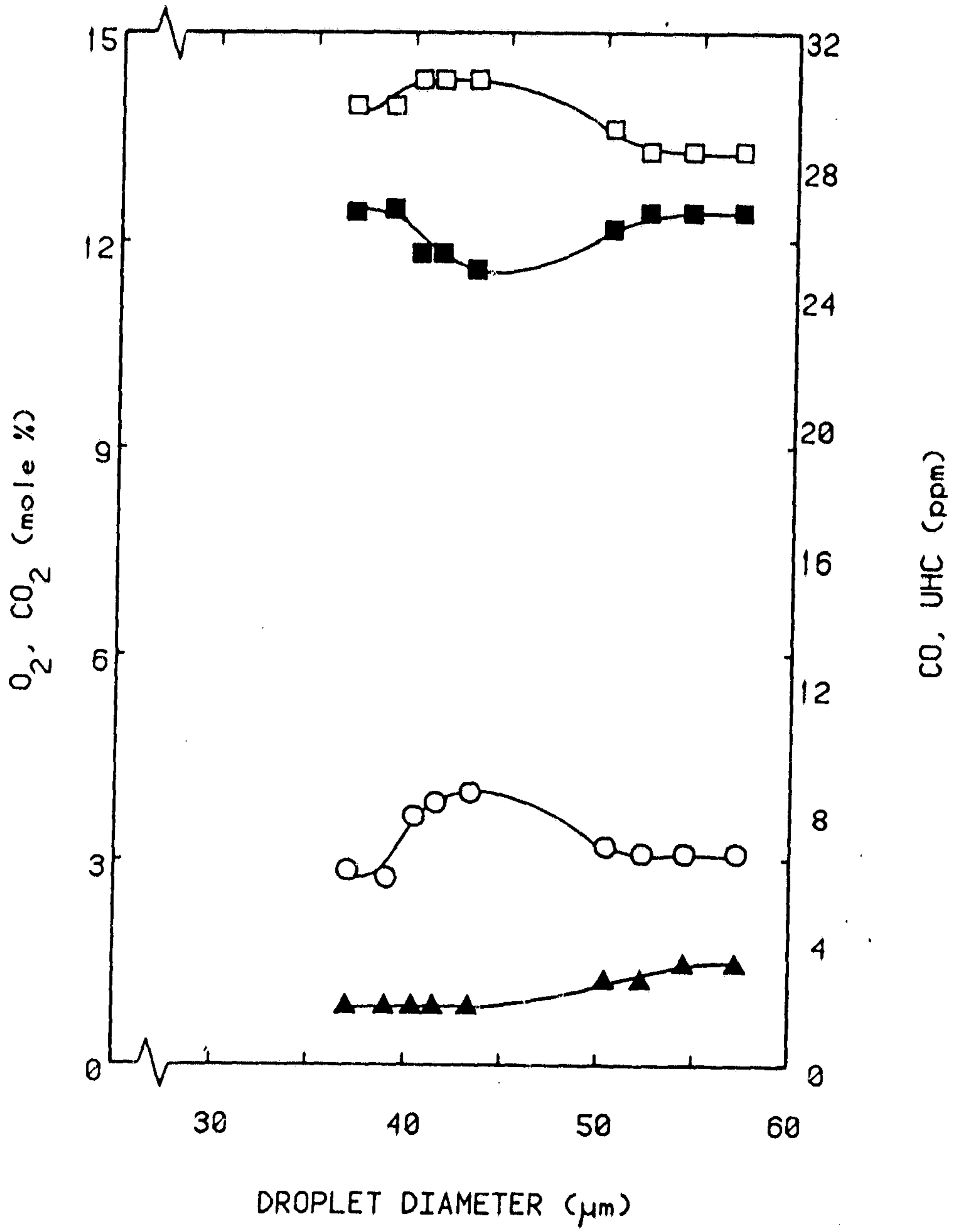

Figure B.8. Droplet size effect on postflame CO, CO_2, O_2 and UHC, for n-octane at $\phi = 1.0$.
□ - CO ; ■ - CO_2; o - O_2; ▲ - UHC.

APPENDIX C

Thermophysical Property Calculations

Certain properties of liquids, such as latent heat of vaporization and vapor pressure, are influenced primarily by temperature. For a mixture of ideal gases, transport properties vary not only with temperature, but also with concentration of the individual components of the mixture. These variations were included in the analytical computations.

The temperature dependence of each property was established as a polynomial expression which fit the tabulated data with best accuracy. At any given temperature, for known species concentrations, the multicomponent transport properties are calculated based on the following formulae (Perry and Chilton, 1973)

density:

$$\rho = \frac{P}{R^{\circ} T \sum_{j=1}^{N'} Y_j / W_j}$$

specific heat:

$$c_p = \sum_{j=1}^{N'} Y_j \, c_{p_j}$$

thermal conductivity:

$$K = \frac{\sum_{j=1}^{N'} X_j K_j W_j^{1/3}}{\sum_{j=1}^{N'} X_j W_j^{1/3}}$$

absolute viscosity:

$$\mu = \frac{\sum_{j=1}^{N'} X_j \mu_j W_j^{1/2}}{\sum_{j=1}^{N'} X_j W_j^{1/2}} .$$

These values were updated during the computations to account for changes in temperature and species concentrations.

APPENDIX D

Temperature Corrections

As pointed out in Chapter 3, a bare Pt/Pt-13% Rh thermocouple was used for temperature measurements. The results presented in Chapter 4 indicate that all temperature readings and, in particular, the maximum flame temperatures are lower than expected. Several factors including convective heat losses to the gas sampling probe, conductive heat losses along the thermocouple wires, radiative heat losses from the thermocouple junction and catalytic reactions on the surface of the junction are considered to be responsible for the discrepancy. The latter case was found to be important only with new thermocouples. Catalytic activity on the thermocouple junction was tested in a manner similar to Kent (1970). After inserting a thermocouple into a flame, the flame was blown out, leaving the thermocouple exposed to the cold fuel/air mixture. It was noticed that while aged thermocouples cooled down quickly to the gas temperature, new ones continued to glow at a temperature of about 800°C, indicating surface reactions on the junction. Reduced catalytic effects were observed after a few hours of operation at high temperatures.

The actual temperature is often calculated from an energy balance on the thermocouple junction (Fristrom and Westenberg, 1965). This requires a knowledge of the local gas properties as well as the emissivity of the junction, which are generally difficult to evaluate. As a result, any correction determined by this method is subject to a high level of uncertainty.

Instead, a more direct approach was taken to estimate the true temperature. Four Pt/Pt-13% Rh thermocouple wires with different wire diameters (0.05 to 0.25 mm), but equal lengths (30 cm), were used to measure the flame temperature of a Bunsen burner at a fixed location. The bead diameter of each thermocouple was approximately 50% larger than the wire diameter. Figure D.1 shows the variations of the flame temperature with the wire diameter. As expected, the losses are lower with smaller wires. In fact, the small heat dissipation resulted in the melting of the 0.05 mm thermocouple wires shortly after a maximum temperature of 1781°C was measured. From these results, the actual flame temperature can be estimated by extrapolating the experimental trend to a thermocouple bead of zero diameter. With the 0.075 mm thermocouple, the combined conductive and radiative corrections are estimated to be about 72°C at a measured flame temperature of 1772°C.

Another source of error in the reported data is related to the interference of the stainless steel gas sampling probe. The probe, as shown previously in Figure 3.2, was adjacent to the thermocouple and is believed to have acted as a heat sink, reducing the convective heat transfer to the thermocouple bead. Without the probe, the Bunsen burner flame temperature was about 222°C higher than that measured in its presence.

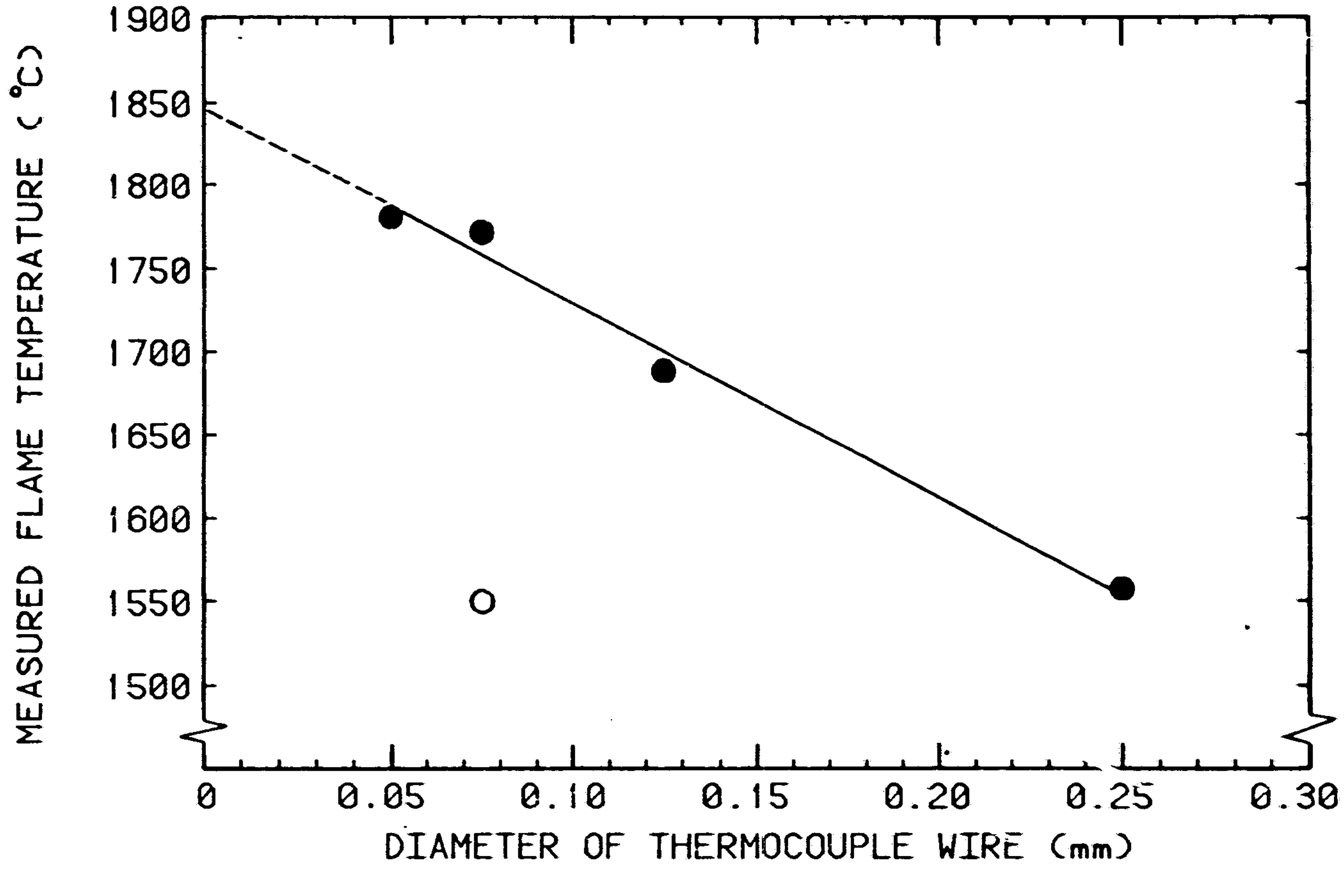

Figure D.1. Effect of gas sampling probe and thermocouple wire diameter on flame temperature measurements.
o – With; ● – Without the gas sampling probe.

In summary, the total corrections for a measured temperature of 1550°C could be as high as 294°C. This amounts to an absolute temperature of about 2117°K which is close to the maximum adiabatic flame temperature. However, these corrections are not constant and require reevaluation at other temperatures. With respect to the volume of the temperature data collected in this study, determination of the actual temperature for all measurements was found to be impractical and, therefore, was not pursued.

APPENDIX E

Computer Programs

E.1 Droplet Interactions

FORTRAN Variable		Definition
A	(N,N)	Interaction matrix.
AL1		Distance between source and particle I.
ETA		Average array burning rate correction factor.
I		Particle index.
IG		Index for number of source generation.
IGEN		Total number of source generation.
J		Particle index.
JJ		Particle index.
K		Index for total number of sources per generation.
K1		Source index in previous generation.
L		Particle index.
N		Number of particles.
R	(N)	Radius of particle I.
S	(IG,K)	Strength of source S.
X	(IG,K)	x-coordinate of source S.
X0	(N)	x-coordinate of particle I.
Y	(IG,K)	y-coordinate of source S.
Y0	(N)	y-coordinate of particle I.
Z	(IG,K)	z-coordinate of source S.
Z0	(N)	z-coordinate of particle I.

```
      PROGRAM INTERACT
C
C     ***********************************************************
C     * PROGRAM TO ACCOUNT FOR DROPLET INTERACTIONS IN ARRAYS *
C     *       OF MONODISPERSE OR POLYDISPERSE DROPLETS        *
C     ***********************************************************
C
       DIMENSION X(19,9000),Y(19,9000),Z(19,9000),X0(19),Y0(19)
       DIMENSION Z0(19),A(19,19),R(19),S(19,9000)
       READ(7,*) N
       READ (7,*) IGEN
       DO 10 I=1,N
 10    READ (7,*) X0(I),Y0(I),Z0(I),R(I)
      DO 11 L=1,N
       A(L,L)=R(L)
       I=L+1
       DO 12 J=1,N-1
       X(1,J)=X0(L)
       Y(1,J)=Y0(L)
      Z(1,J)=Z0(L)
       S(1,J)=R(L)
  12   CONTINUE
       DO 13 IG=2,IGEN
       K1=(N-1)**(IG-2)
       DO 14 K=1,(N-1)**(IG-1)
       IF (I.LE.N) GOTO 50
       I=1
  50   AL1=SQRT((X(IG-1,K1)-X0(I))**2+(Y(IG-1,K1)-Y0(I))**2
     * +(Z(IG-1,K1)-Z0(I))**2)
       S(IG,K)=-R(I)*S(IG-1,K1)/AL1
       IF (I.NE.L) GOTO 60
      A(I,I)=A(I,I)+S(IG,K)
      GO TO 70
  60  A(L,I)=A(L,I)+S(IG,K)
  70   X(IG,K)=X0(I)-R(I)*R(I)*((X0(I)-X(IG-1,K1))/AL1**2)
       Y(IG,K)=Y0(I)-R(I)*R(I)*((Y0(I)-Y(IG-1,K1))/AL1**2)
      Z(IG,K)=Z0(I)-R(I)*R(I)*((Z0(I)-Z(IG-1,K1))/AL1**2)
      IF (FLOAT(K)/(N-1).NE.INT(K/(N-1))) GOTO 80
       K1=K1-1
  80   I=I+1
  14   CONTINUE
  13   CONTINUE
  11   CONTINUE
      WRITE (5,350)
 350  FORMAT (' THE INTERACTION MATRIX ,ALPHA :')
      ETA=0.0
      DO 19 I=1,N
       WRITE (5,300) (A(I,JJ),JJ=1,N)
      DO 19 J=1,N
      ETA=ETA+A(I,J)
  19   CONTINUE
```

```
300    FORMAT (19F7.3)
      WRITE (5,400) ETA/N
400    FORMAT (/,' ARRAY AVERAGE CORRECTION FACTOR =',F6.4)
       STOP
       END
```

E.2 Spray Vaporization

FORTRAN Variable		Definition
A	(N)	$\beta - \gamma$.
A1		Locally defined variable.
ADIAB		Adiabatic/non adiabatic vaporization flag.
AIRFLO		Air flow rate at a given axial location.
AIRMIX	(3)	Curve fit constants for dilution air entrainment.
B	(N)	$1+2\gamma$.
BETA	(N)	Vector of intermediate coefficients β.
BHRAT		Burner diameter to height ratio.
BNO		Evaporation mass transfer number.
C	(N)	$-\beta-\gamma$.
C1		Defined by equation 5-15.
C2		Defined by equation 5-16.
C3		Locally defined variable.
CCONFG	(2)	Curve fit constants for conductivity of fuel vapor as f(T).
CCPFG	(2)	Curve fit constants for specific heat of fuel vapor as f(T).
CHT	(5)	Curve fit constants for distance above orifice as f(TAU).
CLAT	(3)	Curve fit constants for heat of vaporization as f(T)
CON1		Locally defined variable.
CON2		Locally defined variable.
CONG		Conductivity of gas phase.
CONL		Conductivity of liquid fuel.
CONST2		Locally defined variable.
CONST3		Locally defined variable.
CPF		Specific heat of liquid fuel.
CPG		Specific heat of gas phase.
CVAP	(5)	Curve fit constants for vapor pressure as f(T).
CVISFG	(2)	Curve fit constants for fuel vapor viscosity as f(T).
D	(N)	Coefficient vector containing elements of TD.
D1		Locally defined variable.
D2		Locally defined variable.
DELU		U2-U1.
DIFF		Diffusivity.
DISAIR		Dispersion air flow rate.
DR		Radial spacing.
DT		Ramped time increment.
DT0		Initial time increment.
DTINC		Time increment multiplier.
EXTENT		Extent of prevaporization.
F1		Locally defined variable.
F2		Locally defined variable.
FMW		Molecular weight of fuel.
FNAME		Chemical name of fuel.
GAMMA	(N)	vector of intermediate coefficients γ.

FORTRAN Variable		Definition
HT		Burner height.
HTVAP		Heat of vaporization.
I		Local index.
IFP1		Locally defined variable.
JTIME		Time index.
L		Local index.
N		No. of radial meshes.
N2MW		Molecular weight of N2.
NTIME		No. of time steps.
O2MW		Molecular weight of O2.
P		Total pressure.
PRNO		Prandtl No.
PVAPOR		Vapor pressure.
R		Radial position.
REDHT		Height of the reducing section.
REYNO		Reynolds No.
RHOG		Gas phase density.
RHOL		Liquid fuel density.
RS		Droplet radius.
RS0		Initial droplet radius.
RSP		=RS.
RU		Universal gas constant.
SYOW		Inverse average molecular weight.
T		Gas phase temperature.
T0		Initial gas phase temperature.
TAU		Cumulative evaporation time.
TBOIL		Boiling temperature of fuel.
TD	(N)	Droplet temperature.
TDROP0		Initial droplet temperature.
TDROP		Average droplet temperature.
TEVAP		Total evaporation time.
THETAM		Non dimensional temperature evaluated by interpolation.
TOTAIR		Total air flow rate.
TSURF		Droplet surface temperature.
U1		Gas phase velocity at time=TAU-DT.
U2		Gas phase velocity at time=TAU.
V	(N)	Vector containing the computed solution of TD.
VISCG		Gas phase viscosity.
XF		Fuel vapor mole fraction.
XN2		N2 mole fraction.
XO2		O2 mole fraction.
XPLUS		Locally defined variable.
YF		Fuel mass fraction.
YFLG		Liquid fuel mass fraction.
YFLG1		Initial mass fraction of liquid fuel.
YFS		Mass fraction of fuel at droplet surface.
YN2		N2 mass fraction.
YO2		O2 mass fraction.

```
      PROGRAM VAPOR
C
C     ***********************************************************
C     **                SPRAY VAPORIZATION PROGRAM             **
C     **  THIS PROGRAM USES A DROPLET TRACKING TECHNIQUE TO    **
C     **  CALCULATE THE PREVAPORIZATION PARAMETERS ALONG THE   **
C     **                      SPRAY PATH                       **
C      ***********************************************************
C
      REAL N2MW
      COMMON FMW,N2MW,O2MW,CPG,CONG,DIFF,RHOG,VISCG
       COMMON RU,P,XF,XO2,XN2,SYOW
      COMMON CCPFG(2),CCONFG(2),CVISFG(2)
      DIMENSION TD(51),A(51),B(51),C(51),D(51)
       DIMENSION CVAP(5),CLAT(3),AIRMIX(3),CHT(5)
      CHARACTER *11 FNAME
C
C     ----------------- INITIAL CONDITIONS --------------------
C
      N=20
      NTIME=60
      TAU=0.0
      PRINT *,' ENTER DROPLET DIAMETER (MICRONS) :'
      READ (*,*) RS0
      RS0=RS0/2.0*1.0E-6
      RSP=RS0
      RS=RS0
      PRINT *,' ENTER AIR TEMPERATURE (C) :'
      READ (*,*) T0
      T0=T0+273.15
      PRINT *,' ADIABATIC VAPORIZATION (1=Y ,0=N) :'
      READ (*,*) ADIAB
      PRINT *,' ENTER THE HEIGHT OF THE REDUCING SECTIONS (CM) :'
      READ (*,*) REDHT
      READ (8,200) FNAME
      READ (8,210)FMW,RHOL,TBOIL,CONL,CPF,YFLG1,TEVAP,BHRAT
      READ (8,220) (CVAP(I),I=1,5)
      READ (8,230) (CLAT(I),I=1,3)
      READ (8,240) TOTAIR,DISAIR,(AIRMIX(I),I=1,3)
      READ (8,250) (CCPFG(I),I=1,2)
      READ (8,260) (CCONFG(I),I=1,2)
      READ (8,270) (CVISFG(I),I=1,2)
      READ (8,280) (CHT(I),I=1,5)
  200 FORMAT (A11)
  210 FORMAT (8F8.4)
  220 FORMAT (5E10.4)
  230 FORMAT (F8.1,F9.5,F10.5)
  240  FORMAT (2F7.1,F10.1,2F7.1)
  250  FORMAT (2F9.6)
```

```
  260    FORMAT (2E10.3)
  270    FORMAT (2E10.4)
  280   FORMAT (5F8.4)
        O2MW=32.0
        N2MW=28.0
        P=1.0
        RU=0.08205
        T=T0
        TSURF=297.15
        TDROP=297.15
        TDROP0=297.15
        YF=0.0
        YO2=0.231
        YN2=0.769
        DT0=2.0E-4
        DTINC=(2.0*TEVAP/NTIME-2.0*DT0)/(NTIME-1)
        U1=27.59
        DO 5 I=1,N+1
    5   TD(I)=TDROP
        YFLG=YFLG1*TOTAIR/DISAIR
        WRITE (5,101) FNAME
  101   FORMAT (18X,A11,/)
        WRITE (5,102)
  102   FORMAT (' TIME(SEC) HT(CM) D(MIC) Tg(C) Ts(C) Td(C)       B
     *       E')
C
C       ---------------------- BEGIN ITTERATION ----------------------
C
        DO 16 JTIME=1,NTIME
        DT=DT0+(JTIME-1)*DTINC
        TAU=TAU+DT
        IF (TAU.GE.2.7E-4)  GOTO 7
        AIRFLO=DISAIR+AIRMIX(1)*TAU
        GO TO 9
    7   AIRFLO=AIRMIX(2)+AIRMIX(3)*TAU
    9   YFLG=YFLG*DISAIR/AIRFLO
        YF=YF*DISAIR/AIRFLO
        T=(DISAIR*T+(AIRFLO-DISAIR)*T0)/AIRFLO
        DISAIR=AIRFLO
C
C       ------------------------- VELOCITY  --------------------------
C
        HT=CHT(1)
        DO 18 I=2,5
        HT=HT+CHT(I)*(ALOG(TAU))**(I-1)
   18   CONTINUE
        U2=(AIRFLO/6000.0)/(3.14159/4.0*(HT/BHRAT)**2)
        HT=HT/100.0
        DELU=U2-U1
C       ------------------ VAPOR PRESSURE CALCULATIONS ---------------
   17   PVAPOR=CVAP(1)
        DO 20 I=2,5
        PVAPOR=PVAPOR+CVAP(I)*(TSURF-273.15)**(I-1)
   20   CONTINUE
```

```
C
C       -------------------- GAS PROPERTIES -----------------------
C
        CALL FRACT (T,YF,YN2,YO2)
        CALL PROPTY (T,YF,YN2,YO2)
C
C       ------------------ HEAT OF VAPORIZATION -------------------
C
        HTVAP=CLAT(1)
        DO 22 I=2,3
        HTVAP=HTVAP+CLAT(I)*TSURF**(I-1)
   22   CONTINUE
C
        YFS=1.0/(1.0-(1.0-EXP(HTVAP*FMW/8315.0*(1.0/TSURF-1.0/TBOIL)))
     * /(SYOW*FMW))
        IF (YFS.GT.YF) GOTO 40
        YFS=YF
   40   CONST2=CLAT(2)+2.0*CLAT(3)*TSURF
        CONST3=EXP(HTVAP*FMW/8315.0*(1.0/TSURF-1.0/TBOIL))/(SYOW*FMW)*
     * (HTVAP*FMW/8315.0)/(TSURF*TSURF)*YFS*YFS
        D2=-(CPG*(T-TSURF)*(YFS-1.0)-(HTVAP+CPF*(TSURF-TDROP))*(YF-YFS))
     *  /(CPG*(-(YFS-1.0)+CONST3*(T-TSURF))+CONST3*(HTVAP+CPF*
     *  (TSURF-TDROP))-(YF-YFS)*(CONST2+CPF))
        TSURF=TSURF+D2
        IF (ABS(D2).GE.0.005) GOTO 17
        BNO=(YF-YFS)/(YFS-1.0)
C
C       ------------------ DROPLET SIZE CALCULATIONS ---------------
C
        C1=0.25*SQRT(ABS(8.0*(9.81*(RHOG-RHOL)+DELU/DT*RHOL)*RHOG
     *  /(18.0*VISCG*VISCG)))
        C2=CONG/(CPG*RHOL)*ALOG(1.0+BNO)
        C3=0.0
        DO 24 I=1,35
        C3=C3+(-1.0)**(I+1)*(C1*RS**1.5)**(I-1)*RS*RS/(1.5*(I-1)+2.0)
   24   CONTINUE
   38   F1=0.0
        F2=0.0
        DO 30 I=1,35
        F1=F1+(-1.0)**(I+1)*(C1*RS**1.5)**(I-1)*RS*RS/(1.5*(I-1)+2.0)
        F2=F2+(-1.0)**(I+1)*(C1*RS**1.5)**(I-1)*RS
   30   CONTINUE
        F1=C3-F1-C2*DT
        F2=-F2-C2
        D1=-F1/F2
        RS=RS+D1
        IF (ABS(D1).GE.1.0E-8) GOTO 38
        EXTENT=1.0-(RS/RSP)**3
        U1=U2
C
C       ------------------ DROPLET TEMPERATURE -----------------
C
        TDROP0=TDROP
        TD(N+1)=TSURF
```

```
      DR=1.0/N
      A1=DT*CONL/(RHOL*CPF*RS*RS*DR)
      R=0.0
      DO 55 I=2,N
      R=R+DR
      A(I)=A1/R-A1*R/DR
      B(I)=1.0+2.0*A1*R/DR
      C(I)=-A1/R-A1*R/DR
      D(I)=TD(I)
   55 CONTINUE
      C(2)=-2.0*A1
      D(N)=D(N)+(A1/(1.0-DR)+A1*(1.0-DR)/DR)*TD(N+1)
C
C     SOLVE A SYSTEM OF LINEAR EQNS TO GET DROPLET TEMPERATURE PROI
C
      CALL TRIDAG(2,N,A,B,C,D,TD)
      TD(1)=TD(2)
      TDROP=0.0
      DO 52 I=1,N
      CON1=(TD(I+1)-TD(I))/2.0
      CON2=TD(I+1)-CON1*(FLOAT(I)*DR)
      TDROP=TDROP+3.0*(CON1/4.0*((FLOAT(I)*DR)**4-(FLOAT(I-1)*DR)**
     * +CON2/3.0*((FLOAT(I)*DR)**3-(FLOAT(I-1)*DR)**3))
   52 CONTINUE
C
C     ------------------ GAS PHASE TEMPERATURE -------------------
C
      T=(YFLG*(CPF*(TDROP0-(1.0-EXTENT)*TDROP)-EXTENT*(HTVAP+TSURF*
     * (CPF-CPG)))+CPG*T)/(CPG*(1.0+EXTENT*YFLG))
      IF (T.LE.T0) GOTO 14
      T=T0
   14 YF=(YF+EXTENT*YFLG)/(1.0+EXTENT*YFLG)
      YFLG=(1.0-EXTENT)*YFLG/(1.0+EXTENT*YFLG)
      YN2=(1.0-YF)/(1+0.231/0.769)
      YO2=1.0-(YF+YN2)
      RSP=RS
C
C     ---------- THERMAL ENTRY LENGTH SOLN FOR WALL HEATING -------
C
      IF (ADIAB.EQ.1.0) GOTO 11
      IF (HT.LT.REDHT*1.0E-2) GOTO 11
      PRNO=VISCG*CPG/CONG
      REYNO=RHOG*U2*HT/BHRAT/VISCG
      XPLUS=(HT-REDHT*1.0E-2)/(1.43/200.0)/(REYNO*PRNO)
      IF (XPLUS.GT.0.001) GO TO 62
      THETAM=1.0-XPLUS*(1.0-0.962)/0.001
      GO TO 69
   62 IF (XPLUS.GT.0.004) GO TO 63
      THETAM=0.962+(0.001-XPLUS)*(0.962-0.908)/(0.004-0.001)
      GO TO 69
   63 IF (XPLUS.GT.0.01) GO TO 64
      THETAM=0.908+(0.004-XPLUS)*(0.908-0.837)/(0.01-0.004)
      GO TO 69
   64 IF (XPLUS.GT.0.04) GO TO 65
```

```
      THETAM=0.837+(0.01-XPLUS)*(0.837-0.628)/(0.04-0.01)
      GO TO 69
   65  IF (XPLUS.GT.0.08) GO TO 66
      THETAM=0.628+(0.04-XPLUS)*(0.628-0.459)/(0.08-0.04)
      GO TO 69
   66 IF (XPLUS.GT.0.1) GO TO 67
      THETAM=0.459+(0.08-XPLUS)*(0.459-0.396)/(0.1-0.08)
      GO TO 69
   67 IF (XPLUS.GT.0.2) GO TO 68
      THETAM=0.369+(0.1-XPLUS)*(0.396-0.190)/(0.2-0.1)
      GO TO 69
   68 THETAM=0.0
   69 T=T0-(T0-T)*THETAM
C
 11   WRITE (5,290) TAU,HT*100.0,2.0E6*RS,T-273.15,TSURF-273.15,
     * TDROP-273.15,BNO,1.0-(RS/RS0)**3
 290  FORMAT (F8.5,2X,F5.2,F9.3,3(F6.2),F8.5,F7.4)
 16   CONTINUE
      STOP
      END

      SUBROUTINE FRACT(T,YF,YN2,YO2)
      REAL N2MW
      COMMON FMW,N2MW,O2MW,CPG,CONG,DIFF,RHOG,VISCG
       COMMON RU,P,XF,XO2,XN2,SYOW
C
C     ****************************************************************
C     * MASS TO MOLE FRACTION CONVERSION AND AVERAGE DENSITY CALC.   *
C     ****************************************************************
C
      SYOW=YF/FMW+YO2/O2MW+YN2/N2MW
      XF=YF/(FMW*SYOW)
      XO2=YO2/(O2MW*SYOW)
      XN2=YN2/(N2MW*SYOW)
      RHOG=P/(SYOW*RU*T)
      RETURN
      END

      SUBROUTINE PROPTY(T,YF,YN2,YO2)
      REAL N2MW
      COMMON FMW,N2MW,O2MW,CPG,CONG,DIFF,RHOG,VISCG
       COMMON RU,P,XF,XO2,XN2,SYOW
      COMMON CCPFG(2),CCONFG(2),CVISFG(2)
C
C     ****************************************************************
C     *                 GAS PROPERTY CALCULATIONS                    *
C     ****************************************************************
C
C     ------------------------ CP MIXTURE ------------------------
C
      CPG=(YF*(CCPFG(1)+CCPFG(2)*T*1.8)+YO2*(0.36-5.375/SQRT(T*1.8)
     * +47.8/(1.8*T))+YN2*(0.338-123.8/(1.8*T)+4.14E4/(1.8*1.8*T*T)))
     * *4186.9
```

```
C       -------------- THERMAL CONDUCTIVITY OF MIXTURE --------------
C
        CONG=(XF*(CCONFG(1)+CCONFG(2)*T+CCONFG(3)*T*T)*FMW**(1.0/3.0)
     *  +XO2*(0.0078491+6.784E-5*T-4.903E-9*T*T)*O2MW**(1.0/3.0)
     *  +XN2*(0.0143906+4.545E-5*T+1.515E-9*T*T)*N2MW**(1.0/3.0))/
     *  (XF*FMW**(1.0/3.0)+XO2*O2MW**(1.0/3.0)+XN2*N2MW**(1.0/3.0))
C
C
C       -------------- ABSOLUTE VISCOSITY OF MIXTURE ----------------
C
        VISCG=(XF*(CVISFG(1)+CVISFG(2)*T)*SQRT(FMW)
     *  +XO2*(1.697E-5+5.51E-8*T-1.0E-10*T*T)*SQRT(O2MW)
     *  +XN2*(1.697E-5+5.51E-8*T-1.0E-10*T*T)*SQRT(N2MW))/
     *  (XF*SQRT(FMW)+XO2*SQRT(O2MW)+XN2*SQRT(N2MW))
C
        DIFF=CONG/(RHOG*CPG)
        RETURN
        END

        SUBROUTINE TRIDAG(IF,L,A,B,C,D,V)
        DIMENSION A(1),B(1),C(1),D(1),V(1),BETA(51),GAMMA(51)
C
C       ************************************************************
C       *         LINEAR SIMULTANEOUS SYSTEM OF EQNS SOLVER        *
C       *    REF: "APPLIED NUMERICAL METHODS," CARNAHAN ET AL.     *
C       *                 JOHN WILEY & SONS, 1976.                 *
C       ************************************************************
C
        BETA(IF)=B(IF)
        GAMMA(IF)=D(IF)/BETA(IF)
        IFP1=IF+1
        DO 1 I=IFP1,L
        BETA(I)=B(I)-A(I)*C(I-1)/BETA(I-1)
    1   GAMMA(I)=(D(I)-A(I)*GAMMA(I-1))/BETA(I)
        V(L)=GAMMA(L)
        LAST=L-IF
        DO 2 K=1,LAST
        I=L-K
    2   V(I)=GAMMA(I)-C(I)*V(I+1)/BETA(I)
        RETURN
        END
```

E.3 Spray Combustion

FORTRAN Variable		Definition
AIRO		Total oxidizer mass around a burning droplet.
AIRMAS		Cumulative oxidizer mass.
B		Preexponential constant for fuel oxidation reaction.
BRATE1		Backward reaction rate constant for: 02+N2 = 20+N2.
BRATE2		Backward reaction rate constant for: 0+N2 = NO+N.
BRATE3		Backward reaction rate constant for: N+02 = NO+0.
BURND		Burner height.
CF		Stoichiometric molar coefficient for fuel.
CO		Stoichiometric molar coefficient for oxydizer.
CPDT		$\int Cp\ dT$.
DIST		Center-to-center droplet spacing, 2ℓ
DR		= DRI.
DRO		First radial spacing.
DRI	(N)	Ramped radial spacing.
DRLST		Last radial spacing.
E		Activation energy for fuel oxidation reaction.
ELLAST		Locally defined variable.
ELMAS		Locally defined variable.
FRATE1		Forward reaction rate constant for: 02+N2 = 20+N2.
FRATE2		Forward reaction rate constant for: 0+N2 = NO+N.
FRATE3		Forward reaction rate constant for: N+02 = NO+0.
FUO		Total mass of fuel.
FUMAS		Locally defined variable.
J		Local index.
NBRACH		Burning rate correction factor equation flag.
NDROP		Number of droplets in a planar array.
NODEN		Droplet number density.
NOMW		Molecular weight of NO.
PHIO		Overall equivalence ratio.
PI		3.14159
PORUT2		Locally defined variable.
Q		Heat of reaction.
RO		Universal gas constant.
REACT1		Rate of O formation from: 02+N2 = 20+N2.
REACT2		Rate of N formation from: 0+N2 = NO+N.
REACT3		Rate of NO formation from: N+02 = NO+0.
RHO		Gas phase density.
RHODIF		$\rho \times \mathcal{D}$
RHOS		Density at droplet surface.
RVDRDT		Locally defined variable.
SDRLST		Locally defined variable.
SOXF		Stoichiometric oxygen to fuel mass ratio.
SYOWBK		Previous inverse average molecular weight.
T	(N)	Flame temperature.
TAU		Cumulative reaction time.
TENLOG		Log base 10 of nondimensional particle spacing.

FORTRAN Variable		Definition
TGAS		Initial reaction temperature.
TGAS0		Inlet gas phase temperature.
TL0		Boiling temperature of fuel.
TNEW	(N)	Updated flame temperature.
TOTFUL		Sum of cumulative (reacted and unreacted) fuel mass
TOTMAS		Locally defined variable.
TOTMS0		Combined mass of fuel and oxidizer.
TOTOX		Sum of cumulative (reacted and unreacted) oxidizer mass.
V	(N)	Radial velocity.
X1		Local x-coordinate of a droplet.
XN		Mole fraction of N.
XNO		Mole fraction of NO.
XO		Mole fraction of O.
Y1		Local Y-coordinate of a droplet.
YFGAS		Initial fuel vapor mass fraction in gas phase.
YFNEW	(N)	Updated fuel vapor mass fraction in gas phase.
YN2	(N)	Mass fraction of N2 in gas phase.
YN2GAS		Initial mass fraction of N2 in the gas phase.
YN2NEW	(N)	Updated N2 mass fraction in gas phase.
YNO	(N)	Mass fraction of NO in gas phase.
YNONEW	(N)	Updated NO mass fraction in gas phase.
YO2	(N)	Mass fraction of O2 in gas phase.
YO2GAS		Initial mass fraction of O2 in the gas phase.
YO2NEW	(N)	Updated O2 mass fraction in gas phase.
YPMINS		Combined mass fraction of product (no N2) at R+DR(I-1).
YPPLUS		Combined mass fraction of product (no N2) at R+DR(I).
YPROD		Combined mass fraction of product (no N2) at R+DR(N).

```
      PROGRAM COMB
C
C     ***************************************************************
C     **                  SPRAY COMBUSTION PROGRAM                 **
C     **                WITH NO FORMATION KINETICS                 **
C      ***************************************************************
C
      REAL N2MW,NOMW
      COMMON FMW,N2MW,O2MW,NOMW,CPG,CONG,DIFF,RHO,RU,P
      COMMON XF,XO2,XN2,XN,XO,XNO,SYOW
      DIMENSION T(301),TNEW(301),YF(301),YFNEW(301),YO2(301)
      DIMENSION YO2NEW(301),YN2(301),DRI(301)
      DIMENSION YN2NEW(301),YNO(301),YNONEW(301),V(301)
C
C     ------------------ INITIAL CONDITIONS --------------------
C
  351 FORMAT (F7.2,I5,F7.2,F5.2,F7.4)
  352 FORMAT (F7.2,F7.4,F6.1,F6.1,F6.2)
  353 FORMAT (4E10.3)
      READ (7,351) RS0,NODEN,TGAS0,PHI0,EXTENT
      READ (7,352) FMW,CONL,RHOL,TL0,CO
      READ (7,353) HTVAP,Q,B,E
      TAU=0.0
      RS0=RS0/2.0*1.0E-4
      TGAS0=TGAS0+273.15
      DR0=0.2
       CF=1.0
      O2MW=32.0
      N2MW=28.0
      NOMW=30.0
      P=1.0
      R0=8.315*1000.0
      RU=0.08205
      SOXF=CO*O2MW/(FMW*PHI0)
C
C     ---------------- DROPLET CONFIGURATION IN THE ARRAY ----------
C
      CALL CONFIG(RS0,DIST,NODEN,NDROP)
C
      RS0=RS0*1.0E-2
      RS=RS0
      N=INT(-DR0+0.03+SQRT((DR0-0.03)**2-4.0*(1.0-DIST)*0.03)/0.06)-1
      WRITE (5,35) DIST,2.0*RS0*1E6,NODEN,NDROP,PHI0
   35  FORMAT (' INIT DROP SPAC.=',F5.2,' D0 =',F6.2,' NO. DENS
     * =',I4,' DROPS/ARRAY=',I3,' PHI=',F5.3/)
C
       FU0=4.0/3.0*3.14159*RHOL*RS0**3/(1.0-EXTENT)
       TOTMS0=FU0*(1.0+SOXF/PHI0)
      AIR0=FU0*SOXF/PHI0
```

```
      TGAS=1100.0
   18 YFGAS=1.0/(1.0+4.29*SOXF/(EXTENT*PHIO))
      YO2GAS=(1.0-YFGAS)/(4.29)
      YN2GAS=3.29*YO2GAS
      CPDT=(YO2GAS*(0.36*1.8*(TGAS-TGAS0)-2.0*5.375*(SQRT(TGAS*1.8)-
     * SQRT(TGAS0*1.8))+47.8*(ALOG(1.8*TGAS)-ALOG(1.8*TGAS0)))+
     * YN2GAS*(0.338*1.8*(TGAS-TGAS0)-123.8*(ALOG(1.8*TGAS)-
     *  ALOG(1.8*TGAS0))-(4.14E4)/1.8*(1.0/TGAS-1.0/TGAS0))+YFGAS*
     *  (0.0694*1.8*(TGAS-TGAS0)+(5.27E-4)/2.0*1.8*1.8*(TGAS*TGAS-
     * TGAS0*TGAS0)))*2326.0
      YFGAS=YFGAS-CPDT/Q
      YO2GAS=YO2GAS-CPDT/Q*SOXF
      IF (YFGAS.GT.0.001) GOTO 23
      TGAS=TGAS-50.0
      GO TO 18
   23 DO 10 I=1,N+1
      T(I)=TGAS
      YF(I)=YFGAS
      YO2(I)=YO2GAS
      YN2(I)=YN2GAS
      YNO(I)=0.0
      V(I)=0.0
  10  CONTINUE
      T(1)=TL0
      YF(1)=0.80
      YO2(1)=0.0466
      YN2(1)=0.1534
      TNEW(1)=T(1)
      YFNEW(1)=YF(1)
      YO2NEW(1)=YO2(1)
      YN2NEW(1)=YN2(1)
      DT=RS0*0.7E-3
       DRLST=DR0+(FLOAT(N-1))*0.06
      SDRLST=DRLST
      DO 20 I=2,301
      DRI(I)=DR0+(FLOAT(I-2))*0.06
   20 CONTINUE
C
C     --------------------- BEGIN ITTERATION ---------------------
C
      DO 16 JTIME=1,150000
      IF (JTIME.LT.10) GO TO 43
      DT=800.0*RS*RS
   43  TAU=TAU+DT
      CALL FRACT (T,1,YF,YN2,YO2,YNO)
      SYOWBK=SYOW
      RHOS=RHO
C
C     -------------------- DROPLET INTERACTIONS -------------------
C
      CALL CONFAC(DIST,RS0,RS,NDROP,ETA)
C
C     ------------------- BEGIN RADIAL MARCHING ------------------
C
```

```
      IF (RS.GE.1.5E-6) GOTO 339
      FUMAS=0.0
      GO TO 354
 339          FUMAS=4.0/3.0*3.14159*RHOL*RS**3
 354  TOTMAS=FUMAS
      AIRMAS=0.0
      R=1.0
      DO 12 I=2,N
      DR=DRI(I)
      R=R+DR
C
C     --------------------- GAS PROPERTIES -----------------------
C
      CALL FRACT (T,I,YF,YN2,YO2,YNO)
      CALL PROPTY (T,I,YF,YN2,YO2,YNO)
C
C     ----------------- CONSERVATION OF ENERGY -------------------
C
      PORUT2=(P/(RU*T(I)))**2
      TNEW(I)=T(I)+DT*(-V(I)/(RS*DR)*(T(I+1)-T(I-1))/2.0+CONG/(RHO*
     * CPG*RS*RS)*((T(I+1)-T(I-1))/(R*DR)+(T(I+1)-2.0*T(I)+T(I-1))
     * /(DR*DR))+CF*FMW*PORUT2/(RHO*CPG)*XF*XO2*B*EXP(-E/(RO*T(I)))*Q)
C
C     ---------------- CONSERVATION OF FUEL -------------------
C
      PORUT2=(P/(RU*TNEW(I)))**2
      YFNEW(I)=YF(I)+DT*(-V(I)/(RS*DR)*(YF(I+1)-YF(I-1))/2.0+RHO*DIFF/
     * (RHO*RS*RS)*((YF(I+1)-YF(I-1))/(R*DR)+(YF(I+1)-2.0*YF(I)+
     * YF(I-1))/(DR*DR))-CF*FMW/RHO*PORUT2*XF*XO2*
     * B*EXP(-E/(RO*TNEW(I))))
      IF (YFNEW(I).GE.0.0) GOTO 300
      YFNEW(I)=0.0
C
C     --------------- CONSERVATION OF OXIDIZER -----------------
C
 300  YO2NEW(I)=YO2(I)+DT*(-V(I)/(RS*DR)*(YO2(I+1)-YO2(I-1))/2.0+RHO*
     * DIFF/(RHO*RS*RS)*((YO2(I+1)-YO2(I-1))/(R*DR)+(YO2(I+1)
     * -2.0*YO2(I)+YO2(I-1))/(DR*DR))-CO*O2MW/RHO*PORUT2*XF*XO2*
     * B*EXP(-E/(RO*TNEW(I))))
      IF (YO2NEW(I).GE.0.0) GOTO 400
      YO2NEW(I)=0.0
C
C      ++++++++++++++++++++++++++++++++++++++++++++++++++++++++++++++
C     +                         NO KINETICS                          +
C     ++++++++++++++++++++++++++++++++++++++++++++++++++++++++++++++++
C
C     ----------- REACTION RATES FOR ZELDOVICH MECHANISM ------------
C
 400  FRATE1=6.0E10*4.94E8/(RO*TNEW(I))*EXP(-4.94E8/(RO*TNEW(I)))
      BRATE1=1.0E8
      FRATE2=1.36E11*EXP(-3.15E8/(RO*TNEW(I)))
      BRATE2=3.1E10*EXP(-1.4E6/(RO*TNEW(I)))
      FRATE3=6.4E6*TNEW(I)*EXP(-2.62E7/(RO*TNEW(I)))
      BRATE3=1.5E6*TNEW(I)*EXP(-1.62E8/(RO*TNEW(I)))
```

```
      XO=SQRT(FRATE1/BRATE1*RU*TNEW(I)/P*XO2)
      XN=XO*(BRATE3*XNO+FRATE2*XN2)/(FRATE3*XO2+BRATE2*XNO)
C
C     ---------- SOURCE AND SINK TERMS FOR ZELDOVICH MECHANISM ----
C
      REACT1=PORUT2*(2.0*FRATE1*XO2*XN2-2.0*BRATE1*XO*XO*XN2*
     * SQRT(PORUT2))
      REACT2=PORUT2*(FRATE2*XO*XN2-BRATE2*XNO*XN)
      REACT3=PORUT2*(FRATE3*XN*XO2-BRATE3*XNO*XO)
C
C     -------------------- N2 CONSERVATION -----------------------
C
      YN2NEW(I)=YN2(I)+DT*(-V(I)/(RS*DR)*(YN2(I+1)-YN2(I-1))/2.0+RH(
     * DIFF/(RHO*RS*RS)*((YN2(I+1)-YN2(I-1))/(R*DR)+(YN2(I+1)
     * -2.0*YN2(I)+YN2(I-1))/(DR*DR)))
C
C     -------------------- NO CONSERVATION -----------------------
C
      YNONEW(I)=YNO(I)+DT*(-V(I)/(RS*DR)*(YNO(I+1)-YNO(I-1))/2.0+RHC
     * DIFF/(RHO*RS*RS)*((YNO(I+1)-YNO(I-1))/(R*DR)+(YNO(I+1)
     * -2.0*YNO(I)+YNO(I-1))/(DR*DR))+NOMW/RHO*(REACT2+REACT3))
C
C     -------------------- OVERALL O/F RATIO ---------------------
C
      ELMAS=4.0/3.0*3.14159*(R**3-(R-DR)**3)*RS**3*P/(RU*
     * (SYOW+SYOWBK)/2.0*(TNEW(I)+TNEW(I-1))/2.0)
      YPMINS=1.0-(YFNEW(I-1)+YO2NEW(I-1)+YN2NEW(I-1))
      YPPLUS=1.0-(YFNEW(I)+YO2NEW(I)+YN2NEW(I))
      AIRMAS=((YO2NEW(I)+YO2NEW(I-1))/2.0+(YPMINS+YPPLUS)/2.0*
     * (1.0-114./514.0))*ELMAS+AIRMAS
      FUMAS=((YFNEW(I)+YFNEW(I-1))/2.0+(YPMINS+YPPLUS)/2.*114./514.)
     * *ELMAS+FUMAS
      TOTMAS=ELMAS+TOTMAS
      SYOWBK=SYOW
C
C     ---------------------- CONTINUITY -------------------------
C
      IF (RS.LT.1.5E-6) GOTO 64
      RVDRDT=CONL*(T(2)-T(1))/(RS*DRO*HTVAP)
C     V(I)=((P/(RU*TNEW(I)*SYOW)-RHO)/(3.*DT)*RS*(1.-R**3)+
C    *  RVDRDT)/(RHO*R*R)
      V(I)=RVDRDT*(RHOL-RHOS)/(RHO*RHOL*R*R)
 64   IF (JTIME.NE.1.AND.FLOAT(JTIME)/1000..NE.JTIME/1000) GOTO 12
       IF (I.GT.2) GOTO 700
      WRITE (5,444)
 444  FORMAT('       R        T       V       YF      YO2       YN2'
     * ,'      XN        XO         YNO')
       WRITE (5,123) R-DR,INT(T(1)),V(1),YF(1),
     * YO2(1),YN2(1),0.0,0.0,YNO(1)
 700   WRITE (5,123) R,INT(TNEW(I)),V(I),YFNEW(I),
     * YO2NEW(I),YN2NEW(I),XN,XO,YNONEW(1)
 123   FORMAT (1X,F7.1,1X,I5,F7.3,3F7.4,3E10.3)
 12    CONTINUE
```

```
C       --------------- ASSIGN THE NEW VALUES -----------------
C
         DO 14 I=2,N
        T(I)=TNEW(I)
        YF(I)=YFNEW(I)
        YO2(I)=YO2NEW(I)
        YN2(I)=YN2NEW(I)
        YNO(I)=YNONEW(I)
   14    CONTINUE
        IF (RS.LT.1.5E-6) GOTO 66
C
C       -------------------- O/F RATIO CHECK --------------------
C
        ELLAST=TOTMS0-TOTMAS
        YPROD=1.0-(YO2NEW(N)+YFNEW(N)+YN2NEW(N))
   72   TOTOX=AIRMAS+ELLAST*(YO2NEW(N)+YPROD*(1.0-114./514.))
        TOTFUL=FUMAS+ELLAST*(YF(N)+YPROD*114./514.)
        IF (ABS(TOTOX/TOTFUL-SOXF).LT.0.01) GOTO 74
        ELLAST=(SOXF*FUMAS-AIRMAS)/(YO2(N)+YPROD*(1.-114/514.
      *  -SOXF*114./514.)-SOXF*YF(N))
        GO TO 72
   74   DRLST=((ELLAST)/
      *  (4./3.*3.14159*RS**3*P/(RU*SYOW*TNEW(N)))+R**3)**(1.0/3.0)-R
        SDRLST=DRLST+SDRLST
        IF (SDRLST.GE.DRI(N+1)) GOTO 45
        N=N-1
        SDRLST=SDRLST+DRI(N+1)
   45    DRLST=SDRLST
         IF (SDRLST.LE.DRI(N+2)) GOTO 41
        SDRLST=SDRLST-DRI(N+1)
        N=N+1
         DRLST=SDRLST
C
C       ------------ BOUNDARY CONDITIONS AT SURFACE -------------
C
   41    RVDRDT=CONL*(T(2)-T(1))/(RS*DR0*HTVAP)
        RS=RS-DT*RVDRDT/RHOL*ETA
        IF (RS) 99,99,24
   24   V(1)=RVDRDT*(1.0/RHOS+1.0/RHOL)
        RHODIF=CONL/((0.0694+5.27E-4*TL0*1.8)*4186.9)
        YF(1)=(RHODIF*YF(2)/(RS*DR0)+RVDRDT)/(RHODIF/(RS*DR0)+RVDRDT)
        YO2(1)=(RHODIF*YO2(2)/(RS*DR0))/(RHODIF/(RS*DR0)+RVDRDT)
        YN2(1)=(RHODIF*YN2(2)/(RS*DR0))/(RHODIF/(RS*DR0)+RVDRDT)
        YNO(1)=(RHODIF*YNO(2)/(RS*DR0))/(RHODIF/(RS*DR0)+RVDRDT)
        GO TO 68
   66    DO 62 I=1,N
        V(I)=0.0
   62   CONTINUE
        YF(1)=YF(2)
        YN2(1)=YN2(2)
        YO2(1)=YO2(2)
        YNO(1)=YNO(2)
C       T(1)=T(2)
```

```
C      ------------ BOUNDARY CONDITIONS AT AMBIENCE -------------
C
  68    T(N+1)=T(N)
       YF(N+1)=YF(N)
       YO2(N+1)=YO2(N)
       YN2(N+1)=YN2(N)
       YNO(N+1)=YNO(N)
       V(N+1)=V(N)
C
 28    IF (JTIME.NE.1.AND.FLOAT(JTIME)/1000..NE.JTIME/1000) GOTO 16
       WRITE (5,222) TAU,2.0*RS*1.0E6,1.0-(RS/RS0)**3,ETA,
     * JTIME,DR,N
 222    FORMAT (' T(SEC)=',E10.3,';D(MIC)=',F6.3,';E=',F5.3,
     *  ';ETA=',F5.3,';ITER=',I6,';DEL=',F5.1,';N=',I3/)
 16    CONTINUE
  99   STOP
       END

       SUBROUTINE FRACT(T,I,YF,YN2,YO2,YNO)
       REAL N2MW,NOMW
       COMMON FMW,N2MW,O2MW,NOMW,CPG,CONG,DIFF,RHO,RU,P
       COMMON XF,XO2,XN2,XN,XO,XNO,SYOW
       DIMENSION T(1),YF(1),YN2(1),YO2(1),YNO(1)
C
C      *****************************************************************
C      * MASS TO MOLE FRACTION CONVERSION AND AVERAGE DENSITY CALC.
C      *****************************************************************
C
       SYOW=YF(I)/FMW+YO2(I)/O2MW+YN2(I)/N2MW+(1.0-YF(I)-YO2(I)-YN2(
     *  *((114./514.)/18.0+(1.-114.0/514.0)/44.0)
       XF=YF(I)/(FMW*SYOW)
       XO2=YO2(I)/(O2MW*SYOW)
       XN2=YN2(I)/(N2MW*SYOW)
       XNO=YNO(I)/(NOMW*SYOW)
       RHO=P/(RU*T(I)*SYOW)
       RETURN
       END

       SUBROUTINE PROPTY(T,I,YF,YN2,YO2,YNO)
       REAL N2MW,NOMW
       COMMON FMW,N2MW,O2MW,NOMW,CPG,CONG,DIFF,RHO,RU,P
       COMMON XF,XO2,XN2,XN,XO,XNO,SYOW
       DIMENSION T(1),YF(1),YN2(1),YO2(1),YNO(1)
C
C      *****************************************************************
C      *                    GAS PROPERTY CALCULATIONS
C      *****************************************************************
C
C      ------------------------ CP MIXTURE ----------------------------
C
       CPG=(YF(I)*(0.0694+5.27E-4*T(I)*1.8)+YO2(I)*(0.36-5.375/
     *  SQRT(T(I)*1.8)+47.8/(1.8*T(I)))+YN2(I)*(0.338-123.8/(1.8*T(I
     *  +4.14E4/(1.8*1.8*T(I)*T(I)))+(1.0-YF(I)-YO2(I)-YN2(I))*
     *  (0.681*(0.368-148.4/(1.8*T(I))+3.2E4/(1.8*1.8*T(I)*T(I)))
```

```
     * +0.319*(1.102-33.1/SQRT(1.8*T(I))+416.0/(1.8*T(I)))))*4186.9
C
C     --------------- THERMAL CONDUCTIVITY OF MIXTURE --------------
C
      CONG=(XF*(-0.026834+1.329E-4*T(I)-1.741E-8*T(I)*T(I))*
     * FMW**(1.0/3.0)+XO2*(0.0078491+6.784E-5*T(I)-4.903E-9*T(I)*
     * T(I))*O2MW**(1.0/3.0)+XN2*(0.0143906+4.545E-5*T(I)+1.515E-9*
     * T(I)*T(I))*N2MW**(1.0/3.0)+(1.0-XF-XO2-XN2)*(0.681*
     * (-0.0009023+6.915E-5*T(I)-3.688E-9*T(I)*T(I))*44.0**(1.0/3.0)
     * +0.319*(0.0048332+1.303E-4*T(I)-7.059E-9*T(I)*T(I))*
     * 18.0**(1.0/3.0)))/(XF*FMW**(1.0/3.0)+XO2*O2MW**(1.0/3.0)+XN2*
     * N2MW**(1.0/3.0)+(1.0-XF-XN2-XO2)
     * *(0.681*44.0**(1.0/3.0)+0.319*18.0**(1.0/3.0)))
C
      DIFF=CONG/(RHO*CPG)
      RETURN
      END

      SUBROUTINE CONFIG(RS0,DIST,NODEN,NDROP)
C
C     *************************************************************
C      *    PROGRAM TO DETERMINE DROPLET SPACINGS FOR AN EVENLY    *
C      *                DISPERSED MONOSIZED ARRAY                  *
C      *************************************************************
C
      NDROP=0
      BURND=1.43
      PI=3.1415927
      DIST=(2.0/(NODEN*SIN(PI/3.0)))**(1.0/3.0)/(2.0*RS0)
      BURND=BURND/(RS0*2.0)
      DO 15 J=1,INT(BURND/(2.0*DIST*SIN(PI/3.0)))+1
      DO 20 I=1,INT(BURND/(2.0*DIST))+1
      X1=(I-1)*DIST
      IF (FLOAT(J)/2.0.NE.INT(J/2)) GOTO 30
      X1=X1+DIST/2.0
 30   Y1=(J-1)*DIST*SIN(PI/3.0)
      IF (SQRT(X1*X1+Y1*Y1).GT.BURND/2.0) GOTO 20
      NDROP=NDROP+1
      IF (I*J.EQ.1) GOTO 20
      IF(Y1.EQ.0.0) GOTO 40
      NDROP=NDROP+1
      IF (X1.EQ.0.0) GOTO 20
      NDROP=NDROP+2
      GO TO 20
 40    NDROP=NDROP+1
 20    CONTINUE
 15    CONTINUE
      RETURN
      END
```

```
      SUBROUTINE CONFAC(DIST,RS0,RS,NDROP,ETA)
C
C      *************************************************************
C      * SUBROUTINE TO CALCULATE BURNING RATE CORRECTION FACTOR  *
C      * FOR MONODISPERSE SPRAYS.  STATEMENT NUMBERS CORRESPOND  *
C      * TO THE NUMBER OF INTERACTING DROPLETS IN A PLANAR ARRAY.*
C      *************************************************************
C
      TENLOG=ALOG10(2.0*DIST*RS0/RS)
      IF (TENLOG.LT.3.17) GOTO 25
      ETA=1.0
      GO TO 27
   25 NBRACH=(NDROP-1)/6-8
      GO TO (55,61,67,73,79,85,91,97,103,109,115,121,127,133,139,
     * 145,151,157),NBRACH
   55 ETA=-1.2436435+TENLOG*(2.2164602-0.8041338*TENLOG+0.1235272*
     * TENLOG*TENLOG-0.0064171*TENLOG**3)
      GO TO 27
   61 ETA=-1.218263+TENLOG*(2.1265647-0.7282704*TENLOG+0.098952*
     * TENLOG*TENLOG-0.0036453*TENLOG**3)
      GO TO 27
   67 ETA=-1.2337979+TENLOG*(2.0958116-0.6898761*TENLOG+0.0856408*
     * TENLOG*TENLOG-0.0021527*TENLOG**3)
      GO TO 27
   73 ETA=-1.1997394+TENLOG*(1.9788084-0.5967735*TENLOG+0.0559048*
     * TENLOG*TENLOG+0.0012112*TENLOG**3)
      GO TO 27
   79 ETA=-1.1988726+TENLOG*(1.9448054-0.5593372*TENLOG+0.0432551*
     * TENLOG*TENLOG+0.0026203*TENLOG**3)
      GO TO 27
   85 ETA=-1.1423215+TENLOG*(1.8058571-0.4514555*TENLOG+0.0088748*
     * TENLOG*TENLOG+0.0065384*TENLOG**3)
      GO TO 27
   91 ETA=-1.1428598+TENLOG*(1.7650879-0.4115640*TENLOG-0.0042657*
     * TENLOG*TENLOG+0.0079962*TENLOG**3)
      GO TO 27
   97 ETA=-1.0798480+TENLOG*(1.6162612-0.2968254*TENLOG-0.0409864*
     * TENLOG*TENLOG+0.0122215*TENLOG**3)
      GO TO 27
  103 ETA=-1.0748937+TENLOG*(1.5707712-0.2552938*TENLOG-0.0544528*
     * TENLOG*TENLOG+0.0137137*TENLOG**3)
      GO TO 27
  109 ETA=-1.0080442+TENLOG*(1.4162596-0.1363881*TENLOG-0.0927271*
     * TENLOG*TENLOG+0.0181601*TENLOG**3)
      GO TO 27
  115 ETA=-0.9990754+TENLOG*(1.3675382-0.0938431*TENLOG-0.1063837*
     * TENLOG*TENLOG+0.0196740*TENLOG**3)
      GO TO 27
  121 ETA=-0.9380671+TENLOG*(1.2264606+0.0151967*TENLOG-0.1417152*
     * TENLOG*TENLOG+0.0238125*TENLOG**3)
      GO TO 27
```

```
127   ETA=-0.9125118+TENLOG*(1.1476325+0.0791626*TENLOG-0.1622019*
     * TENLOG*TENLOG+0.0261359*TENLOG**3)
      GO TO 27
133   ETA=-0.8509631+TENLOG*(1.006496+0.1884841*TENLOG-0.1978621*
     * TENLOG*TENLOG+0.0303513*TENLOG**3)
      GO TO 27
139   ETA=-0.8368802+TENLOG*(0.9543458+0.2317049*TENLOG-0.2115844*
     * TENLOG*TENLOG+0.0318774*TENLOG**3)
      GO TO 27
145   ETA=-0.7636684+TENLOG*(0.7898749+0.3588799*TENLOG-0.2532952*
     * TENLOG*TENLOG+0.0368515*TENLOG**3)
      GO TO 27
151    ETA=-0.7478763+TENLOG*(0.7367701+0.4021712*TENLOG-0.2670025*
     * TENLOG*TENLOG+0.0383796*TENLOG**3)
      GO TO 27
157   ETA=-0.6827373+TENLOG*(0.5896260+0.5165399*TENLOG-0.3047329*
     * TENLOG*TENLOG+0.0429093*TENLOG**3)
 27   RETURN
      END
```

E.4 Sample Input Data

E.4.1 Droplet Interactions Program

```
7
6
  0.000    0.000   0.000 1.0
 20.000    0.000   0.000 1.0
-20.000    0.000   0.000 1.0
 10.000   17.321   0.000 1.0
 10.000  -17.321   0.000 1.0
-10.000  -17.321   0.000 1.0
-10.000   17.321   0.000 1.0
```

E.4.2 Spray Vaporization Program

```
N-OCTANE
114.2    707.0    398.15   0.132    2205.0   0.0663   0.1703   12.45
2.267E0    0.2138E0    8.594E-3    1.42E-4     1.28E-5
368370.0 421.2021   -1.4705
3400.0 1300.0 7253000.0 3272.0  498.0
0.0694   0.000527
 -1.306E-1  7.997E-4
 7.2029E-7 1.7494E-8
 31.59  9.935   1.372   0.095   0.0026
```

E.4.3 Spray combustion Program

```
  47.68  400   23.64 1.00 0.43
 114.20 0.0199 707.0 380.0 12.50
   3.027E5   4.460E7   1.150E11   1.260E8
```

VITA

Hamid Sarv was born [redacted] in [redacted] He attended Drexel University where he received the B.S. degree in Mechanical Engineering in 1979. During his undergraduate study, he obtained cooperative work experience at the Franklin Institute Research Laboratories, Ecolaire Inc., and Drexel University. He continued his graduate study at Drexel and obtained the M.S. and Ph.D. degrees in Mechanical Engineering in 1981 and 1985, respectively. During this period, he served as a research/teaching assistant in the ME department and co-authored four papers.

Mr. Sarv is a member of SAE, ASME, and Sigma Xi.